Università degli Studi di Urbino Carlo Bo

Department of Pure and Applied Science

Ph.D. PROGRAMME in: Basic Sciences and Applications

CURRICULUM: Chemical and Pharmaceutical Sciences

CYCLE XXXIV

DESIGN, SYNTHESIS AND CHARACTERIZATION OF POLYAMINE-BASED FLUORESCENT CHEMOSENSORS FOR SELECTIVE RECOGNITION OF METAL CATIONS IN SOLUTION

ACADEMIC DISCIPLINE: CHIM/03

Coordinator:
Chiar.mo Prof. Alessandro Bogliolo

Supervisor:
Chiar.mo Prof. Luca Giorgi

Ph.D. student:
Daniele Paderni

ACADEMIC YEAR 2020/2021

To my Family

Contents

Abstract

This project describes the design, synthesis, photochemical characterization, coordination properties and X-ray crystal structures of some fluorescent polyamino-ligands, four of which (L1-L4) were found to have interesting photochemical and coordination properties (Scheme 1). Each structure contains one or two fluorophores linked to a polyamine building block with open-chain or cyclic topology and is able to signal the presence of a specific metal ion in solution by changing its emission properties.

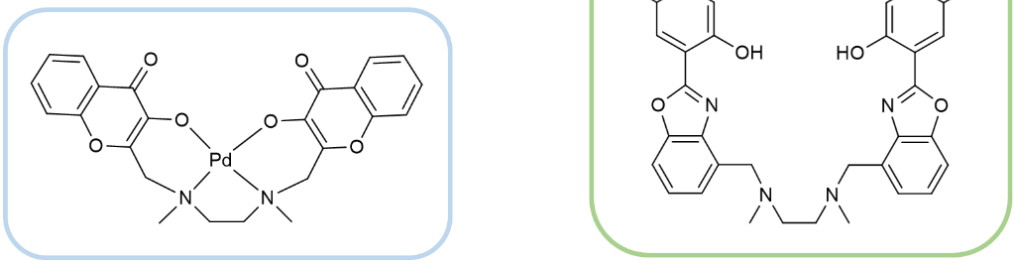

[Pd(H_{-2}**L1**)] **L2**

L3 **L4**

Scheme 1. The ligands synthesized during this project.

L1 contains two hydroxychromone units linked as side arms to an ethylenediamine moiety, this ligand can be pre-organized by the coordination of a Pd(II) ion giving rise to the [Pd(H_{-2}**L1**)] species in which the four oxygen atoms bearing to the two hydroxychromone units form a negatively charged pocket able to interact with hard metal cations, such as rare earth ions. This system can be used as a selective fluorescent probe to detect the presence of Gadolinium in environmental water, due to a chelation enhancement of the fluorescence effect (CHEF) upon the coordination of Gd(III).

L2 is an open-chain ligand containing two HNBO fluorophores (hydroxynaphthylbenzoxazol) linked to a dimethylethylenediamine fragment. In DMSO solution this ligand absorbs at 450 nm and is weakly fluorescent. Studies performed with Alkali and Alkaline Earth ions showed that the emission at 530 nm dramatically increases only in the presence of Mg(II) ions. Competition experiments demonstrate that the presence of Li(I), Na(I), K(I), Ca(II), Sr(II) and Ba(II) do not prevent the ability of the sensor to signal the presence of Mg(II), thus it can be used to sense this ion also in real samples such as commercial drinkable water. The presence of Mg(II) can be qualitatively appreciated with the naked eye as a yellow emission by lighting the sample with a 360 nm UV lamp.

L3 is a polyamine cyclophane macrocycle in which 2,6-bis(5-(2- methylphenyl)-1,3,4-oxadiazol-2-yl)pyridine (POXAPy) acts as a fluorescent sensor and the polyamine as a metal ion binding unit. **L3** performs as a PET-mediated chemosensor, with a maximum emission wavelength close to 360 nm. This gives rise to a signal that is visible to the naked eye in the blue visible range. **L3** is able to detect Zn(II) and Cd(II) metal ions in an aqueous solution at pH = 7, with the coordination of the ions switching ON the emission through a CHEF effect. In contrast, paramagnetic metal ions like Cu(II) and Ni(II) completely quench the already low emission of **L3** at this pH value.

L4 contains the 2,6-bis(benzoxazol-2-yl)phenol fluorophore (BPhB) and shows peculiar double emission properties. The ligand is able to coordinate a Zn(II) ion in aqueous environment with concomitant keto-enol tautomerism giving rise to large Stokes shifts. Upon excitation at 342 nm the protonated form of the ligand shows a double emission at 380 nm and 507 nm, due to Excited State Intramolecular Proton Transfer (ESIPT), while in the deprotonated form only an emission band at 475 nm is observed. At pH = 7 both protonated and deprotonated forms are present in solution, thus by exciting at 342 nm an intense emission at 507 nm can be observed, while by exciting at 405 nm the emission band is centered at 476 nm. At pH = 7, the addition of selected transition metal ions causes the quenching of the keto band at 507 nm and the formation of a new band relative to the deprotonated form at 458 nm for Zn(II), Cd(II) and Pb(II). Zn(II) and Cd(II) ions give rise to highly fluorescent complexes while the other tested metal ions (Ni((II), Cu(II), Hg(II) and Pb(II)) form weakly fluorescent species. Under a UV lamp at 360 nm a solution of **L4** at pH = 7 appears green. Due to the ratiometric nature of the signal the presence of Zn(II) and Cd(II) ions can be detected through a clear change of color from green to blue.

Chapter 1 - Introduction

1.1 Chemosensors, a general overview

1.1.1 Definition of a Chemosensor

A modern multidisciplinary research area grew in the last decades in the context of supramolecular chemistry, involving inorganic, organic, physical and analytical chemistry. In this new field, researchers work on the design and synthesis of molecular sensors able to selectively detect the presence of a species of interest in different matrices depending on the application. Usually, a chemosensor can be defined as a molecular device containing three units, each one having a specific function:[1] (i) a *receptor unit*, that is the fragment involved in the recognition process of the analyte; (ii) a *signalling unit*, that has the ability to produce a signal in response to the binding; (iii) a *spacer*, that connects receptor and signalling units, allowing for their electronic interaction and the regulation of their distance and spatial arrangement[2] (Figure 1). These systems can be considered as ligands obtained through organic synthesis, starting from singular molecular precursors. The synthetic receptors are designed in order to obtain a stable and selective interaction with a specific analyte. Depending on the class of substrates (cations, anions, neutral organic/inorganic/biological molecules), different parameters should be considered during the development of chemosensors. Among all analytes, anions and metal ions arose special interest because of their central role in human life and environment.[3] The interaction with the substrate must result in a change of a specific property. Depending on the application, different signalling transduction strategies are possible. The most common systems are photochemical sensors (UV-Visible and fluorescence spectroscopy) and electrochemical sensors[4] (voltammetry). Independently from the nature of the signal, one of the reasons for the great success of these molecular devices in biology and analytical chemistry is their possibility to work in the same concentration range of the chemical analytes involved in biological or environmental samples they are developed for. The topology of the ligands can be different depending on the choice

of the molecular precursor, ranging from open chain to macrocyclic variants. Typically, analogues can be obtained by changing only the recognition moiety, maintaining the same signalling unit. This can be helpful in trying to find out the best performing system for a certain analyte in specific experimental conditions.

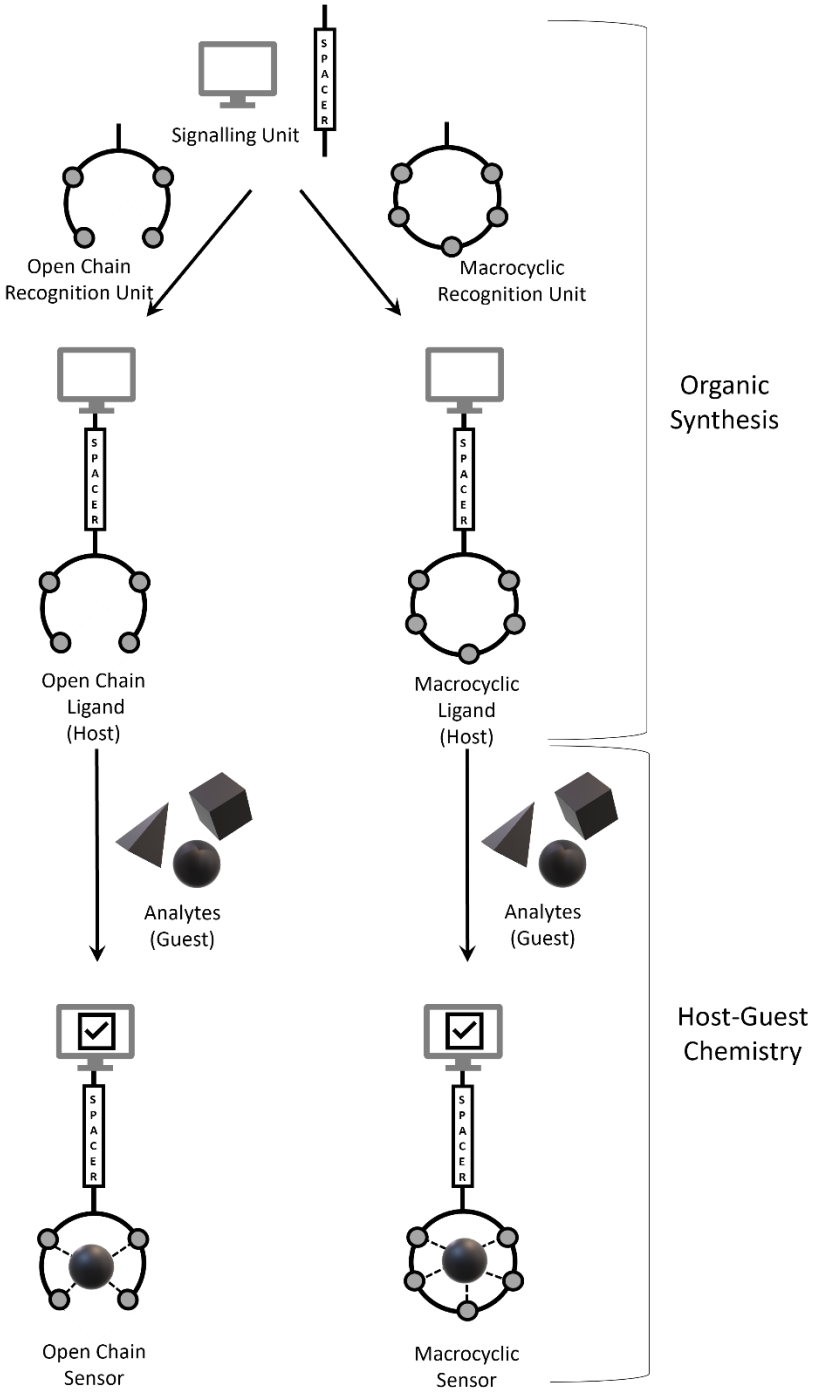

Figure 1. General schematic representation of a chemosensor.

1.1.2 Properties of Chemosensors

To obtain a good molecular device it is important to consider, ever since the design step, which are the requirements for a real application (Figure 2). To this end, the most commonly used methods for the development of a sensor are the *combinatorial processes* and *rational design*.[5] Typically, the real matrices are complex in terms of the number of different components. Examples of biological and environmental real samples are cells, blood and urine, tap/river/sea water and soil. For this reason, one of the most important property of a chemosensor is the selectivity towards a class of substrates, or even better, towards a specific species. Another fundamental characteristic is the response time: depending on the technique used, the detection of the signal emitted upon the binding of the guest must be fast enough to make the experiment more practical. In host-guest chemistry, this factor is influenced by the kinetic of the complex formation. The sensibility of the sensor is another important aspect that needs to be considered: the higher the sensibility, the lower is the detection limit, meaning that the system is able to detect the substrate even in those samples where it is present in trace amounts.[6] The interaction between substrate and receptor must therefore involve a change of a physico-chemical property, attesting the occurred recognition. The sensibility also depends on the technique employed.

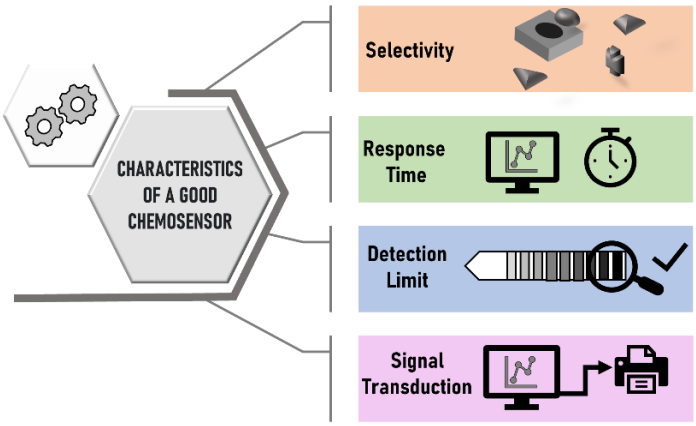

Figure 2. Characteristics of a good chemosensor.

1.1.3 Applications of Chemosensors

The applications of chemosensors can be endless. Suffice it to think how many times and in how many contexts humans wonder if something is contained in a sample. Depending on the user, the development of a specific probe able to recognise the analytes of interest can be based on different techniques, some of them being too difficult to be used without specific expertise, economic and instrumental resources. Nevertheless, the recognition can be appreciated also by people which had a fast and easy training, such as in the case of colorimetric sensors: everyone can indeed observe the colour change of a solution. Therefore there is a huge push for the development of sensors suitable to be used in everyday life. Some of them possess biological applications, such as the detection of specific analytes (organic or inorganic) in cells, blood, urine and saliva. Other sensors feature environmental applications, being able to signal the presence in solution of different kind of metals, metabolites and anions. Such systems also find utility in food and agricultural industry.

No matter what are the user, the scope, the technique and the analyte, the research is trying to assess systems more and more robust and efficient.

1.2 Host-Guest Chemistry

1.2.1 Definition of Host-Guest Chemistry

After the birth of Supramolecular Chemistry, defined by Jean-Marie Lehn (Nobel Prize in 1987) as "*the chemistry of molecular assemblies and of the intermolecular bond*", the most colloquial and popular definition of this branch of chemistry, extracted from Lehn's statement, is: "*the chemistry of the non-covalent bond*".[7] For this reason, it is easy to figure out that if the recognition process involves weak interactions this leads to the formation of supramolecular species, while if the interaction is mediated by covalent bonds (for example in the case of metal coordination bonds) a new molecular species is obtained (coordination product). In this regard, three historical concepts explain the Receptor-Substate chemistry, the most recent coming from Paul Ehrlich and dating from 1906. He introduced the concept of a receptor in biology: "*Corpora non agunt nisi fixata*" explaining that a molecule must bind to the receptor to perform its effect. In 1894, Emil Fisher gave a definition which still today remains the most famous one. He introduced the concept of "*lock and key*", in which the geometry and shape of the guest must be complementary to those of the host (Figure 3).

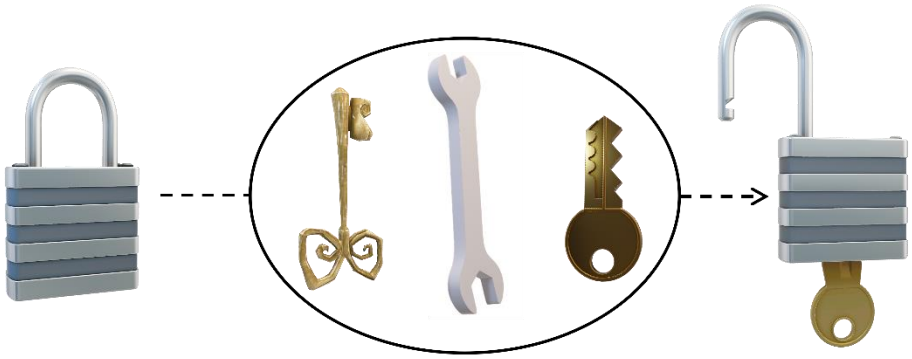

Figure 3. Schematic representation of the "Lock and Key theory".

This way of thinking led scientists to conceive the concept of *molecular recognition*, namely the ability of a host to discriminate a specific guest. The first definition in this field was given by Alfred Werner in 1893 with his *theory of* "*coordination chemistry*". He correctly deduced that a metal ion can be coordinated by ligands through "dative bonds".[8]

Therefore, since its earliest definitions, the Host-Guest chemistry mainly focuses on a molecule (host) that binds another molecule (guest) to produce a complex (if the binding involves a coordinate covalent bond) or a supramolecule (if the binding involves a non-covalent interaction). For this reason, in recent years scientists working in the field of supramolecular photochemistry gave a different definition of a supramolecular compound, considering it as a set of compounds that once assembled (through covalent or not-covalent interaction) feature new properties compared to those possessed by the singular components. With this in mind, it is possible to insert the research area of sensing in the context of the host-guest chemistry, in the middle between supramolecular and coordination chemistry (Figure 4).

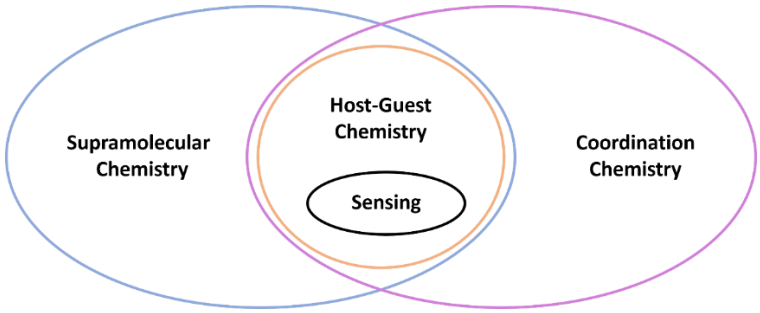

Figure 4. Research context of sensing area.

The host is considered as a molecule having a central cavity with convergent binding sites (with a concave binding site),[5] such as Lewis basic donor atoms or H-bond donors. The guest can be a species such as an inorganic anion, cation or organic molecule with divergent binding sites such as Lewis acid cations or H-bond acceptors.

As mentioned before, in host-guest chemistry both non-covalent and covalent interactions are involved: coordinative bond, ion-ion interaction, ion-dipole interaction, dipole-dipole interactions, hydrogen bonding, cation-π interaction, anion- π interaction, π- π interaction, Van der Waals forces, Crystal Close Packing, Closed Shell interaction. It is essential to consider all the interactions that can occur between the host and the guest as well as with their surrounding such as ion pairing, gas phase, solvation.[9] They are called weak interactions, but they are not weak at all. Just think at the synergy of all hydrogen bonds in the rearrangement of the two DNA strands (Figure 5), where the most important information about our existence on planet Earth are conserved. Their power lies in the fact that they are not irreversible bonds, allowing for processes such as replication, transcription and translation of the genetic material.[10]

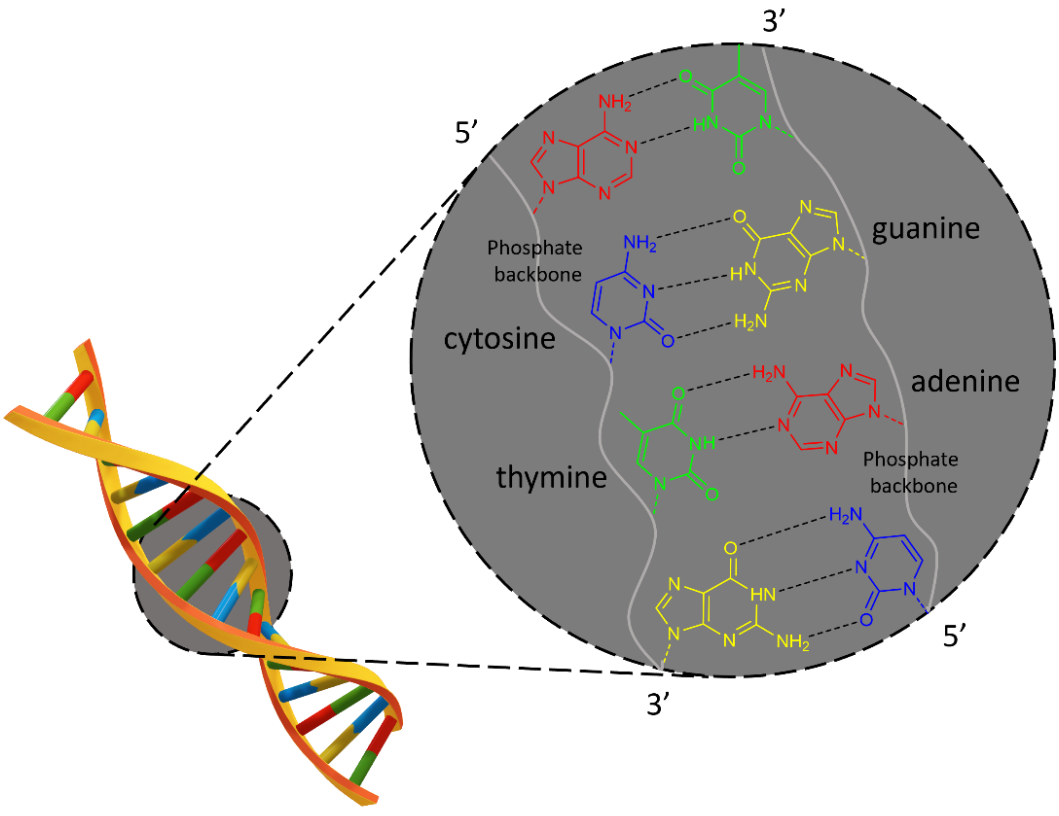

Figure 5. Hydrogen bonds involved in the DNA double helix.

Host molecules are distinguished in two different classes: Cavitands and Clathrands.[11] The former feature a permanent intramolecular cavity that endures both in the solid state and in solution. The latter possess instead an extramolecular cavity, that usually forms by the gap between different host units, and therefore exists only in the solid state. The aggregates, cavitands and clathrands, formed upon the interaction with the guest are called respectively *cavitates* and *clathrates*. A third concept is related to two subunits forming an aggregate through non-covalent interactions: it does not fit with the host-guest theory, instead it matches the self-assembly definition and exists both in solution and in the solid state[7] (Figure 6).

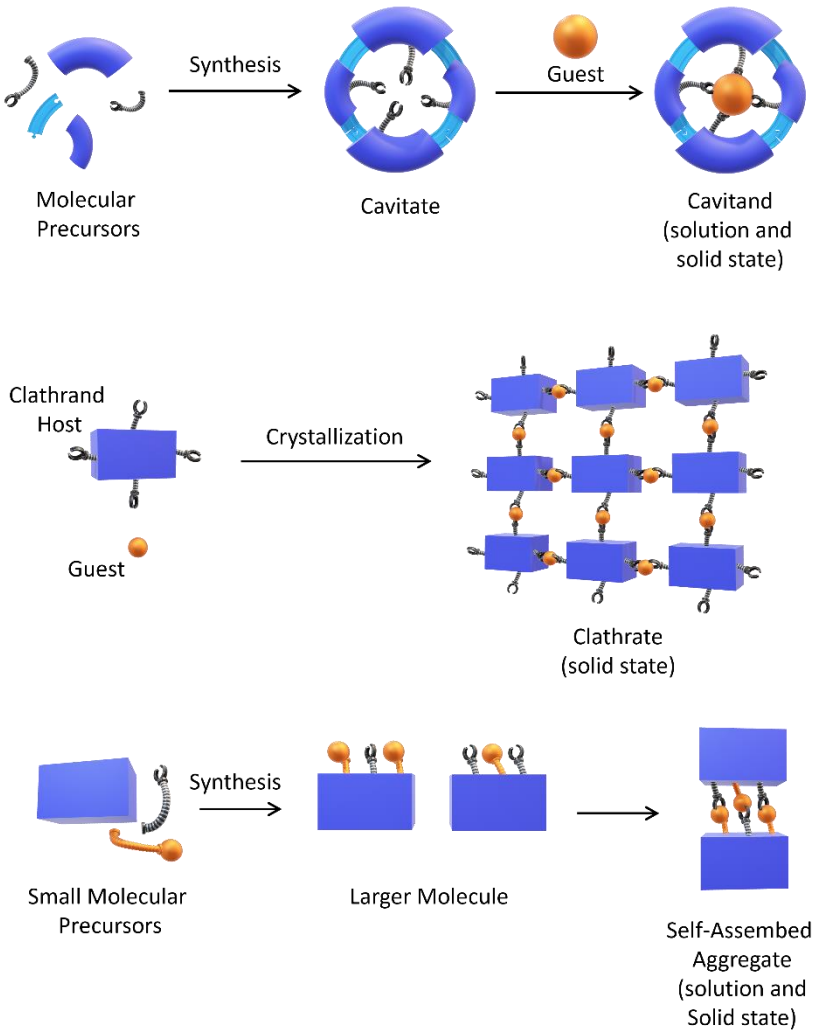

Figure 6. Classification of host-guest compounds.

1.2.2 Binding Constant: Definition, Use and Measurement

In terms of thermodynamics, the stability of a complex in a given solvent at a specific temperature is measured by the binding constant (*K*). This parameter is crucial in this context because it gives a value of the host-guest affinity in solution.[12] *K* can be described as the equilibrium constant for the following reaction:

$$M(H_2O)_n^{m+} + L \rightleftarrows ML^{m+} + nH_2O$$

$$K = \frac{[ML^{m+}]}{[M(H_2O)_n^{m+}][L]}$$

(M = metal; L = host ligand)

A high value of *K* means a high concentration of bound metal, which results in a more stable complex. If more than one metal ion is involved in the complexation, the *K* values are measured for both 1:1 and the 1:2 Ligand to Metal complexes.

$$M(H_2O)_n^{m+} + L \overset{K_1}{\rightleftarrows} ML^{m+} + nH_2O$$

$$M(H_2O)_n^{m+} + ML^{m+} \overset{K_2}{\rightleftarrows} M_2L^{(2m)+} + nH_2O$$

$$K_2 = \frac{[M_2L^{2m+}]}{[M(H_2O)_n^{m+}][ML^{m+}]}$$

In this case an overall binding constant, β, can be defined:

$$\beta = (K_1 \times K_2)$$

More often, the binding constant is reported in logarithmic units (log *K):*

$$log\ \beta = log\ (K_1 \times K_2) = log\ K_1 + log\ K_2$$

Binding constants can also be described in terms of the rate constants (*k)* of both complexation and decomplexation steps:

$$M(H_2O)_n^{m+} + L \underset{k_{-1}}{\overset{k_1}{\rightleftharpoons}} ML^{m+} + nH_2O$$

$$K = \frac{k_1}{k_{-1}}$$

K can be measured by using all the techniques that can give information about the concentration of the complex. In those cases in which the *K* value is too high, a competing host is added to reduce the apparent binding constant, then the true value can be extrapolated from the constant of the guest for the host with the lower affinity.[7] In the following, the different experimental techniques that are commonly used to determine binding constants are reported.[13]

Potentiometry. If the ligand is prone to be protonated, the protonation constant (pK_a) can be determined using pH electrodes as in a simple acid-base titration. The first step concerns the dissociation of the conjugated acid HL^+ (pK_a). Then, upon the addition of the metal ion the basicity of the ligand is perturbed by the competition between the metal and the proton for the lone pairs of the donor atoms, affecting the shape of the curve.

$$K_a = \frac{[H^+]\,[L]}{[HL^+]};\ HL^+ \underset{}{\overset{K_a}{\rightleftharpoons}} L \underset{}{\overset{K_1}{\rightleftharpoons}} ML^+ \underset{}{\overset{K_2}{\rightleftharpoons}} M_2L^+ \ldots$$

NMR (Nuclear Magnetic Resonance). If the exchange of bound and unbound guest is slow on the NMR time scale, *K* may be evaluated. Usually, in a NMR titration small amounts of guest are added to a known concentration of host dissolved in a deuterated solvent,

recording a NMR spectrum after each addition. As a result, from the changes in chemical shift (Δδ) two information can be obtained. The first one is the regioselectivity of guest binding, that can obtained by looking at the location of the nuclei that are more affected. The second one can be extrapolated from the shape of the curve in the plot of Δδ as a function of added guest concentration, obtaining information about *K*. The titration curves can be analysed by a computer program using the equation:

$$\delta_{Calc} = \sum_{m=1}^{m=i} \sum_{n=0}^{n=j} \frac{\delta_{mn} \beta_{mn} m [G]^m [H]^n}{[G]_{Total}}$$

(δ = chemical shift; mn = host-guest ratio; H = host; G = guest; β = stepwise *K*)

UV-Vis Spectroscopy. Spectrophotometric titrations are based on the monitoring of the absorption band at a specific wavelength, that is typical for that species. A plot of absorbance (Abs) against concentration of added guest can be built and a specific software can be used to extrapolate *K*. This technique offers the advantage to be more sensitive, allowing for a lower concentration of the species to be used. In UV-Vis is possible to see isosbestic points, allowing to better appreciate the conversion of the free ligand into complex (without intermediate species).

Fluorescence Spectroscopy. This technique is based on the proportionality between emission intensity and fluorophore concentration. In the case of a 1:1 complex with a:

$$K_{HG} = \frac{[HG]}{[H][G]}$$

the emission intensity F can be calculated as:

$$F = k_G [G] + k_{HG} [HG]$$

where k_G and k_{HG} represent proportionality constants for the guest and the 1:1 host-guest complex respectively. When in the solution there is only presence of the ligand, fluorescence intensity can be calculated as:

$$F_0 = k^0_G [G]_{Total}$$

where $[G]_{Total} = [G] + [HG]$. From the combination of these two formulas it is possible to obtain the following equation, that gives the possibility to determine *K*:

$$\frac{F}{F_0} = \frac{{k_G}/{k_G^0} + \left({k_{HG}}/{k_G^0}\right) K_{HG}[H]}{1 + K_{HG}[H]}$$

This equation can be simplified in those cases in which either the guest or the complex are not emissive, such as when the complexation turns on the system, or in the case of quenching by the host. This means that $k_G = k^0_G$ and $k_{HG} = 0$, therefore:

$$\frac{F_0}{F} = 1 + K_{HG}[H]$$

A plot of F_0/F vs [H] from the titration of the host with a guest can give a straight line of slope K_{HG}.

1.3 Polyamine-based Fluorescent Sensors for Metal Ions

1.3.1 General Aspect

Cation coordination chemistry has given birth to the area of selective binding of particular substrates by using "pre-programmed" receptors.[7] An incredible number of host ligands has been prepared in the last few decades, exhibiting useful properties.[14-22] The development of fluorescent chemical sensors able to selectively detect metal ions in solution has attracted the special interest of many academic research groups worldwide.[23-34] The reason behind this is the growing need for a system having a greater efficiency in both biological and environmental fields. A molecular device able to convert cations recognition in solution into a change of a specific chemico-physical property of the free ligand is an easy and fast method to reach out the desired goal. As mentioned above, different techniques are employed for metal ions monitoring, including electrochemical ones, such as potentiometry[35] and cyclic voltammetry[36], and optical ones, such as phosphorescence[37,38], colorimetric, UV-Visible[39,40] and fluorescence spectroscopies. However, in the last few decades many fluorescent chemosensors have been developed for the determination of metal ions in solution due to the fact that they represent a sensitive, simple and fast technique. The greatest goal which drives the design is selectivity, that can be intended towards either a class of elements or a specific one. The thermodynamic selectivity of the interaction is represented by the ratio between the receptor affinity (measured by binding constants) for a specific metal vs all the others. In molecular recognition the binding must be both strong and selective. It is very complicated to design a selective synthetic sensor because the selectivity is influenced by many factors, such as the size and the electronic complementarity between the guest and the host cavity, the electrostatic charge, the nature of the solvent, the preorganization of the host, the free energies of solvation, the donor groups orientation, enthalpic and entropic contributions.[41]

Fluorescent probes can be considered as switches able to signal the presence of the analyte through a spectral shift or a change in the emission intensity. For these systems the limit of detection depends on the affinity towards the ions, while the detectability of the emission sets out the response sensitivity. Since it is easier to recognize small variations in emission intensity than a shift of the spectra in terms of wavelength, the majority of sensors are intensity-based. Usually, to obtain these cationic probes researchers follow a rational design but they often rely on their intuition because the excited-states dynamics of fluorescent compounds generally are not as straightforward.[5] Despite this, research continues in this field to get new sensors that can be increasingly selective and performing. Depending on the application, the molecular device must be soluble in the solvent selected for the experiments and able to produce, in that medium, the change of the properties after the interaction with the analyte.

Considering application fields of chemosensors, ranging from biological to environmental ones, it is intuitive to think that the best solvent in which the system should be able to work is water. For this reason, during the design, researchers try to obtain ligands soluble in aqueous solution. Often, however, it is not possible to get the desired water solubility and some tricks can be used to overcome the problem. One of these is to dissolve the ligand in a solvent mixture with different water/organic solvent ratios. The second one is to dissolve the ligand into the minimum quantity of organic solvent, followed by the addition of an amount of this solution to the aqueous solution of the sample which has to be analysed. Sometimes the addition of an amount of organic solvent is necessary because the receptor is not able to work as a sensor in water due to the quenching effect of water on the fluorescence emission. In the following, a classification of the three groups of metals for which these systems are more commonly developed is reported, namely Alkali and Alkaline-Earth, Transition and Rare Earth (lanthanides) metals.

Alkali and Alkaline-Earth Metals. The great interest for the detection of alkali and alkaline-Earth Metals in solution comes from the fact that they play crucial roles at physiological level, such as the stabilization of DNA conformation, ion membrane transporters, enzyme cofactors, signal transduction.[42] Therefore, real-time determination of their content in physiological fluids, drinkable water and food is still important to monitor their level in human body, so as to avoid dysregulation in the physiological processes they are involved in. Sodium ion (Na^+) is crucial in the regulation of fluids balance and in the responses of nerves and muscles.[43] The largest amount of ingested sodium comes from food. Studies have shown that a lot of people consume excessive amounts of Na^+, much more than the physiological need,[44,45] which can cause high blood pressure and an increased risk of cardiovascular disease and stroke.[46]

Potassium ion (K^+) plays an essential role in many biological processes and is thus considered one of the most important cations in physiology. The intracellular concentration of K^+ is about 150 mM, thirty times higher than the extracellular level. Imbalances of the gradient concentration can be related to certain diseases including diabetes, heart disease, anorexia and Alzheimer's disease (AD).[47]

Magnesium ion (Mg^{2+}) is the most abundant divalent cation at the intracellular level and plays several key roles including DNA stabilization, enzyme cofactor, regulator of Ca^{2+} signalling, enzyme-driven metabolic reactions.[48] Beyond its involvement in diseases such as diabetes, osteoporosis and heart disease,[49,50] some studies confirmed its important activity as a modulator of the cell function. It was observed that the concentration of Mg^{2+} decrease leads to cell death, on one hand,[51,52] while, on the other hand, high levels can occur in some neuronal diseases such as AD and Hypertension.[53-55] The main part of chemosensors reported in the literature are not able to distinguish between Mg^{2+} and Ca^{2+}.[56-63] For this reason, the development of chemosensors that offer selectivity for Mg^{2+} *vs* Ca^{2+} represents an hard and open challenge.

Calcium ion (Ca^{2+}) is the most abundant cation in the human organism and acts on important functions in many biological phenomena. For such a reason, it is a very important challenge to be able to quantify the intracellular concentration of free Ca^{2+} due to the fact that imbalances of this element are correlated to many diseases such as neurodegeneration and heart disease. [64]

Transition Metals. For this group of elements, a large number of fluorescent probes was developed. The reason behind this is that in both environmental and biological systems some of them are essential while some others are detrimental when present in high concentration.[65]

Iron(III) ion (Fe^{3+}) is the most abundant essential transition metal in the human organism. For its fluorescence quenching nature, to obtain systems able to recognise this metal with a "Turn-on" response of the emission is a very challenging task. It acts as cofactor in proteins and as electron and oxygen carrier, meaning that its deficiency can lead to low oxygen delivery to cells causing anaemia, kidney damage and low blood pressure.[66] On the contrary, an excess of this cation in cells can lead to the formation of reactive oxygen species (ROS) causing damage of biological macromolecules. Several diseases are correlated to this aspect, such as Alzheimer's and Parkinson's disease.[67]

Zinc(II) ion (Zn^{2+}) is the second most abundant transition metal ion in the human body[68,69] and plays crucial activities in human body, such as catalysis, brain activity, cellular transport and gene transcription. High concentration of this metal is correlated to Alzheimer's disease while its deficiency can be correlated to particular conditions, such as growth retardation.[70,71]

A huge number of fluorescent sensors for Zn^{2+} is reported in the literature and still this is a current topic. To this purpose, several types of fluorophores have been used, such as quinoline, coumarin, rhodamine, fluorescein, Dipyrromethene boron Difluoride, 4-amino-1,8-naphthalimide, porphyrin and pyrene. [72-83] Especially for the biological application, Zn^{2+}

sensor have to be able to operate in water. Due to the vast number of these sensors, the current focus of the scientists is to develop systems with better analytical parameters, such as the limit of detection (LOD), the limit of linearity (LOL) and the limit of quantitation (LOQ). Another important skill to consider is the selectivity because some of them give the same response for Cd^{2+}.[84-87] For this reason, the development of fluorescent chemosensor selective for Zn^{2+} with only little interference from Cd^{2+} is still an open challenge.

Copper(II) ion (Cu^{2+}) is the third most abundant transition metal ion in the human organism and it plays several important roles in many physiological processes. In addition to its cofactor activity in different enzymes it is considered an environmental pollutant when present in high concentration, leading to several neurodegenerative, gastrointestinal, metabolic and inflammatory disorders.[88,89] Great efforts have been made in this context in trying to obtain fluorescent or colorimetric probes able to interact and signal the presence of Cu^{2+} in solution. This is still an open and hard challenge, due to the paramagnetic properties of this d^9 element that usually turns off the fluorescence emission.

Cadmium(II) ion (Cd^{2+}) is toxic due to its easy absorption and accumulation in various organisms, from plants to humans. Cd^{2+} is used in many human activities, in fact it is present in batteries, paints, plastics and fertilizers. The intake of high doses of this metal leads to its accumulation in spleen and kidney, causing several pathological conditions such as renal disfunction and different forms of cancer. Because of its dangerousness, Cd^{2+} pushes researchers to find increasingly effective methods for its detection.

Mercury(II) ion (Hg^{2+}) is one of the most toxic elements in nature because of its strong affinity for thiol groups in proteins, causing serious damage to the organism and, depending on the exposure, even death. In this case Nature does not help because some bacteria are able to convert both elemental and ionic form of Hg to methylmercury, allowing it to enter the food chain.[90] For this reason its detection in the environment is essential.

Rare Earth Metals. These particular metals are considered rare due to the fact that the separation processes of these elements as pure substances is considered an economical challenge because they are not frequently found in concentrated form.[91] Indeed, looking at the abundances of the most common metals compared to those of rare earth elements (REEs), except for Promethium that is a radioactive manmade element, it is clear that REEs are not rare at all. Today, lanthanides find lots of applications, especially in components of many technological devices and everyday electronics: Yttrium in ceramics, metal alloys, lasers, computer monitors (etc.); Lanthanum in electric car batteries, digital cameras (etc.); Cerium in catalysts, optical glasses (etc.); Neodymium in high-power magnets for laptops, lasers, communication devices (etc.); Samarium in high-temperature magnets, electric motors etc.; Europium in liquid crystal displays (LCDs), fluorescent lighting systems, glass additives (etc.); Gadolinium in NMR imaging contrast agents; Terbium in phosphors for lighting and displays; Dysprosium and Holmium in high power magnets and lasers; Ytterbium in fiber-optic technology, solar panels, alloys (etc.); Lutetium in X-ray phosphors.[92,93] For all these reasons, an incredible increase of the demand for REEs together with their recovery and reuse have generated a strong interest of researchers working in several fields.

REEs are stable in aqueous solution mainly in their trivalent state, however Cerium can be also found as a tetra-positive cation, while Europium, Samarium and Ytterbium can be found as divalent ions. REEs have very similar chemical properties, there is only a small variation along the series attributable to the different ionic radii and atomic numbers that are inversely correlated. Many studies on REEs are ongoing, especially related to their complexation equilibria in aqueous solution, that represents an emerging, important and challenging field in modern inorganic chemistry.[92]

The search for ligands suitable to achieve selective complexation of trivalent REEs metal ions represents a challenging task, considering that the coordination properties of these ions are complicated by not well defined stereo-chemical requirements and uncertain coordination

numbers, especially in aqueous solution. Also for these metals, the need for a fast and easy response to the presence of REEs in a sample has become of primary interest. Fluorescent and electrochemical chemosensors represent the favourite choice to obtain such a response, indeed they are characterized by a high efficiency and high sensitivity. There are only few examples of selective chemosensors for RE ions in the literature, and for this reason and for the aspects already mentioned above, the development of these systems represents one of the most innovative and hard challenge for scientists working in this field.[94-100]

1.3.2 Polyamine Receptor Units

Polyamine binding units have been attracting great interest in the last decades in the development of molecular sensors for metal cations. The reasons behind this are their water solubility and ability to coordinate metal ions in solution. Another important aspect is their easy functionalization,[101-102] thus a large number of analogues can be obtained, which help finding the best performing system for a specific cation in specific experimental conditions. Using different receptor units it is possible to obtain ligands with different topologies, open-chain or macrocyclic molecules.

Depending on the desired topology, several synthetic strategies can be used. The most common reaction retrieved in the literature is the nucleophilic substitution between an amine group and an alkyl halide. In this context, the protection and deprotection of the amine functional groups play an important role. Indeed, the presence of more amine groups in the same chain can lead to poly-substitution reactions and this can be overcome using previously protected receptor units.

Moreover, a polymerization subproduct can be obtained when both fluorophore and polyamine chains contain two electrophilic and two nucleophilic groups, respectively. Working in high dilution conditions, together with the slow addition of the fluorophore to the reaction mixture (Scheme 2), can guide the reaction in the direction of the 1:1 product, avoiding the formation of the 2:2 and other subproducts .

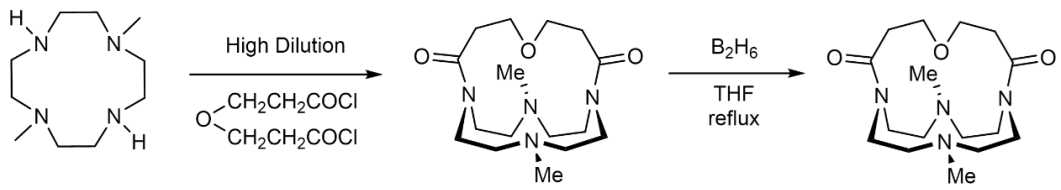

Scheme 2. Example of a cyclization reaction performed in high dilution.

Among other synthetic approaches,[103-107] one of the most popular involves a metal ion as a templating agent (Scheme 3).

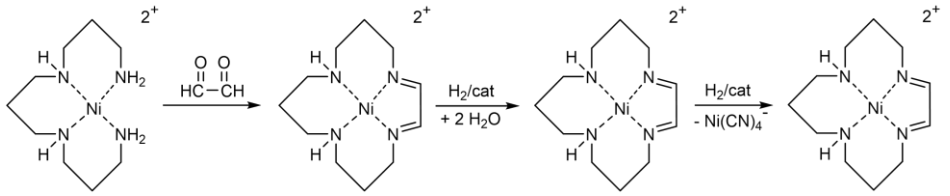

Scheme 3. Example of a cyclization reaction performed using Ni(II) as metal templating agent.

In this kind of synthesis, the metal ion plays a fundamental role, acting through two different mechanisms that can work singularly or contemporarily. The first mechanism is defined as *thermodynamic templating effect*, in which the ion is strongly coordinated to the ligand, thus the equilibrium is shifted towards the macrocyclic species. In the second mechanism, called *kinetic templating effect,* the metal ion promotes the formation of the cyclic compound by driving the steric requirement of the reaction. In terms of coordination there must be a good compromise between stiffness and flexibility of the molecular structure to obtain a complex with significant selectivity and stability.[108,109] A high flexibility allows the ligand to adapt its conformation to the stereochemical requests of the metal ion giving the complex a high stability; on the other hand, however, it reduces the selectivity of the ligand. The stiffness is directly correlated to the preorganization. During the formation of the complex, the ligand needs to rearrange to meet the metal ion steric requests. If the ligand already possesses a preorganized structure allowing for the interaction with the metal ion, high stability and good selectivity are achieved. Looking at the host and its affinity for the receptor, selectivity can be defined, in thermodynamic terms, as the ratio of the binding constants for one guest over another:[110]

$$Selectivity = \frac{K_{GUEST1}}{K_{GUEST2}}$$

In kinetic terms, selectivity relates instead to the rate of transformation of the competing substrate: the system is said to be selective for the fastest transformed guest, rather than for the strongest bound guest. Other important aspects to consider are guest selectivity and inter-guest discrimination. While thermodynamic selectivity is referred to binding constants, the inter-guest discrimination is referred to other observable results of specific host-guest interactions. Fluorescent sensors are a good example for this discrimination, because the strongest interacting guest with the host is not necessarily the receptor that gives the largest change in fluorescent emission intensity or in colour change, suggesting that the change in a specific physical property may not be directly proportional to the binding affinity. In the construction of supramolecular compounds, the involved interactions are weak if considered singularly, but they can be significantly stronger if considered as the result of the sum of all individual interactions. The Chelate effect is well known in coordination chemistry and it is based on the fact that metal complexes of bi-dentate ligands are significantly stronger than their mono-dentate analogues (Scheme 4). In the example below:

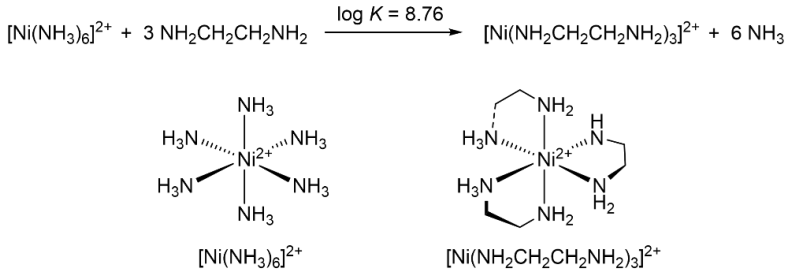

Scheme 4. Scheme of the replacement of ammonia with 1,2-diaminoethane.

the equilibrium constant value (log K = 8.76) for the replacement of ammonia with 1,2-diaminoethane indicates that the chelate complex is 10^8 times more stable. The particular stability of chelate complexes in solution can be rationalised on both thermodynamic and kinetic bases. From a thermodynamic standpoint, the reaction between a metal and a chelator produces an increase of the number of free particles (in the example, four in the reagents and seven in the products), and therefore leads to a favourable entropic

contribution in terms of total free energy of the reaction ($\Delta G^0 = \Delta H^0 - T\Delta S^0$). This contribution is also reinforced by a statistical factor, because to obtain the dissociation of the complex both bonds of the metal-donating atoms need to break simultaneously. From a kinetic standpoint, the reaction rate of the bond formation between the metal ion and either a mono-dentate ligand (L) or the first donating atom of a chelator ligand (L-L) is probably similar. However, the second bond with L-L occurs faster because its *effective concentration* is higher than that of a second molecule of mono-dentate ligand (L). The desolvation of the metal ion and the ligand usually takes place during the formation of a coordination complex, therefore if the chelator ligand shows a lower degree of solvation with respect to the mono-dentate ligand, the complexation enthalpy is more favourable, meaning a smaller energy demand for the desolvation process. On the other hand, fewer solvent molecules released during the complexation process represents an unfavourable entropic contribution. This means that both contributions compensate with each other and free energy variations are hardly affected by solvation. In the absence of a metal ion, the molecular structure of the guest is arranged in a suitable conformation for the coordination. This state corresponds to a minimum of conformational energy. The coordination of a metal cation, according to its size, can alter the positions of donating atoms causing an increase of the conformational energy of the ligand. The size of the coordinating cavity is a crucial structural parameter to determine the properties of the metal complex and is directly correlated to the number of atoms that make up the macrocycle cavity. A study conducted through molecular mechanics shows a regular increment of 0.10-0.15 Å of the cavity medium radius for every carbon atom.[111] The same study also evidences that small differences in the size (0-05 Å) are predictable between constitutional isotopomers of the same ligand. As mentioned before, the coordination usually entails an increase of the conformational energy of the ligand. This effect is due to the internal angular repulsion of the chelating ring and/or to the internal steric repulsion in the aliphatic chain that binds to each other donating atoms.

1.3.3 Fluorescence Mechanisms

As mentioned before, a fluorescent sensor for a metal ion must signal its presence by changing fluorescence properties, such as the emission intensity, the wavelength or the appearance of a new fluorescence bands. In general, the coordination of a metal ion can lead to two types of response, opposed to each other, namely an enhancement of the fluorescence emission, called Chelation Enhancement Fluorescence effect (CHEF) or a quenching of the fluorescence emission, called Chelation Enhancement Quenching effect (CHEQ). Both effects can cause either a blue or a red shift of the emission band. Hereafter, a list of the mechanisms responsible for the fluorescence response is reported.[112]

Paramagnetic fluorescence quenching. In a variety of metal complexes, the intersystem crossing (*isc*), that usually is a forbidden transition, becomes faster because of the influence of a paramagnetic metal ion located close to the fluorophore. The Paramagnetic Effect is the main cause of the fluorescence quenching by the d^9 Cu(II) ion. Metal complexes containing this metal ion undergo isc by excitation, from S1 to T1 state of the fluorophore that is deactivated by bimolecular non-radiative processes (Figure 7). Sensors for paramagnetic ions (Cu(II), Cr(III), Fe(III), Co(II)) are mainly based on the quenching of the emission.

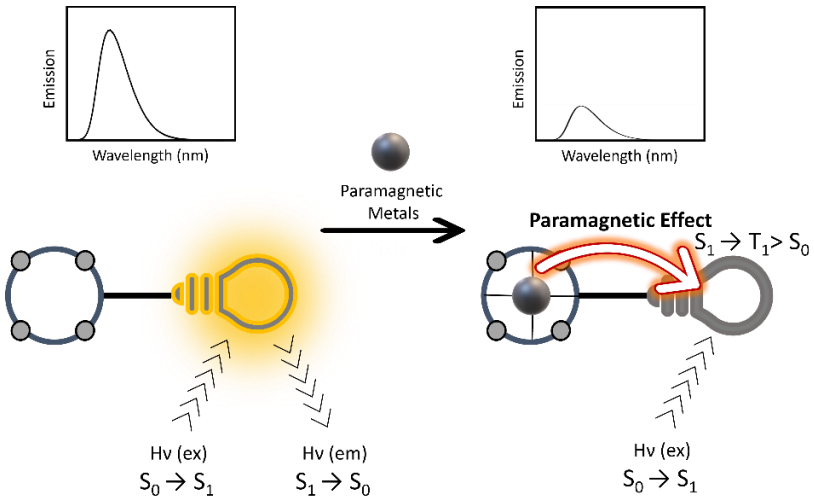

Figure 7. Paramagnetic fluorescence quenching.

Photoinduced Electron Transfer (PET). PET effect is a deactivation process caused by an internal red-ox reaction between a species able to donate or accept an electron and the excited state of the fluorophore. In the excited and ground state the properties of the species are different: as a result of its higher energy content, the excited state features both reducing and oxidant powers stronger than its corresponding ground state. Usually, in fluorescent probes for metal ions the PET effect occurs from a lone pair of a donating atom of the receptor moiety (e.g. P. O. N. S) to the HOMO of the excited state of the fluorophore (Figure 8). Once the metal ion is coordinated, the lone pair is involved in the interaction and this prevents PET causing the switching-ON of the emission. This effect is highly dependent on the solvent polarity which influences the oxidation potential of lone pairs of the coordinating atoms.[113] The more the polarity the easier the PET effect, thus the quenching effect is more effective in high polar media. Fluorescent sensors that work according to this mechanism do not cause a shift in the emission band upon the ion complexation.

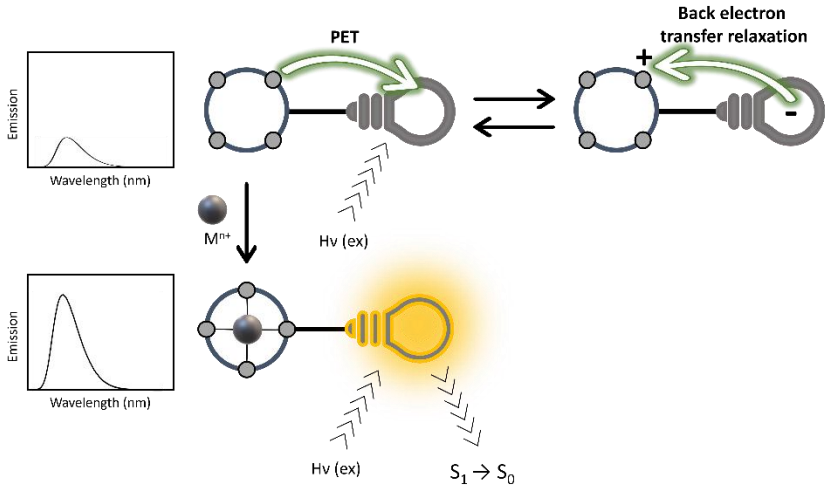

Figure 8. Photoinduced electron transfer (PET).

Photoinduced Charge Transfer (PCT). In this mechanism, a transfer of an electron between the electron donor and the acceptor group is at the base of the fluorescence response,

promoting a change in the emission intensity. PCT sensors involve a partial charge transfer within a fully conjugated π system. In these probes the receptor unit and the fluorophore moiety are integrated in the same structure, to the contrary of PET sensors in which the two units are separated by a linker. In this case, the complexation of the metal ion leads to an alteration of electron energy levels causing both a variation in the emission wavelength and a fluorescence turn-ON or OFF, depending on the fluorophore structure, the analyte and the complexation mode (Figure 9).

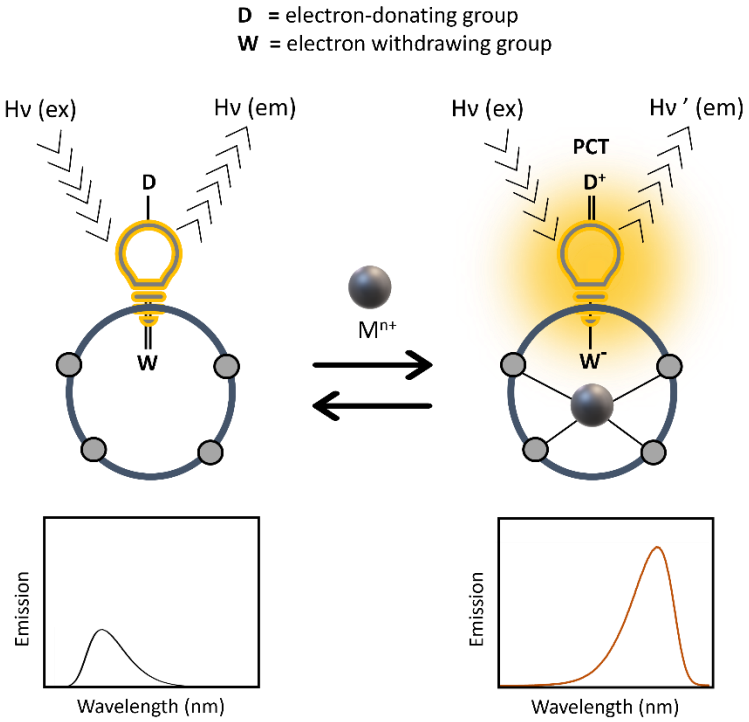

Figure 9. Photoinduced charge transfer (PCT).

Fluorescence Resonance Energy Transfer (FRET). In this mechanism there is an interaction between the electronic excited state of a fluorophore and another fluorescent moiety. During the excitation, energy is transferred from the donor to the acceptor group, without any emission of photons. This means that if FRET occurs when exciting one of the two fluorescent moieties, the emission of the other one is detected. Some conditions are

essential: the interaction is distance-dependent, thus the donor and the acceptor groups must be sufficiently close to each other (10-100 Å); the absorbance of the acceptor must overlap the emission of the donor; donor and acceptor transition dipoles orientation must be approximately parallel. FRET depends on the inverse of the sixth power of the distance between the fluorophores. The interaction with a metal forces the two units (A and B) to stay closer or farther away from each other. In the former case, the distance between the units prevents FRET, thus upon excitation of fluorophore A, the emission of fluorophore A can be detected (Figure 10). After the coordination of the metal ion, fluorophore units are closer switching on FRET, which is why exciting fluorophore A the emission of B is detected.

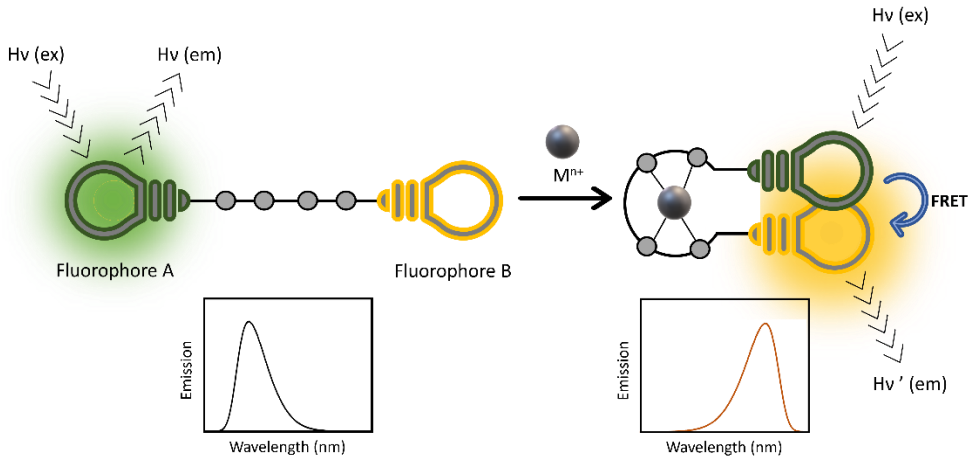

Figure 10. Fluorescent resonance energy transfer (FRET).

Excimer or exciplex formation. If the interaction between the ground and the excited state component in a metal probe is strong enough, new luminescent species called excimers or exciplexes form. The formation of these new species is a reversible process. The monomer emission is at a higher energy compared with excimer or exciplex emissions, that usually show a weak and broad band. The interaction with the metal ion may either favour or prevent the excimer or exciplex formation, thus influencing the emission (Figure 11). Not only, a quantitative measure of the metal ion content can be obtained from the ratio between the

emission intensities of monomer and excimer. These sensors are indeed defined as "ratiometric".[114]

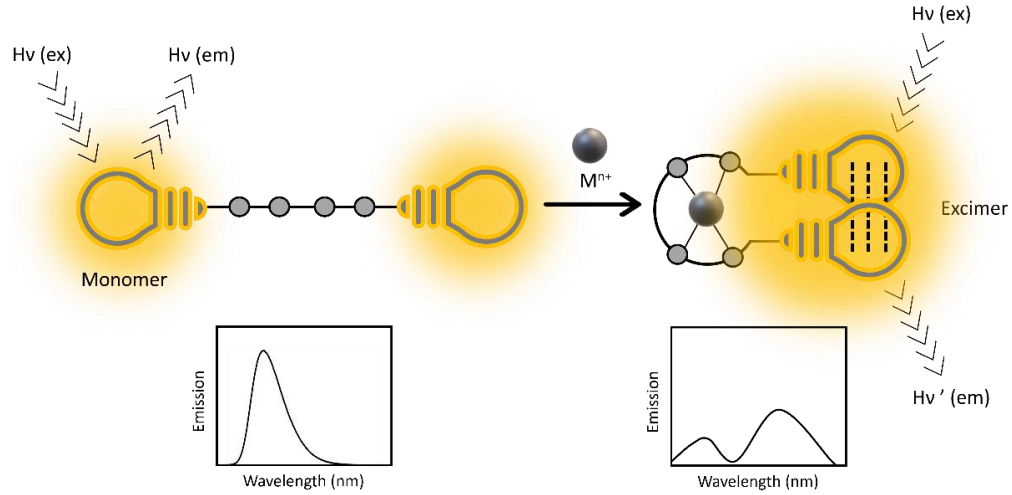

Figure 11. Excimer or exciplex formation.

Irreversible reaction-based sensors: ***Chemodosimeters***. These particular sensors usually work in an OFF-ON mode, and they are mainly used for those metals that normally quench the emission (e.g. Cu(II)). The metal ion converts the non-emissive starting ligand, through an irreversible chemical reaction, into an emissive system (Figure 12). They often require some specific conditions such as high temperature and organic solvents.

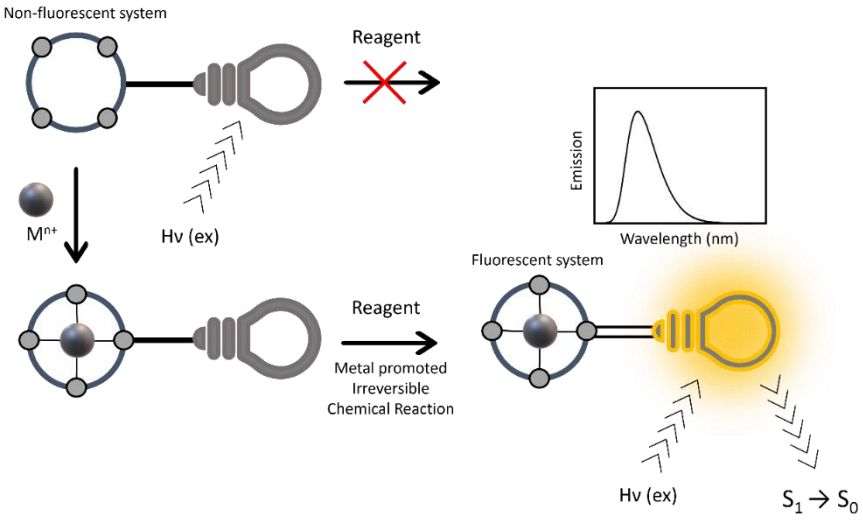

Figure 12. Irreversible reaction-based sensors.

Excited-State Intramolecular Proton Transfer (ESIPT). ESIPT is a four-level photochemistry process that involves an enol (E) to keto (K) transformation in the excited state, through an intramolecular hydrogen bond, during which a proton is transferred from a hydroxyl group to an electronegative atom, giving rise to a high stokes shift.[115] For this reason, the presence of an unsaturated H-bond acceptor, such as C=N– or C=O, and a H-bond donor like –NH– or –OH is essential. In the ground-state these systems are stable in their E forms. Upon the excitation (E*), there is a redistribution of the electronic density causing an increase of both the acidity of the hydrogen bond donor and the basicity of the acceptor, giving rise to the K* form, that is the most stable form in the excited state. If the excited keto-form radiatively decays, a reverse proton transfer (RPT) takes place to give back the original E form, and this can be detected through a change in fluorescence emission along with a marked red-shift of the wavelength. This is attributed to the fact that in the ground-state the enol form is more stable than keto form, while in the excited state the stability is inverted, resulting in a higher absorption energy gap between E and E* than between K* and K. ESIPT fluorophores can be often used as ratiometric sensors because of the dual-emission spectra arising from the emission bands of the enol (E*) and keto (K*) excited states (Figure 13).

Figure 13. ESIPT-based sensor.

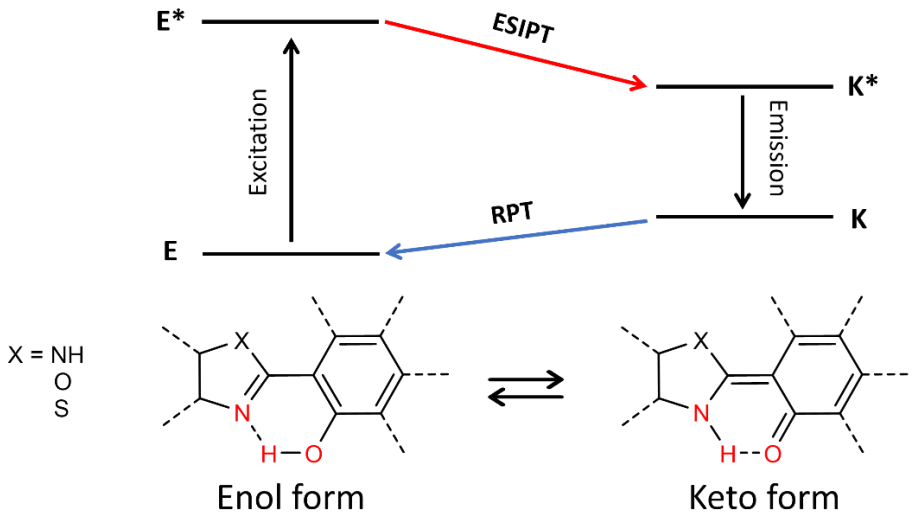

1.4 Research Objectives

The objectives of this research are the design, synthesis and characterization of fluorescent chemosensors for the selective recognition of metal cations in solution. A fluorescent chemosensor contains a polyamine unit acting as receptor and a fluorophore moiety acting as signalling unit. The molecular topology of both receptor and fluorophore is crucial for the selectivity towards a specific substrate and drives the signal transduction mechanism. The principal aim is to obtain different systems able to coordinate hard metal ions such as Alkali, Alkaline Earth and Rare Earth metal ions as well as Transition metal ions. For this purpose a series of ligands was synthesized and studied using UV-Vis, Fluorescence, NMR, and X-ray diffraction techniques. The more promising systems will be in deep evaluated in order to be used as chemosensors in simulated and real samples of biological and environmental interest and public health concerns.

Chapter 2 - Discussion

2.1 Results and Discussion of [Pd(H_{-2}L1)]

The content of this chapter has been published in: D.Paderni, L.Giorgi, E.Macedi, M.Formica, P.Paoli, P.Rossi, V.Fusi. *Dalton Trans.*, 2021, 50, 15433 DOI: 10.1039/D1DT01753E.

This project starts from a search previously carried out by the Supramolecular Chemistry Group of the University of Urbino. This study evidenced that the metal-receptor [Cu(H_{-2}**L**)] (Figure 14), a bis-maltol polyamine coordinated with Cu(II) in 1:1 ratio is able to bind hard cations such as lanthanide ions in a 2:1 [Cu(H_{-2}**L**)] : RE(III) ions ratio in aqueous solution.[116, 117] Given the limited availability in the literature of selective fluorescent sensors for RE(III) ions, this was an excellent starting point for the design of a system able to work as fluorescent chemosensor for lanthanide ions.

The binding of **L** with Cu(II) generates the neutral [Cu(H_{-2}**L**)(H_2O)] complex, in which the Cu(II) ion is penta-coordinated by the N_2O_2 donor atoms set of the deprotonated form of **L** and a water molecule, forcing the four oxygen atoms of **L** to converge, thus generating an electron-rich pocket suitable to host hard cations such as RE(III) ions. Two [Cu(H_{-2}**L**)(H_2O)] units stabilize one RE(III) ion, giving rise to the $\{Gd[Cu(H_{-2}\mathbf{L})(H_2O)]_2(H_2O)\}^{3+}$ trinuclear species in water, whose structure is resumed in Figure 14. In this complex the Gd(III) ion is stabilized by nine oxygen atoms, eight deriving from the two preorganized [Cu(H_{-2}**L**)(H_2O)] units and one from a water molecule.

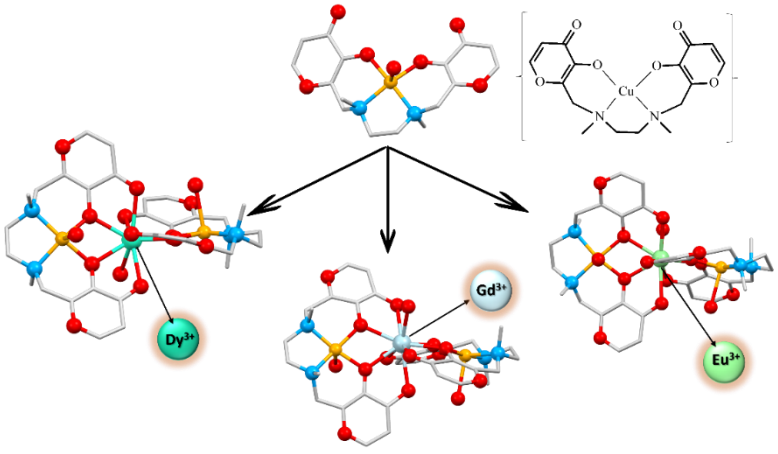

Figure 14. Metal Receptor [Cu(H_{-2}**L**)] based on maltol units and its trinuclear species.

In order to add fluorescent properties to this system while maintaining the same molecular coordination framework of **L**, the new ligand **L1** has been synthesized (Scheme 5). The synthetic strategy replaced the two maltol units of **L** by two fluorescent 3-hydroxy-4-chromone fragments, both linked to the same polyamine unit. The synthetic pathway (see Experimental Section, chapter 3.2.1) is simple, reliable and inexpensive: no protective groups are needed, the purification processes in every steps only consisted in precipitation and crystallization procedures, not involving time- and solvent-consuming flash column chromatography. Moreover, all carbon atoms contained in the reagents are found in the final product, in agreement with the "carbon economy" paradigm,[118] thus contributing to the development of green ecological processes based on low energy consumption and low pollution. As observed in the case of **L**, to force the four chromone oxygen atoms to converge and form a negatively charged pocket, an appropriate transition metal ion must be employed to preorganize **L1**. The choice of the preorganizing metal ions must not affect the fluorescence, namely the metal ion should not quench the emission of the system. For its known paramagnetic properties, Cu(II) does not match this purpose. Thus, in order to increase the conjugation of the system trying to improve the fluorescence properties, other metal ions with square planar coordination requirements were tested, such as Pd(II), Pt(II). Among these metal ions, Pd(II) was found to be the most promising in terms of stability and photochemical response of the complex.

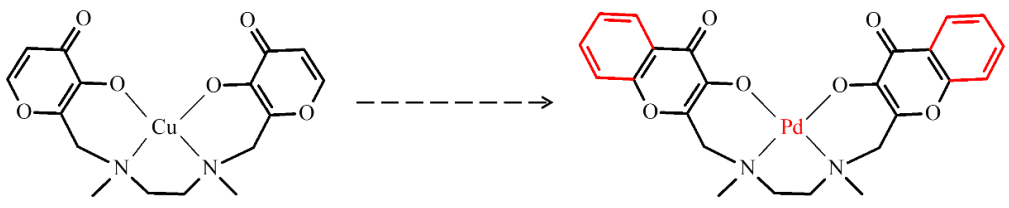

[Cu(H$_{-2}$L)] **[Pd(H$_{-2}$L1)]**

Scheme 5. Structural modifications to obtain [Pd(H$_{-2}$**L1**)].

2.1.1 Solid state studies

In the [Pd(H_{-2}**L1**)] complex, the Pd(II) cation is tetracoordinated by two nitrogen atoms of the ethylendiamine bridge and by one oxygen atom of each 3-hydroxy-4-chromone moiety of the (H_{-2}**L1**)$^{2-}$ species (Figure 15).

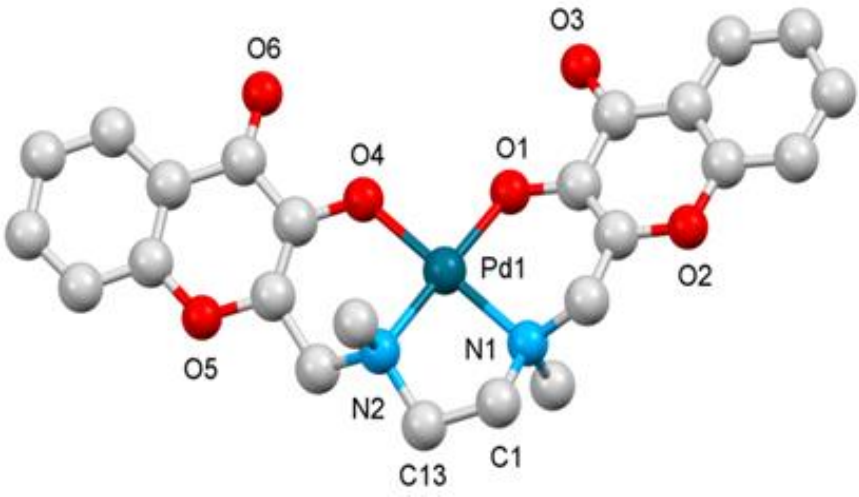

Figure 15. Ball and stick view of [Pd(H_{-2}**L1**)]. For the sake of clarity hydrogen atoms were not reported and labels were added only for non-carbon atoms and for carbon atoms C1 and C13, that are cited in Table x1

The resulting coordination geometry is square planar with distances and angles (Table 1) in agreement with those found for similar complexes in the Cambridge Structural Database (CSD v. 5.41, November 2019 update 3 August 2020).[119] The conformation taken by the ligand clearly resembles the one adopted by the related ligand (H_{-2}**L**)$^{2-}$ in similar complexes.[117,120]

An electron-rich area forms upon the coordination of the Pd1 ion, with the oxygen atoms O1, O3, O4 and O6 defining an approximated isosceles trapezoid, whose dimensions are 2.777(6) and 6.018(6) Å (bases), 2.661(6) and 2.703(5) Å (legs) (Table 1).

This negatively charged pocket features the right dimensions and donor atoms position to allow the coordination of a second metal cation, as already observed in polynuclear complexes of similar ligands. [117,120]

Table 1. Selected bond distances (Å) and angles (°) for [Pd(H_{-2}**L1**)](H_2O)$_6$.

Distances	**(Å)**	**Angles**	**(°)**
Pd1-O1	2.006(4)	O1-Pd1-O4	87.4(2)
Pd1-O4	2.014(4)	O1-Pd1-N1	91.6(2)
Pd1-N1	2.038(5)	O1-Pd1-N2	179.0(2)
Pd1-N2	2.033(5)	O4-Pd1-N1	177.6(2)
O1···O4	2.777(6)	O4-Pd1-N2	93.6(2)
O1···O3	2.661(6)	N1-Pd1-N2	87.4(2)
O3···O6	6.018(6)		
O4···O6	2.703(5)	N1-C1-C13-N2	-53.8(7)
		A / B[1]	19.2(1)
		A / C	15.2(1)
		B / C	20.3(1)

[1]A = mean plane defined by: O1, O4, N1, N2; B = mean plane defined by the non-hydrogen atoms of the 3-hydroxy-4-chromone bearing the O1-O3 oxygen atoms; C = mean plane defined by the mean plane defined by non-hydrogen atoms of the 3-hydroxy-4-chromone bearing the O4-O6 oxygen atoms.

In the asymmetric unit of [Pd(H_{-2}**L1**)](H_2O)$_6$ one [Pd(H_{-2}**L1**)] complex and six crystallization water molecules are present.

Similarly to the complexes of the analogous ligand (H_{-2}**L**)$^{-2}$, N1, N2, O1 and O4 are quite coplanar (being the maximum deviation due to N2, 0.023(6) Å), with the Pd(II) cation lying on the mean plane defined by these four atoms.

The aromatic rings form an angle of 19.2(1) and 15.2(1)°, respectively, with the mean plane defined by the four coordinating atoms (Table 1), while the angle between them is 20.3(1)°. Finally, the two methyl groups point in opposite direction with respect to the coordinating plane (Figure 16).

A search performed in the CSD allowed us to retrieve 25 structures of metal complexes having the fragment reported in Scheme 1, none of these is a palladium complex and six containing the related ligand **L1**, [117,120] where the metal cation is coordinated by the four oxygen atoms of the two maltol moieties and is out of the mean planes defined by these donor atoms of

about 0.50 Å (range = 0.007 – 0.744 Å, mean value = 0.492 Å) while the angle O3-M-O6 (Scheme 6) is in the 142-170° range, with a mean value of 151°.

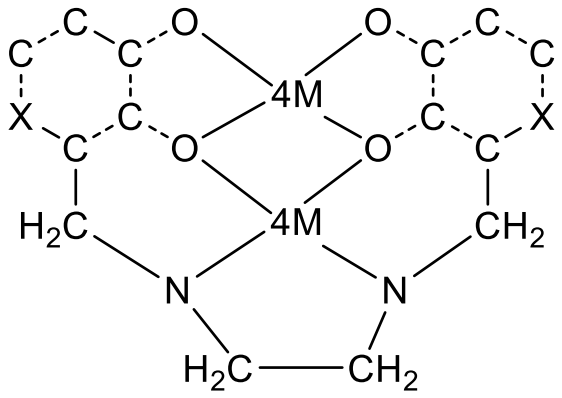

Scheme 6. Fragment searched in the CSD. X = any atom; 4M = any metal: dashed line = any bond type.

The trapezoidal area described by the four oxygen atoms of the two maltol rings has dimensions similar to those found in [Pd(H$_{-2}$**L1**)](H$_2$O)$_6$: 2.371-3.055 Å (mean value 2.515 Å) and 4.724-5.548 Å (mean value 5.013 Å) for the two bases, 2.547-2.662 Å (mean value: 2.609 Å) and 2.539-2.707 Å (mean value 2.606 Å) for the legs.

Interestingly, a water molecule is located within this area in compound [Pd(H$_{-2}$**L1**)](H$_2$O)$_6$ (Figure 16), interacting via hydrogen bonds with oxygen atoms of the two 3-hydroxy-4-chromone moieties (Table 2). The molecule lies in the mean plane defined by the four oxygen atoms O1, O3, O4 and O6 (deviation of O2w from the mean plane = 0.226(6) Å). Finally, the O3…O2w…O6 angle is 162.6(2)°.

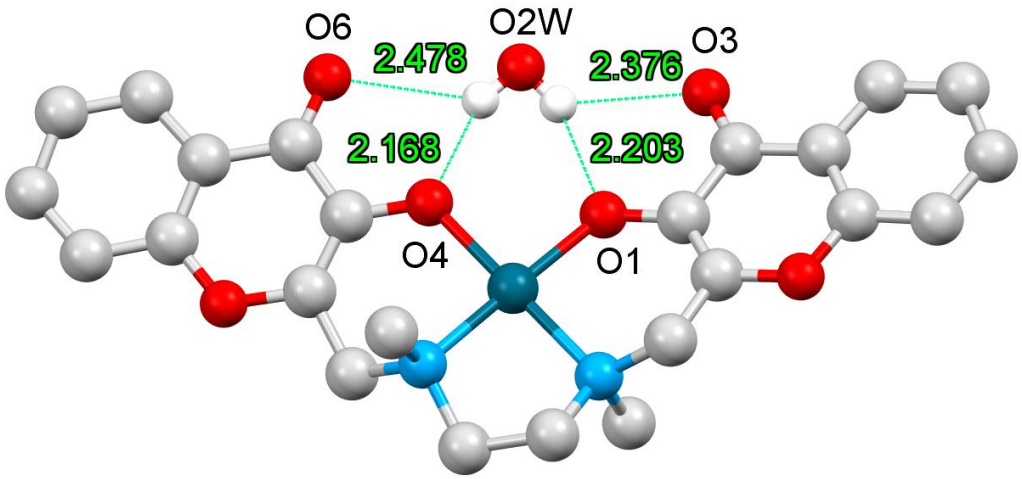

Figure 16. Ball and stick view of the water molecule (O2w) in the negative pocket of [Pd(H$_{-2}$**L1**)].

Table 2. Selected hydrogen bond distances (Å) and angles (°) for [Pd(H$_{-2}$**L1**)](H$_2$O)$_6$.

X-H···Y	X···Y (Å)	H···Y (Å)	X-H···Y (°)
O1w-H1w1···O4w	2.867(9)	2.040(6)	168(6)
O1w-H1w2···O1^1	2.854(8)	2.02(2)	170(2)
O2w-H2w1···O4	2.882(6)	2.17(5)	144(2)
O2w-H2w1···O6	3.104(6)	2.48(3)	132(2)
O2w-H2w2···O1	2.916(6)	2.20(4)	144(3)
O2w-H2w2···O3	2.985(6)	2.37(5)	131(3)
O3w-H3w2···O1w^2	2.780(8)	1.97(6)	161(6)
O3w-H3w1···O5w^3	2.992(7)	2.19(6)	160(5)
O4w-H4w2···O6w^4	2.856(7)	2.07(5)	154(5)
O4w-H4w1···O5w^5	2.839(9)	2.10(8)	146(7)
O5w-H5w2···O4w	3.081(8)	2.26(4)	164(3)
O5w-H5w1···O2w	2.771(8)	1.93(3)	171(2)
O6w-H6w2···O3w	2.828(9)	2.05(4)	154(4)
O6w-H6w1···O6^2	2.941(7)	2.22(6)	144(3)

^{1}= x,y+1,z; ^{2}= x-1/2,-y+3/2, z-1/2; ^{3}= x-1/2,-y+1/2, z-1/2; ^{4}= -x+1,-y+1,-z+1; ^{5}= -x+3/2, y+1/2,-z+3/2

Concerning the crystal packing, due to the presence of a π···π interaction (distance between the centroid of one 3-hydroxy-4-chromone moiety and the mean plane containing the other ring= 2.288(7) Å; angle between the line connecting the centroids of the two rings and the mean plane defined by one ring = 16.0(2)°) involving one 3-hydroxy-4-chromone moiety and a symmetry related unit (-x+1, -y+1, -z+1), a dimer forms (Figure 17).

Different dimers are connected via a net of hydrogen bonds that involves the six crystallization water molecules giving rise to a ribbon that propagates along the b axis direction. Such ribbons interact via weak hydrogen bonds.

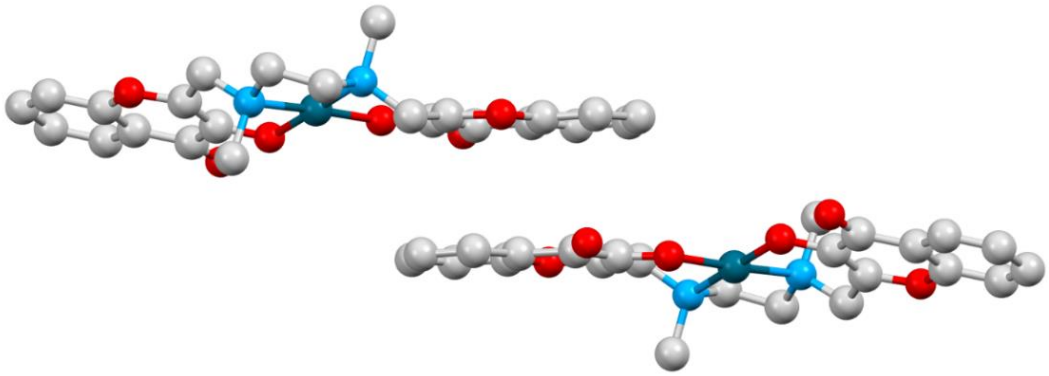

Figure 17. The [Pd(H$_{-2}$**L1**)] dimer.

Table 3. Crystallographic data and refinement parameters for [Pd(H$_{-2}$**L1**)](H$_2$O)$_6$.

	[Pd(H$_{-2}$**L1**)](H$_2$O)$_6$
Formula	$C_{24}H_{34}N_2O_{12}Pd$
M	648.93
T (K)	100
λ (Å)	1.54184
Crystal system, space group	Monoclinic, $P2_1/n$
Unit cell dimensions (Å, °)	a = 13.8990(5) b = 9.2755(5); β = 100.880(5) c = 20.2093(5)
V (Å^3)	2558.6(3)
Z, ρ (mg/cm3)	4, 1.685
μ (mm^{-1})	6.468
F(000)	1336
Crystal size	0.22 X 0.28 X 0.32
2θ range (°)	8.52 – 144.96
Reflns collected / unique (R_{int})	19062 / 5059 (0.1034)
Data / parameters	5059 /388
Final R indices [I > 2σ]	R1 = 0.0606, wR2 = 0.1317
R indices (all data)	R1 = 0.0926, wR2 = 0.1498
GoF	1.063

2.1.2 Acid-Base behaviour

pH-dependent UV-Vis absorption spectra of **L1** in aqueous solution were performed to understand its acid-base properties. In acidic media (pH=2) **L1** shows three main absorption bands at λ_{max} = 325, 282 and 235 nm (ε = 9800, 7700 and 26600 $dm^3\ mol^{-1}\ cm^{-1}$, respectively). By increasing the pH, the first band gradually decreases and a new band at 365 nm (ε = 7500 $dm^3\ mol^{-1}\ cm^{-1}$) appears, while the other two bands were red-shifted reaching λ_{max} = 295 and 240 nm (ε = 3800 and 17700 $dm^3\ mol^{-1}\ cm^{-1}$, respectively) at pH=12 (Figure 18). Three isosbestic points at 340, 270 and 245 nm are visible. The changes in the absorbance spectra are caused by the deprotonation of hydroxychromone moieties. By looking at the trend of the absorbance at 365 nm as a function of the pH values, two deprotonation steps at pH = 4.5 and pH = 9.5 can be observed (inset of Figure 18).

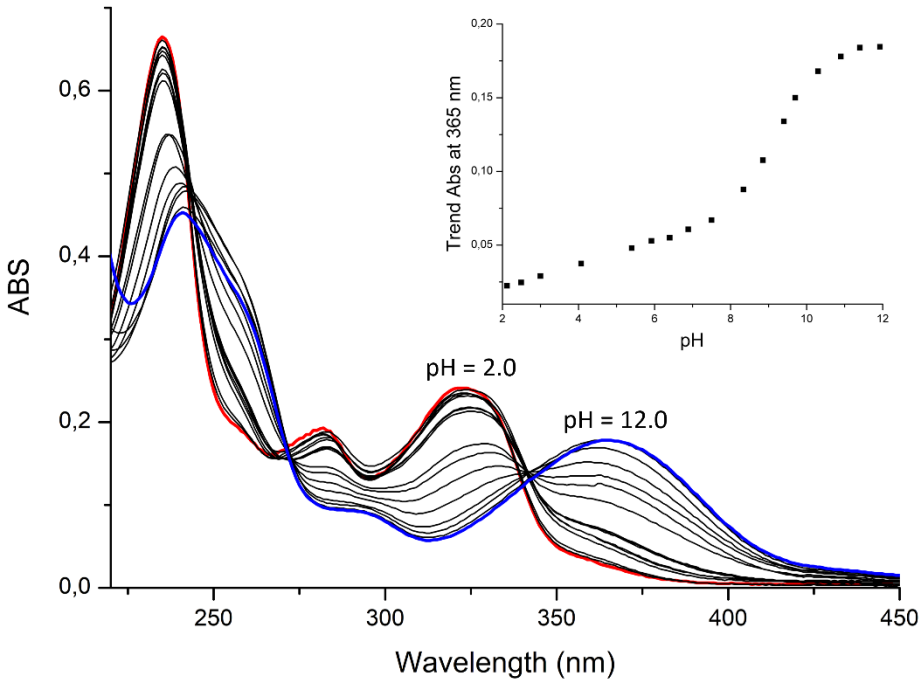

Figure 18. UV-Vis absorption spectra of **L1** registered in aqueous solution in the pH range 2 - 12. [**L1**] = $1 \cdot 10^{-5}$ mol dm^{-3}, pH was adjusted by adding HCl and NaOH aqueous solutions. Inset: trend of absorbance at 365 nm as a function of pH.

2.1.3 Coordination behaviour

In order to evaluate the interaction between **L1** and Pd(II) ion, pH-dependent UV-Vis absorption and emission studies were performed by either adding one equivalent of K_2PdCl_4 to an aqueous solution of the ligand or dissolving the preformed $[Pd(H_{-2}\mathbf{L1})](H_2O)_6$ complex in water in the 2-12 pH range (Figure 19).

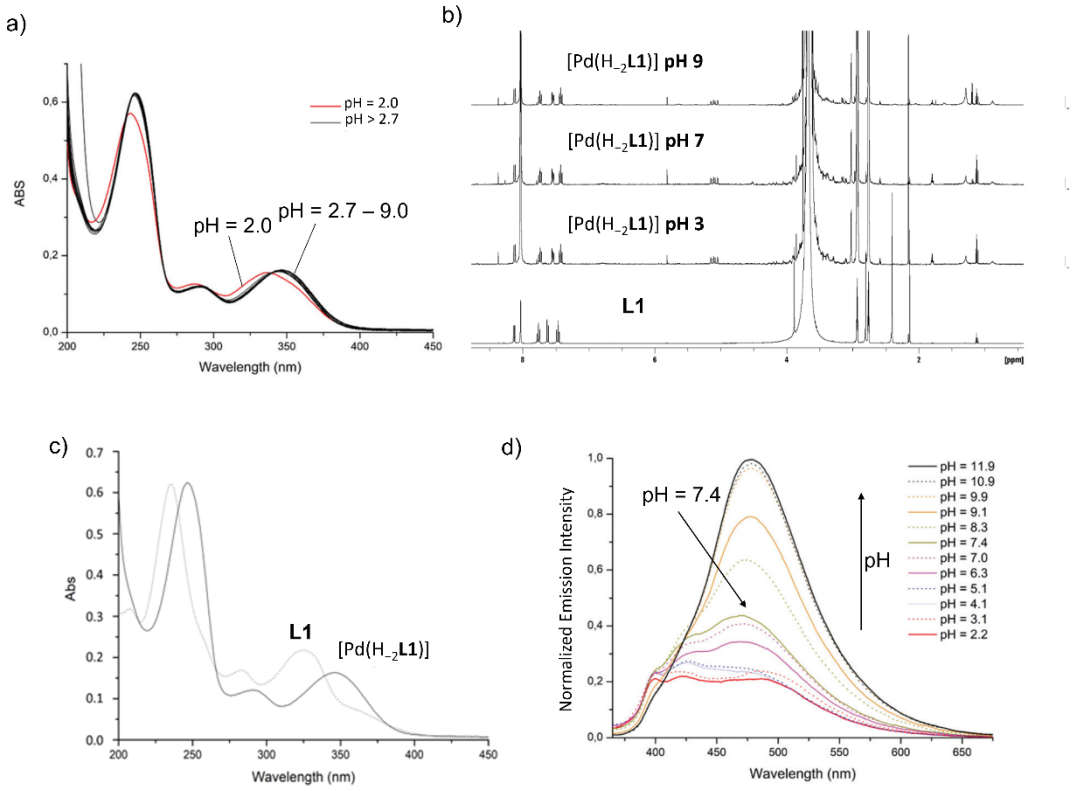

Figure 19. a) UV-Vis absorption and d) emission spectra of preformed $[Pd(H_{-2}\mathbf{L1})]$ in aqueous solution in the pH range 2 – 12. $[Pd(H_{-2}\mathbf{L1})] = 1{\cdot}10^{-5}$ mol dm^{-3}, pH was adjusted by adding HCl and NaOH aqueous solutions, $\lambda_{ex} = 350$ nm. b) ^{1}H-NMR spectra of ligand **L1** and $[Pd(H_{-2}\mathbf{L1})]$ complex in DMF-*d7* prepared at pH = 3, 7 and 9: the complex was obtained as crystals by adding one equiv. of K_2PdCl_4 to a hydroalcoholic solution of **L1** and setting the pH value at 3, 7 and 9. The three solid complexes were filtered, washed, dried and dissolved in DMF-*d7* to acquire the spectra. c) UV-Vis absorption spectra of **L1** (dashed line) and $[Pd(H_{-2}\mathbf{L1})]$ (solid line) in aqueous solution at pH = 7. $[\mathbf{L1}] = 1{\cdot}10^{-5}$ mol dm^{-3}, $[[Pd(H_{-2}\mathbf{L1})]] = 1{\cdot}10^{-5}$ mol dm^{-3}, aqueous TRIS 0.01 mol dm^{-3}.

Both approaches gave the same result, the absorption spectrum shows a band at 350 nm that remains unchanged in the 2.7 – 9.0 pH range (Figure 19a), suggesting that the complex is stable almost in this pH range. This is also confirmed by ^{1}H NMR measurements (Figure 19b).

For comparison, in Figure 19c the absorption spectra of the free ligand and the preformed Pd(II) complex at pH=7 are reported.

The complex is more fluorescent than the free ligand, nevertheless it is still weakly emissive in aqueous solution (ϕ_{em} = 0.005 at pH = 7). Figure 19d shows that the emission wavelength of the system is pH-dependent, moving from λem = 500 nm in acidic solutions to 460 nm at pH>5.

The solution studies to understand the coordination properties of [Pd(H$_{-2}$**L1**)] towards RE(III) ions were performed at pH = 7 using TRIS (tris(hydroxymethyl)methylamine) as buffer system. UV-Vis and fluorescence titrations of a [Pd(H$_{-2}$**L1**)] solution were performed by adding aqueous solutions of Ce(III), Nd(III), Sm(III), Tb(III) and Yb(III) ions as chloride salts and La(III), Gd(III) and Dy(III) as sulphate salts. For all experiments, UV-Vis spectra gave only minimal changes, while significant effects can be observed in the fluorescence emission results.

Among all RE(III) ions tested, only Gd(III) and La(III) showed a CHEF effect together with a blue-shift from 460 to 423 nm (Figure 20a), while the other RE(III) ions caused a CHEQ effect (Figure 20b). At pH = 7 the emission quantum yields of [Pd(H$_{-2}$**L1**)] in the presence of 1 equiv. of Gd(III) or La(III) are, respectively, ϕ_{em}=0.041 and 0.010.

The observed change in the emission properties confirms the interaction between [Pd(H$_{-2}$**L1**)] and RE(III) ions, more likely in a similar way to that observed in the previous studies on [Cu(H$_{-2}$**L1**)(H$_2$O)].[116,117] Indeed, the equilibrium constants (log *K*) for the addition of Gd(III) ions to an aqueous solution of the Pd-based receptor (pH = 7, TRIS 0.01 mol dm^{-3}), suggest the presence of both {Gd[Pd(H$_{-2}$**L1**)]}$^{3+}$ and {Gd[Pd(H$_{-2}$**L1**)]$_2$}$^{3+}$ species (table 4).

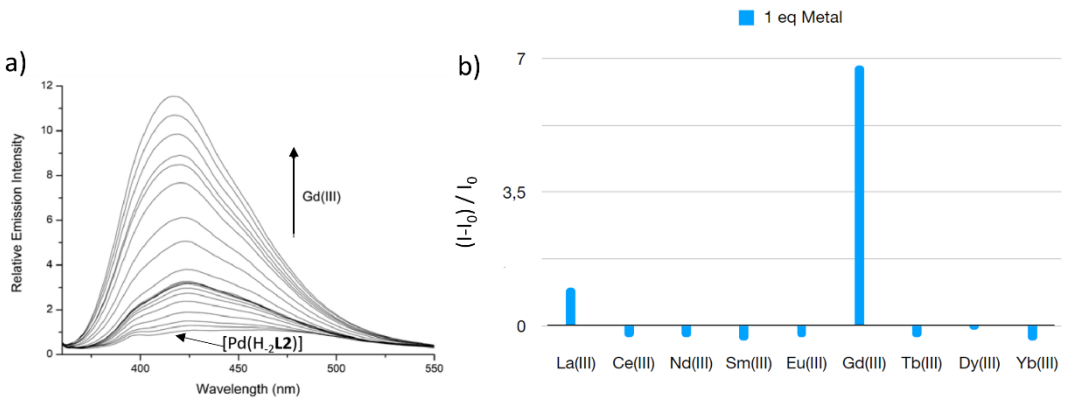

Figure 20. a) Fluorescence titration of [Pd(H$_{-2}$**L1**)] with Gd(III) in aqueous solution at pH = 7 (TRIS 10^{-3} mol dm^{-3}). [[Pd(H$_{-2}$**L1**)]]= $1\cdot10^{-5}$ mol dm^{-3}, addition of 0→10 equiv. of Gd(III) as an aqueous solution of $Gd_2(SO_4)_3$ (λ_{ex}=350 nm). b) Variation of emission intensity at 423 nm of [Pd(H$_{-2}$**L1**)] by adding 1 equiv. of RE(III) ion in aqueous solution at pH = 7 (R=[Pd(H$_{-2}$**L1**)], TRIS 10^{-3} mol dm^{-3}, λ_{ex}=350 nm).

Table 4. Logarithms of the equilibrium constants (log *K*) spectrofluorimetrically determined in aqueous solution at pH=7 (TRIS 0.01 mol dm^{-3}).

Reaction	**Log *K***
Pd(H$_{-2}$**L1**)] + Gd^{3+} = {Gd[Pd(H$_{-2}$**L1**)]}$^{3+}$	4.9(1)[a]
[Pd(H$_{-2}$**L1**)] + {Gd[Pd(H$_{-2}$**L1**)]}$^{3+}$ = {Gd[Pd(H$_{-2}$**L1**)]$_2$}$^{3+}$	3.1(2)

[a] Values in parentheses are the standard deviations on the last significant figure

Considering our previous studies,[116,117] it can reasonably be expected that in both species the Gd(III) ion is coordinated by the 3-hydroxychrom-4-one oxygen atoms of one or two [Pd(H$_{-2}$**L1**)] units and the coordination sphere is probably completed by water molecules. A similar arrangement can also be expected for the species formed with the other tested cations.

The photochemical properties of 3-hydroxychrom-4-one based systems are already well known.[121] They are typically more fluorescent in an apolar media than in water, being strongly influenced by the characteristics of the solvent, such as the polarity and H-bond donor capability. For this reason the low emission of [Pd(H$_{-2}$**L1**)] in aqueous solution can be attributed to a rearrangement of the H-bond network between the complex and the water

molecules occurring upon excitation, that contributes to a thermal dissipation of the excited state energy.[122] This consideration is also confirmed by the solid state structure (see solid state discussion) that shows the ability of [Pd(H_{-2}**L1**)] to form strong H-bonds between a water molecule and the four oxygen atoms of the two 3-hydroxychrom-4-one side arms. Based on this information, an hypothesis to explain the enhancement of the fluorescence intensity after the addition of Gd(III) can be rationalized. After the formation of the $\{RE[Pd(H_{-2}\mathbf{L1})]\}^{3+}$ or $\{RE[Pd(H_{-2}\mathbf{L1})]_2\}^{3+}$ species, the water molecule is replaced by the metal ion causing the de-solvation of [Pd(H_{-2}**L1**)]. In this way the system should gain in emission quantum yield. Open-shell RE(III) cations are characterized by f-energy states generated by the partial filling of the 4f orbital (Figure 21b), which enables them to act as energy transfer acceptors. The UV-excitation of RE(III) complexes causes an energy transfer from the excited state of the ligand to the metal, generating an f-excited state centred on the RE(III) ion, with a process called "antenna effect". If a solvent molecule is coordinated to the metal ion, e.g. a water molecule, the f-excited state of RE(III) ion dissipates the energy *via* vibrational coiling. This results in a total quenching of the fluorescence emission (Figure 21a).

The coordination of La(III) confirms this hypothesis: indeed, it is a closed-shell f^0 ion, showing a unique ^1S state and lacking of accessible excited ones, thus it is able to increase the fluorescence emission intensity of the metal receptor.

Apart from La(III), the f^7 Gd(III) is the only one, among the tested RE(III), that does not have low energy accessible excited states (Figure 21b). Indeed, due to the stability of the high spin f^7 configuration, corresponding to an ^8S fundamental state, the first excited state of Gd(III) lies probably at higher energy than the excited state of the receptor,[92] causing the described CHEF effect. The larger enhancement of the emission caused by Gd(III) with respect to La(III) can be attributed to their difference in ionic radii,[116,117] that provides Gd(III) with a greater Lewis acid character, producing a stronger interaction with the receptor. The proposed

mechanism is in agreement with both fluorescence properties of the 3-hydroxychrom-4-one-based system in water[122] and the RE(III) complex properties in solution.

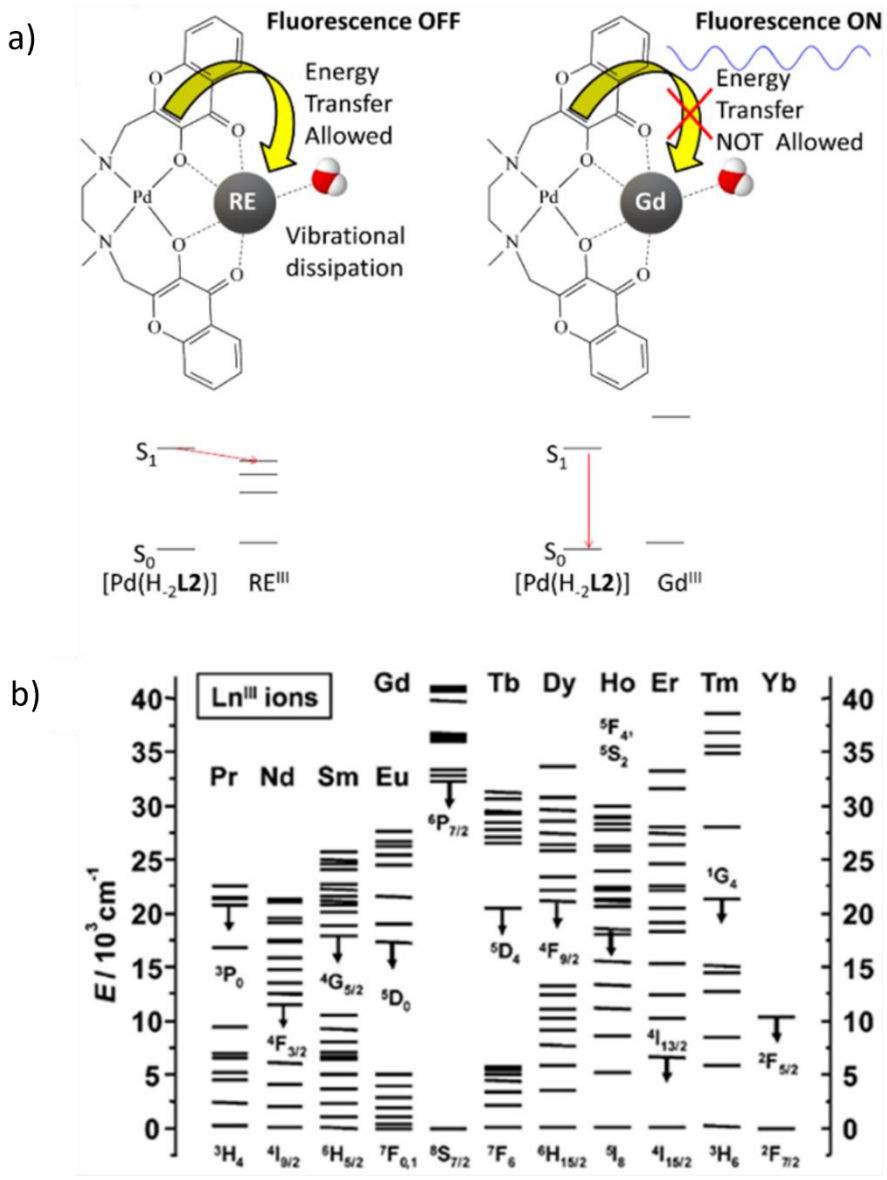

Figure 21. Scheme of the probable transduction mechanism a) and partial energy diagrams of lanthanide trivalent ions. b) Reprinted with permission from Ref. [92]. Copyright © 2006, American Chemical Society.

2.1.4 Competition Experiment

A series of competition experiments were performed to test the selectivity of the system towards Gd(III) in the presence of other ions, such as rare earth elements, Alkali, Alkaline earth and transition metals, common anions such as sulphate, nitrate, chloride and phosphate (Figure 22). Bar plots in figure 22 show that the presence of high concentration (0.01 mol dm^{-3}) of Alkali and Alkaline earth metal ions and anions such as sulphate or phosphate did not substantially influence the response to Gd(III) (Figure 22b and 22d). Fluorescence emission intensity is reduced by 20% in the presence of nitrate and chloride. The results of the same experiments performed with transition metal ions such as Ni(II), Cu(II), Zn(II), Cd(II) and Pb(II) and other RE(III) ions show that these metal ions compete with Gd(III) quenching fluorescence to a large extent (Figures 22a and 22c). When 10 equivalents of these cations with respect to Gd(III) are added to the solution, the signal decreases up to 5-10%. Cu(II), probably due to its paramagnetic properties, totally quenched the emission, while La(III), that, as said before, causes a little increase of the [Pd(H_{-2}**L1**)] signal, increases the overall response.

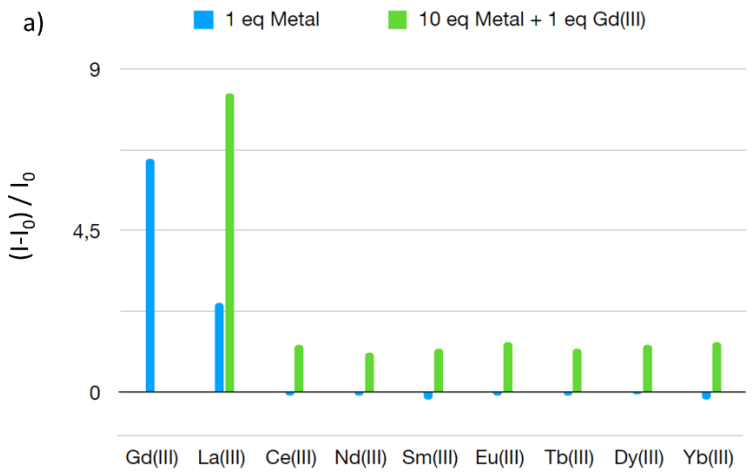

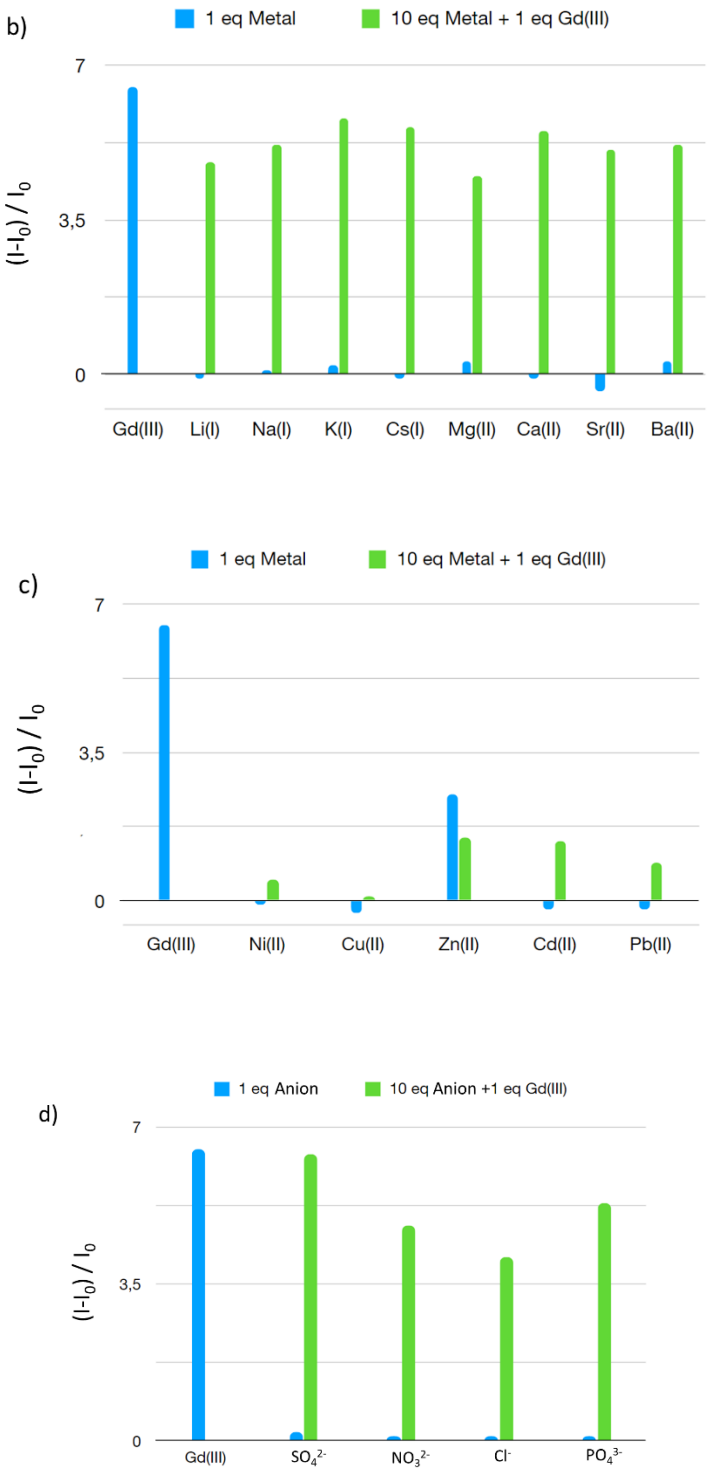

Figure 22. Effect of the presence of other ions on the fluorescence response to [Pd(H$_{-2}$**L1**)] sensor ($1 \cdot 10^{-5}$ mol dm^{-3}). a) Blue bars: RE(III) ion; green bars: co-presence of Gd(III) and 10 equiv. of RE(III) ion. b) Blue bars: alkali/alkaline earth metal ion; green bars: co-presence of Gd^{III} and 10 equiv. of alkali/alkaline earth metal ion. c) Blue bars: transition metal ion; green bars: co-presence of Gd(III) and 10 equiv. of transition metal ion. d) Blue bars: anion; green bars: co-presence of Gd(III) and anion.

2.1.5 Real Samples Analysis

Considering a possible application of the sensor for the detection of Gd(III) in the environment, the observed competition with the other RE(III) and transition metal ions does not prevent the utility of the system to work as a fluorescent chemosensor for the detection of Gd(III) in environmental samples. In order to assess the ability of [Pd(H_{-2}**L1**)] in the recognition of Gd(III) for environmental concerns, fluorescent experiments were performed on tap water samples polluted by addition of Gd(III) as sulphate salt from 1.0 to 10 ppm (Figure 23). By exciting at 350 nm, the emission caused by [Pd(H_{-2}**L1**)] in distilled water and in tap water samples are similar to each other, meaning that the presence of the cations and anions contained in the real samples does not perturb the signal. On the contrary, the same experiments performed on polluted samples show an increase of the signal at 423 nm and the intensities agree with Gd(III) contents. The system reaches a plateau upon the addition of 4 ppm of Gd(III). The enhancement of fluorescence emission intensity is also visible to the naked eye under a 360 nm lamp.

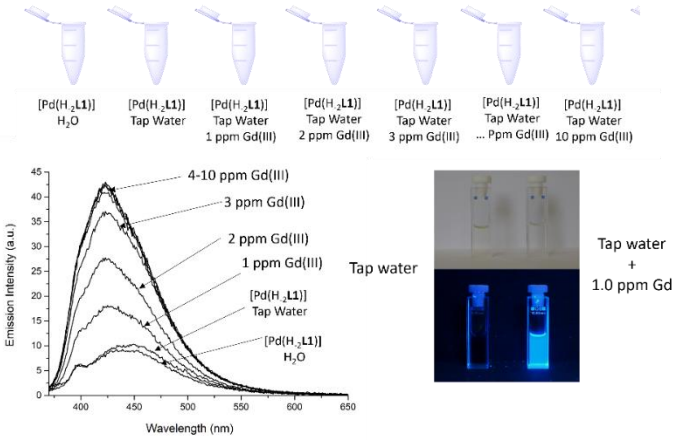

Figure 23. Experimental conditions: to each sample of tap water (5 cm^3), 0.5 cm^3 of 0.1 mol dm^{-3} pH=7 TRIS buffer and 0.5 cm^3 of a $5 \cdot 10^{-4}$ mol dm^{-3} ethanolic [Pd(H_{-2}**L1**)] solution were added. The samples were polluted by the addition of Gd(III) as sulphate salt from 0.1 to 10 ppm. Emission spectra were acquired after 10 min by exciting at 350 nm.

The Limit of Detection (LOD) and the Limit of Quantification (LOQ) were determined through the linear regression method.[123] This methodology allows to make a calibration curve by plotting the fluorescence signal (Y) of a series of standard solutions with a known concentration of the analyte (X). The linearity of the system can be expressed using the equation of the line Y = A + BX as a mathematic model, where A is the intercept and B is the slope of the line. Both parameters can be calculated with the minimum square method together with their respective standard deviations S_A and S_B. The response is the ratio between the emission intensity of each sample and the emission intensity of the blank at 423 nm by exciting at 350 nm (Figure 24). The limit of linearity was observed to be in the concentration range 0-4 ppm (2.5 10^{-5} mol dm^{-3}) of gadolinium (R=0.99), the LOD is 0.4 ppm ($2.2 \cdot 10^{-6}$ mol dm^{-3}) and the LOQ is 1.2 ppm ($7.0 \cdot 10^{-6}$ mol dm^{-3}).

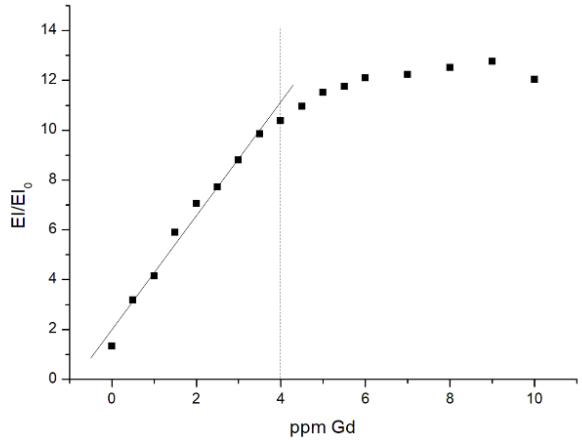

Figure 24. Trend of the normalized emission intensity at 423 nm (λ_{ex}=350 nm) of tap water samples polluted with Gd(III) (0-10 ppm).

Linear regression from 0 to 4 ppm:

Y=A + B·X;

A=1.998 (S_A = 0.278),

B=2.244 (S_B = 0.117),

R=0.9907.

The LOD and LOQ were calculated as:

LOD=$3S_A$ /B = 3·0.278/2.244=0.372≈0.4 ppm

LOQ=$10S_A$ /B = 10·0.278/2.244=1.23≈1.2 ppm

2.1.6 Conclusion

[Pd(H_{-2}**L1**)] has been synthesized and characterized. The synthetic pathway to obtain this Pd-based complex is inexpensive and easily reproducible. No protective groups and flash column chromatography are needed. The free ligand is obtained with a one-pot procedure using the Mannich reaction conditions and the process is in agreement with the "carbon economy" paradigm because the carbon atoms of all reagents are found in the final ligand **L1**.

Solution studies in the presence of RE (III) revealed that the [Pd(H_{-2}**L1**)] complex is able to interact with Gd(III) causing a switch-ON of the fluorescence emission intensity at 423 nm. This fluorescent probe can be used to detect the presence of gadolinium in real samples following a simple protocol, with a LOD of 0.4 ppm of Gd(III), using a simple 350 nm Wood lamp as illuminating source. The chance to set-up a technique to monitor Gadolinium in real samples can give a fundamental support towards studies aimed at the determination of long-term ecotoxicological data, biochemical effects, degradation, metabolism and bioaccumulation processes of the Gd(III) ion and its compounds.

Since today only hotspots with high levels of Gd(III) were considered dangerous for aquatic environments, this can be useful to assess more detailed environmental risks due to Gd(III). Among future objectives, this system can be improved in several directions. It could be linked to nanoparticles or surfaces trying to amplify the signal. It could also be coupled with different fluorophore fragments in order to displace the emission towards the visible region via energy transfer processes.

To the best of our knowledge, this is the first example of a fluorescent chemosensor for Gd(III) able to work in real aqueous samples. [Pd(H_{-2}**L1**)] complex is able to detect Gd(III) also with the contemporary presence of high concentrations of interfering anions and cations, such as other RE(III) or alkali and alkaline earth metals, however its quantification is not possible in their presence. For this reason, another future goal is aimed at improving the selectivity

towards the other metals, for example by increasing the number of the donor atoms or varying the molecular topology of the metal receptor.

2.2 Results and Discussion of L2

A series of ligands containing the 2-(2-hydroxy-3-naphthyl)-4-methylbenzoxazole (HNBO)[124] as fluorophore moiety (Scheme 7) has been tested as chemosensor for alkali and alkaline earth metal ions. The ligands were previously synthesized by us; in the present project the synthesis has been optimized, increasing the yield of the process.

The three ligands of the series contain an aliphatic amine/polyamine chain as the receptor unit, which is linked to the HNBO moiety through a methylene linker. Ligands **La**, **Lb** and **L2** (Scheme 7) have been synthesized via a nucleophilic substitution between the amine/polyamine fragment and the fluorophore, prior bromination at the benzylic position of HNBO. The latter was previously synthesized as reported in the literature.[125]

Both **La** and **Lb** contain a single HNBO fluorophore moiety; they feature a dimethylamine and a N,N,N'-Trimethylethylenediamine fragment, respectively, at the benzylic position of HNBO as the binding unit. **L2** shows the most complex structure, bearing two HNBO moieties each one linked to a nitrogen atom of a N,N'-Dimethylethylenediamine fragment (Scheme 7).

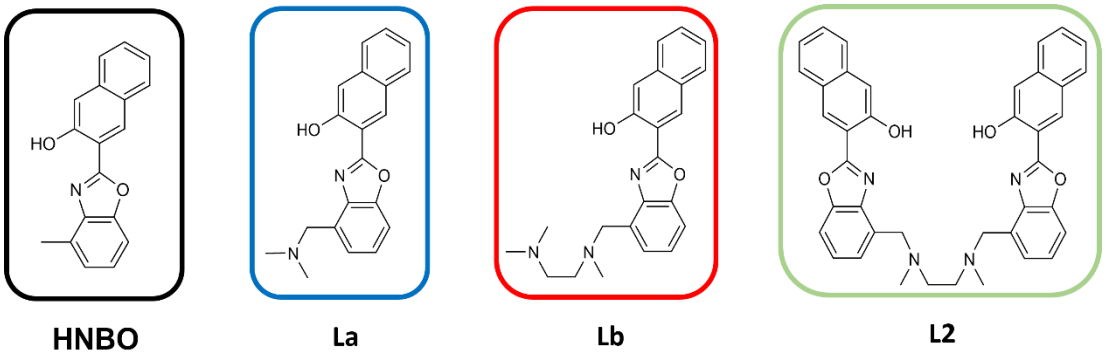

Scheme 7. Ligands synthesized based on HNBO unit as fluorophore moiety.

Following the objectives, a series of preliminary studies were performed to test the emission behaviour of the three ligands towards alkali and alkaline earth metal ions in dimethyl sulfoxide (Figure 25).

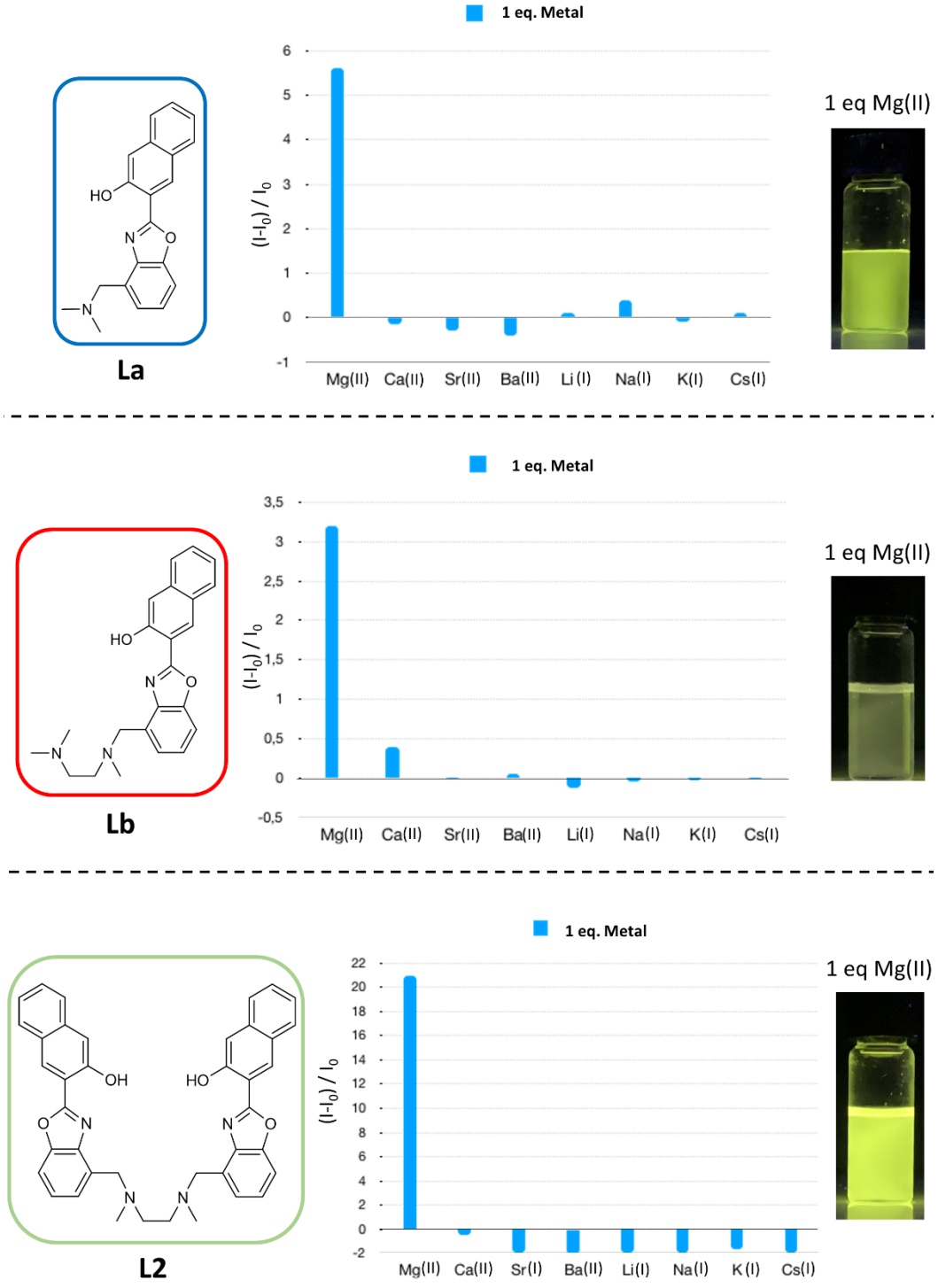

Figure 25. Bar plots of the maximum emission intensity (λem **La** = 540 nm; λem **Lb** = 535 nm; λem **L2** = 537 nm) recorded by exciting (λex) at **La** = 444 nm; **Lb** = 444 nm; **L2** = 450 nm. [**L**] = $1.2 \cdot 10^{-5}$ mol dm^{-3} DMSO + 1.5 % H_2O; *I*= $1.2 \cdot 10^{-3}$ mol dm^{-3} NMe_4Cl. $(I-I_0) / I_0 = 0$ corresponds to the emission of the free Ligand. The spectra were recorded after the addition of 1 equivalent of the metal (Mg(II), Ca(II), Sr(II), Ba(II), Li(I), Na(I), K(I), Cs(I)) to the solution of the ligand.

Dimethyl sulfoxide was chosen because it guarantees good solubility and photochemical properties to the ligands. The bar plots in Figure 25 show what happens to the emission of the ligands after the addition of 1 equivalent of Mg(II), Ca(II), Sr(II), Ba(II), Li(I), Na(I), K(I), Cs(I) to a $1.2 \cdot 10^{-5}$ mol dm^{-3} DMSO solution of **La**, **Lb** and **L2** (Figure 25). The results suggested that only the presence of Mg(II) caused an increase of the signal for all three systems. HNBO without further molecular functionalisation did not give any fluorescence response in the presence of all tested metal cations. By comparing the relative fluorescence emission intensity of the three molecular systems in the presence of Mg(II) (Figure 26), **L2** shows the highest enhancement of the intensity, being the best performing sensor for Mg(II). For this reason, **L2** was selected to continue the study.

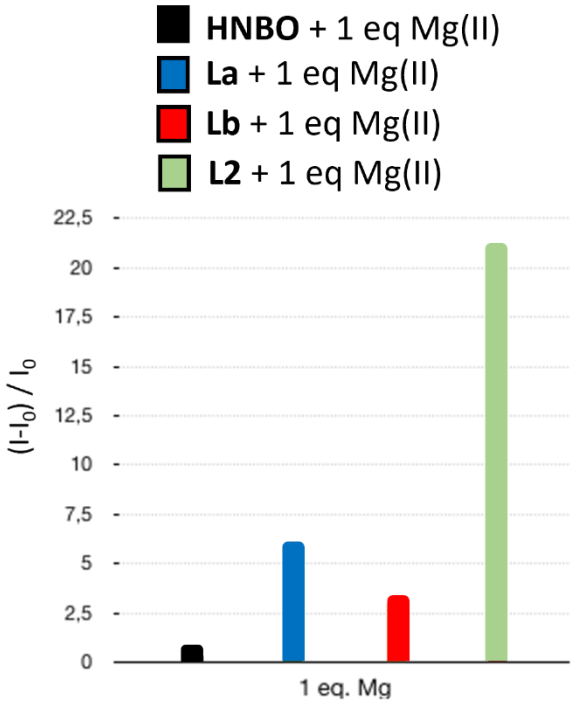

Figure 26. Bar plots of the maximum emission intensity (λem **La** = 540 nm; λem **Lb** = 535 nm; λem **L2** = 537 nm) recorded by exciting (λex) at **La** = 444 nm; **Lb** = 444 nm; **L2** = 450 nm. [**L**] = $1.2 \cdot 10^{-5}$ mol dm^{-3} DMSO + 1.5 % H_2O; *I*= $1.2 \cdot 10^{-3}$ mol dm^{-3} NMe_4Cl. $(I-I_0) / I_0 = 0$ corresponds to the emission of the free Ligand. The spectra were recorded after the addition of 1 equivalent of Mg(II) to the solution of the ligand.

2.2.1 Solution studies

Given the great ability of **L2** to detect Mg(II) ions, further solution studies were performed to better understand the system. UV-Vis and fluorescence titrations were carried out by adding an increasing amount of Mg(II) to a $1.2 \cdot 10^{-5}$ mol dm^{-3} DMSO solution of **L2**. Two equivalents of tetrabutylammonium hydroxide (TBAOH) were added to the solution of **L2** to help the deprotonation process to obtain the $(H_{-2}\mathbf{L2})^{-2}$ species, since the Mg(II) cation does not affect the acid dissociation of the naphthol group. During the UV-Vis titration reported in Figure 27a, a new absorption band grows at 450 nm, ascribable to the deprotonation of the naphthol moiety induced by the coordination of Mg(II). By exciting at 450 nm (Figure 27b) a great enhancement of the fluorescence emission intensity (λem = 537 nm) occurs, which is linear up to one equivalent and then the signal remains constant, suggesting that the system reaches the saturation with the formation of the species with a 1:1 ligand to Mg(II) ratio.

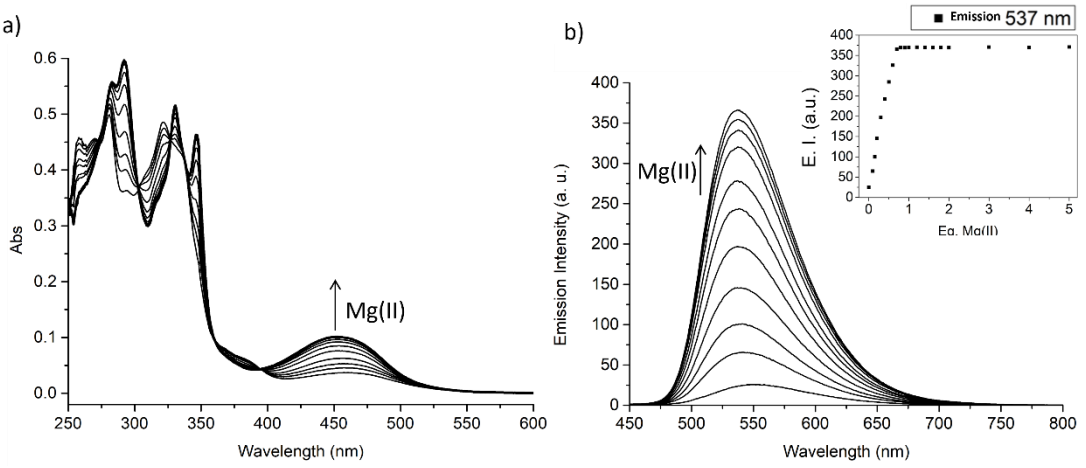

Figure 27. UV-Vis absorption (A) and emission (B) spectra of **L2** ($1.2 \cdot 10^{-5}$ mol dm^{-3}) registered in DMSO (+ 1.5% H_2O), *I*= $1.2 \cdot 10^{-3}$ mol dm^{-3} NMe_4Cl upon addition of $Mg(ClO_4)_2$ (from 0.1 to 1.0 equivalents). λex = 450 nm.

In order to gain a deeper insight into the nature of the complex, a ^1H NMR titration was performed by adding Mg(II) to a DMSO solution of **L2**. Also in this case, two equivalents of TBAOH were added to the solution of **L2**, to start from the deprotonated $(H_{-2}\mathbf{L2})^{-2}$ species. No

variation of the chemical shifts was detected following the addition of 1 equivalent of Mg(II), suggesting the formation of the mononuclear species (Figure 28a). By comparing the spectra of (H_{-2}**L2**)$^{-2}$ before and after the addition of 1 equivalent of Mg(II) (Figure 28b), it is possible to see that all aromatic signals shift downfield.

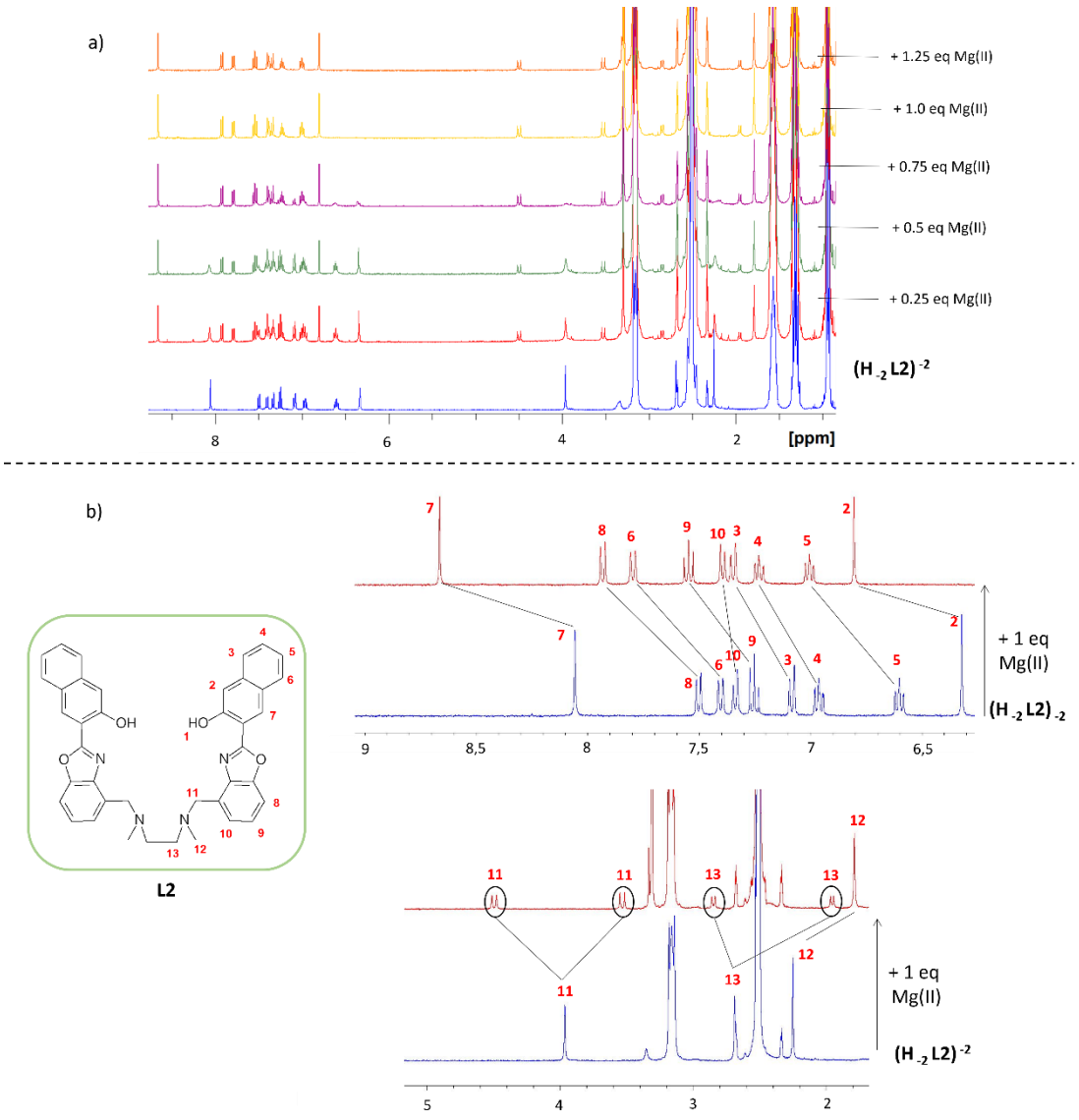

Figure 28. a) ^{1}H NMR spectra of **L2** ($7.5 \cdot 10^{-3}$ mol dm^{-3}) registered in a DMSO-d_6 in the presence of two equivalents of TBAOH following the addition of $Mg(ClO_4)_2$. b) Shits of the resonances obtained by comparing (H_{-2}**L2**)$^{-2}$ species before (blue line) and after the addition of one equivalent of Mg(II) (red line).

Since **L2** contains two fluorophore units, but only one series of signals is visible, pointing at a C2v symmetry for the complex as well as for the free ligand, it is possible to suggest a cooperation between the two fluorophore moieties in the ion complexation. In the aliphatic region, the resonance of proton 12 shifts upfield, while those of protons 11 (benzylic position) and 13 (methylene group of the polyamine chain) splits in characteristic AB systems suggesting the stiffening of the structure upon the ion complexation. Following these considerations, it can be hypothesized a complexation mechanism in which the two fluorophores are forced to stay on the same side with respect to the amine scaffold upon the binding of Mg(II) (Figure 29a). A possible mechanism explaining the observed enhancement of the fluorescence is the PET effect from the HOMO of the benzylic nitrogen atoms to the HOMO of the excited fluorophore moiety. This effect occurs only when benzylic nitrogen atoms bear free lone pairs, in other words are not involved in the coordination. Following the stabilization upon coordination, the lone pairs are not available anymore, thus PET effect is prevented and the emission is switched ON (Figure 29b).

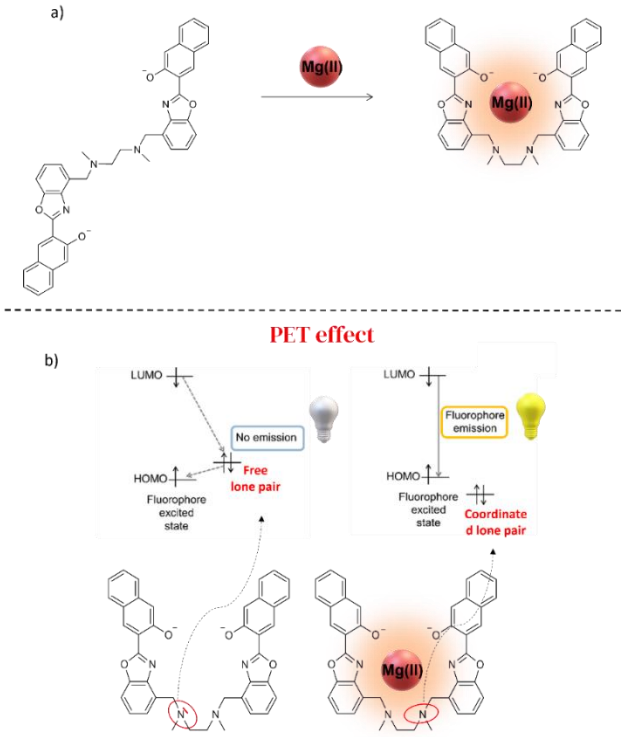

Figure 29. a) Proposed complexation mechanism; b) Proposed mechanism (PET) for the enhancement of the fluorescence of **L2** caused by Mg(II).

2.2.2 Competition Experiments

To evaluate the selectivity of the sensor, different competition experiments were performed. One equivalent of Mg(II) was added to different DMSO solutions of **L2** containing Ca(II), Sr(II), Ba(II), Li(I), Na(I), K(I) and Cs(II). In the bar plot reported in Figure 30 is possible to observe that the individual presence of the other cations does not prevent the emission of the system caused by Mg(II).

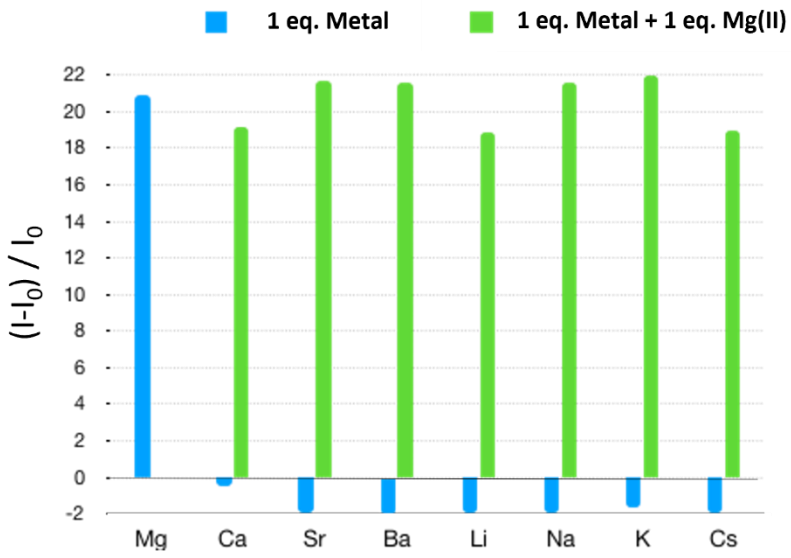

Figure 30. Bar plots of the maximum emission intensity (λem **L2** = 537 nm) recorded by exciting (λex) at 450 nm. **L2 =** $1.2 \cdot 10^{-5}$ mol dm^{-3} DMSO + 1.5 % H_2O; *I*= $1.2 \cdot 10^{-3}$ mol dm^{-3} NMe_4Cl. $(I-I_0) / I_0 = 0$ corresponds to the emission of the free Ligand. The spectra were recorded after the addition of 1 equivalent of Mg(II) to the solutions of the ligand already containing 1 equivalent of the metals Ca(II), Sr(II), Ba(II), Li(I), Na(I), K(I), Cs(I).

Moreover, **L2** is able to detect Mg(II) also in a mixture of all tested cations. Figure 31a shows the enhancement of the fluorescence emission intensity after the addition of one equivalent of Mg(II) to a solution containing an equimolar mixture of Ca(II), Sr(II), Ba(II), Li(I), Na(I), K(I) and Cs(II). Figure 31b (bottom) shows the emission enhancement of **L2**, both in the absence and in the presence of a mixture of the other alkali and alkaline-earth metal ions, which is visible to the naked eye under a 360 nm UV lamp.

The addition of 1 equivalent of Mg(II) to a DMSO solution of **L2** also induces a colour change from colourless to yellow, again both in the absence and in the presence of a mixture of the other alkali and alkaline-earth metal ions, as depicted in Figure 31b (top).

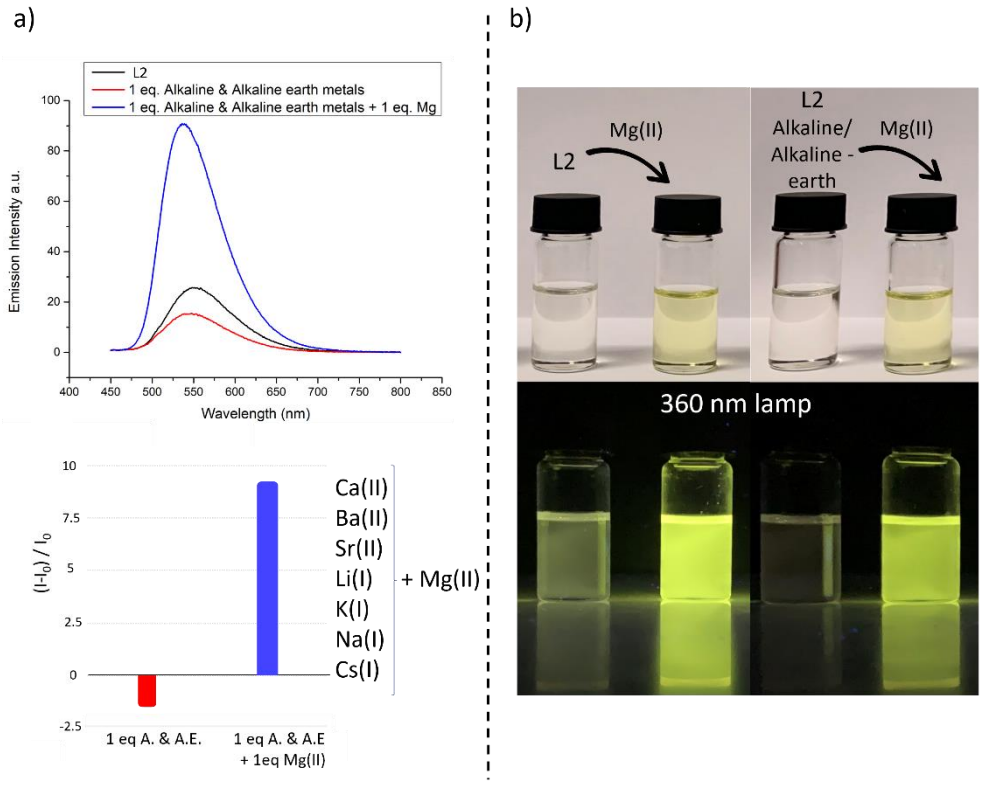

Figure 31. a) Bar plot of the maximum emission intensity (λem **L2** = 537 nm; bottom) and emission spectra recorded by exciting (λex) at 450 nm. **L2** = $1.2 \cdot 10^{-5}$ mol dm^{-3} DMSO + 1.5 % H_2O; *I*= $1.2 \cdot 10^{-3}$ mol dm^{-3} NMe_4Cl. $(I-I_0) / I_0 = 0$ corresponds to the emission of the free Ligand. The spectra were recorded after the addition of 1 equivalent of Mg(II) to the solution of the ligand already containing an equimolar mixture of the metals Ca(II), Sr(II), Ba(II), Li(I), Na(I), K(I), Cs(I). b) Colour change (top) and enhancement of the fluorescence visible to the naked eye under a 360 nm lamp (bottom) after the addition of 1 equivalent of Mg(II).

Systems found in the literature able to detect the presence of Mg(II) in solution are usually also sensitive to the presence of other cations, such as Ca(II) and Zn(II), in other words they are not selective towards Mg(II). As reported above, notably the fluorescence emission of **L2** is switched ON in the presence of Mg(II) but not in the presence of Ca(II). Therefore, the observed selectivity for Mg(II) against Ca(II) was investigated more in depth.

Figure 32a reports the superimposition of the UV-Visible spectra of **L2** after the addition of 1 equivalent of Mg(II) and after the addition of 1 equivalent of Ca(II). In both cases an increase of the absorption at 450 nm occurs, but the increase is much bigger in the case of Mg(II), suggesting a stronger interaction between **L2** and Mg(II) than between **L2** and Ca(II).

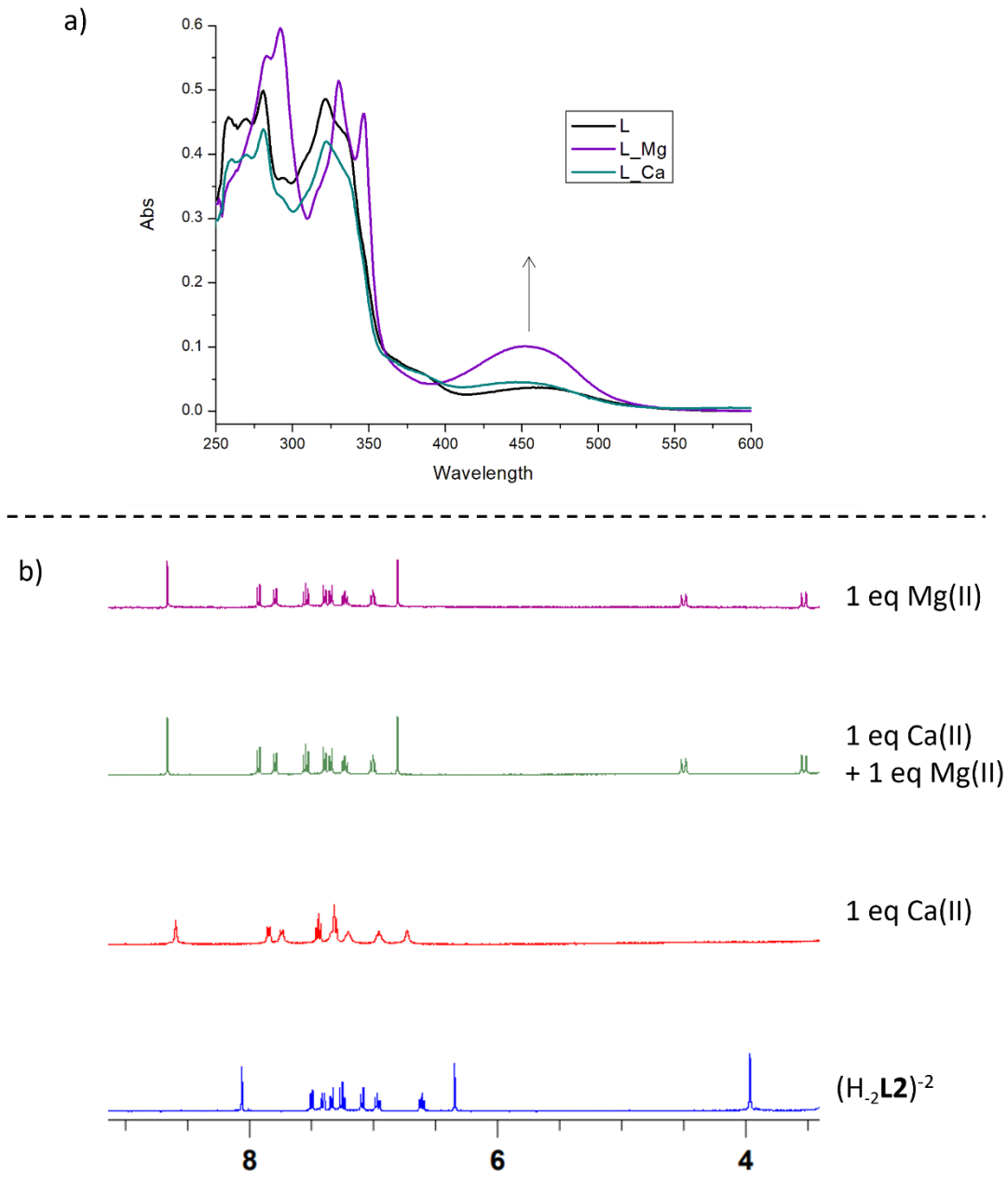

Figure 32. a) Superimposition of UV-Vis absorption spectra of **L2**, **L2** + 1 eq Mg(II), **L2** + 1 eq Ca(II) in DMSO (1.5% H_2O), [**L2**] = $1.2\cdot10^{-5}$ mol dm^{-3}, *I*= $1.2\cdot10^{-3}$ mol dm^{-3} NMe_4Cl. b) Stacked ^1H NMR spectra of **L2**, **L2** + 1 eq Ca(II), **L2** + 1 eq Ca(II) + 1 eq Mg(II), **L2** + 1 eq Mg(II) registered in DMSO-d_6 in the presence of two equivalents of TBAOH. [**L2**] = $7.5\cdot10^{-3}$ mol dm^{-3}.

^{1}H NMR experiments were carried out by adding 1 equivalent of Ca(II) or Mg(II) to a DMSO-d_6 solution of $(H_{-2}\mathbf{L2})^{-2}$ (Figure 32b).

Looking at the spectrum recorded upon the addition of Ca(II), there is a change in chemical shifts suggesting a complexation between the ligand and Ca(II). In this case protons in benzylic position do not split in characteristic AB systems suggesting that probably the interaction with Ca(II) is less efficient. The addition of 1 equivalent of Mg(II) to this solution further modifies the spectrum, with all resonances coinciding with those of the Mg(II) complex. This result suggests that **L2** has a larger affinity for Mg(II) than for Ca(II), in other words Mg(II) replaces Ca(II) in the complex with the ligand. The system performance was tested also in the presence of some transition metal ions, such as Zn(II) and Cd(II). Figure 33 shows the enhancement of the emission of the system caused by the addition of 1 equivalent of Mg(II), Zn(II) and Cd(II) to a solution of all three ligands in DMSO.

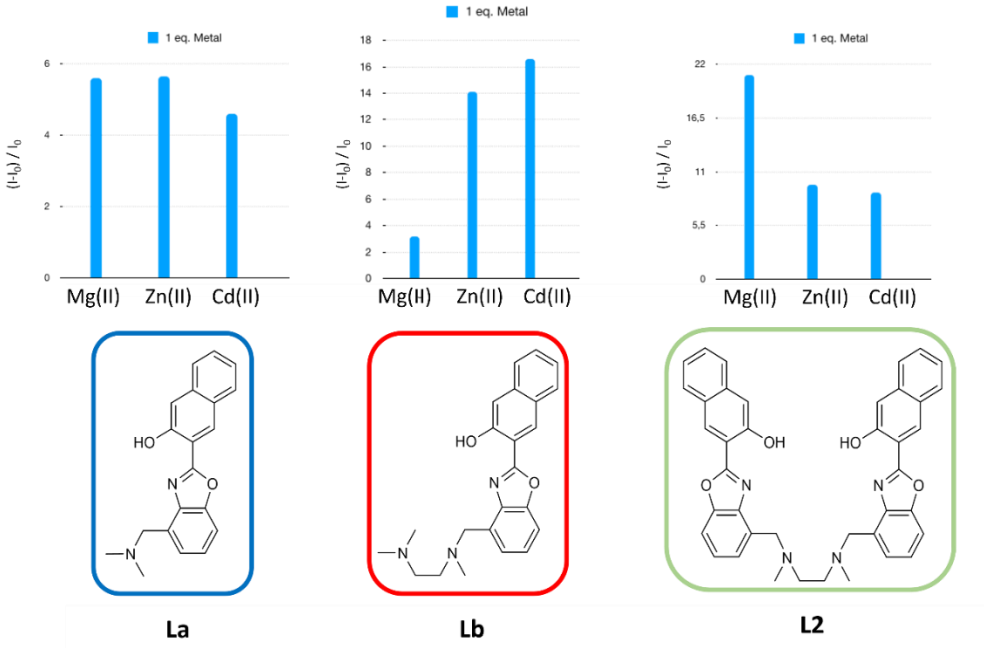

Figure 33. Bar plots of the maximum emission intensity (λem **La** = 540 nm; λem **Lb** = 535 nm; λem **L2** = 537 nm) recorded by exciting (λex) at **La** = 444 nm; **Lb** = 444 nm; **L2** = 450 nm. [**L2**] = $1.2\cdot10^{-5}$ mol dm^{-3} DMSO + 1.5 % H_2O; *I*= $1.2\cdot10^{-3}$ mol dm^{-3} NMe_4Cl. $(I-I_0) / I_0 = 0$ corresponds to the emission of the free Ligands. The spectra were recorded after the addition to the solution of the ligands 1 equivalent of the metals Mg(II), Zn(II), Cd(II), Pb(II).

Zn(II) and Cd(II) switch ON the fluorescence emission of all systems, but only in the case of **L2** the enhancement is lower than that produced by Mg(II). **La** features indeed a similar emission intensity for Mg(II), Zn(II) and Cd(II), while **Lb** shows a larger intensity for Zn(II) and Cd(II) than for Mg(II). This is a remarkable result, also considering both the great selectivity of **L2** for Mg(II) with respect to the other alkali and alkaline earth metal ions as well as the bigger selectivity of **L2** for Mg(II) with respect to the other ligands of the series.

The Limit of Detection (LOD) and the Limit of Quantification (LOQ) were determined through the linear regression method.[123] The response is the ratio between the emission intensity of each sample and the emission intensity of the blank at 550 nm by exciting at 450 nm (Figure 34). The limit of linearity was observed to be in the concentration range 0-20 ppm ($1.2 \cdot 10^{-5}$ mol dm^{-3}) of Mg(II) (R=0.99), the LOD is 1.0 ppm ($1.5 \cdot 10^{-6}$ mol dm^{-3}) and the LOQ is 3.2 ppm ($4.9 \cdot 10^{-6}$ mol dm^{-3}).

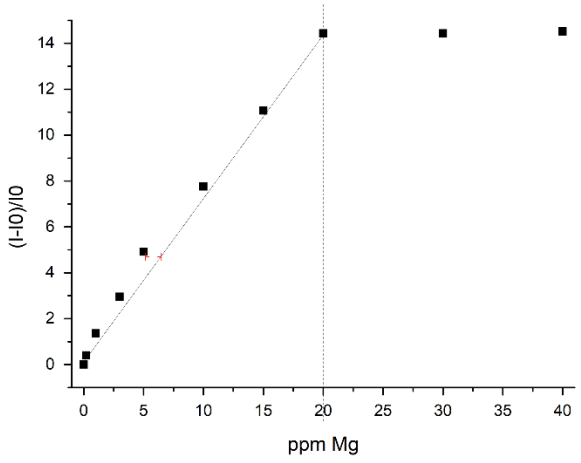

Figure 34. Trend of the normalized emission intensity at 537 nm (λ_{ex}=450 nm) of samples polluted with Mg(II) (0-5 ppm).

Linear regression from 0 to 50 ppm:

Y = A + B·X;

A = 0.59244 (S_A = 0.22544),

B = 0.70425 (S_B = 0.02312),

R = 0.99678.

The LOD and LOQ were calculated as:

LOD= $3S_A$ / B = 3·0.22544 / 0.70425 = 0.96 ppm (0.048 eq)

LOQ = $10S_A$ / B = 10·0.22544 / 0.70425 = 3.2 ppm (0.16 eq)

2.2.3 Real Samples Analysis

To assess the behaviour of this fluorescence probe for Mg(II) in real samples, thus containing different cations and anions with respect to those analysed so far, different brands of still water and tap water samples of different origin were selected. The experiments consisted in the addition of a little amount of the water samples (1.5 %, 37.5 µL) to a $1.2 \cdot 10^{-5}$ M DMSO solution of **L2** (2.5 ml) (Figure 35).

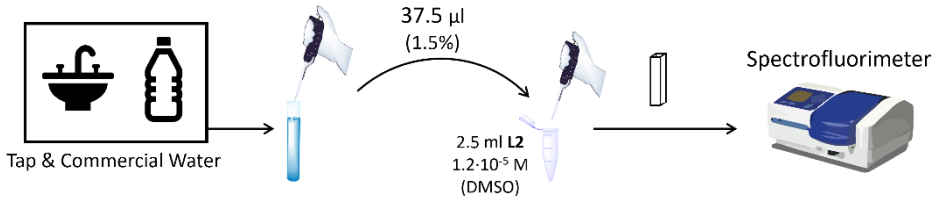

Figure 35. Experimental condition used to carry out experiments with real samples.

Three different brands of commercial water were selected. Figure 36 reports their labels, showing the Mg(II) contents, and their fluorescence analysis, performed after the addition of 37.5 µL of the real sample (red line) or of distilled water (black line) to a DMSO solution of **L2**.

The addition of Sample 1 (4.2 ppm of Mg(II)) to a solution of **L2** entails an enhancement of the emission intensity compared to the emission intensity of **L2** in the presence of distilled water. Sample 2 features a higher content of Mg(II) than the first one and the spectrum acquired upon its addition shows indeed a larger enhancement of the signal compared to the previous one. The third sample is a water brand that is sold as really low in Mg(II) and actually its content is not even reported in the label. Indeed, in this case the spectrum does not show any increase of the fluorescence emission intensity.

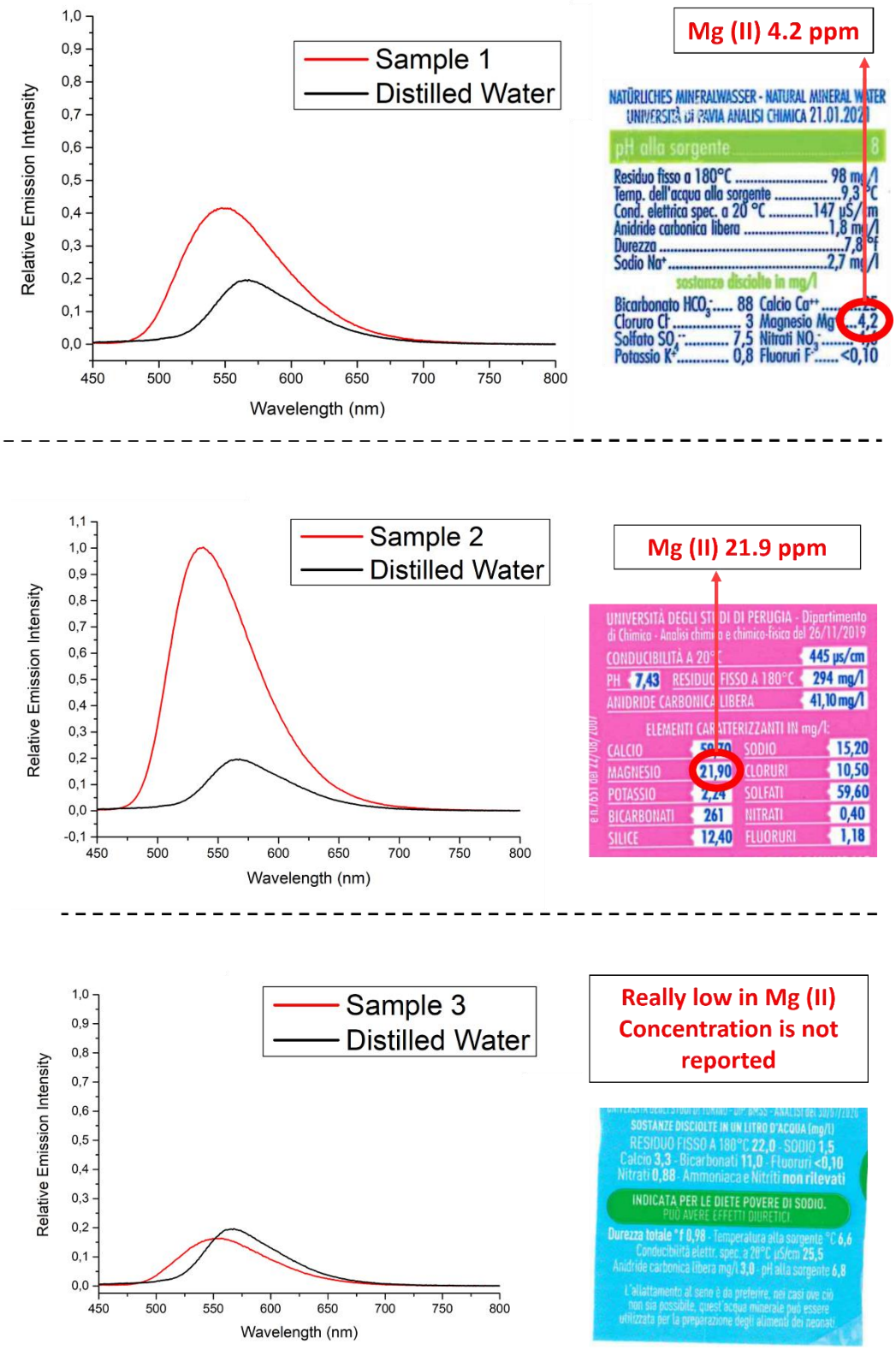

Figure 36. Top: Emission spectra recorded by exciting (λex) at 450 nm. [**L2**] = $1.2 \cdot 10^{-5}$ mol dm^{-3} DMSO + 1.5 % H_2O; *I*= $1.2 \cdot 10^{-3}$ mol dm^{-3} NMe_4Cl. $(I-I_0) / I_0 = 0$ corresponds to the emission of the free Ligand. The spectra were recorded after the addition of 37.5 µL of commercial water to a DMSO solution of **L2**. Bottom: labels of the commercial waters.

Two samples of tap water coming from two different Italian cities were selected and tested with **L2**. In Figure 37 the quantities of some cations such as Mg(II), Ca(II), K(I) and Na(I) obtained through ion chromatography are reported. As it is possible to observe from the spectra, the fluorescence emission intensities of the sensor upon the addition of the two tap water samples are again in agreement with their Mg(II) contents. For both samples, a colour variation of the solution is observed; moreover, the increase of the fluorescence is also visible to the naked eye under a 360 nm UV lamp.

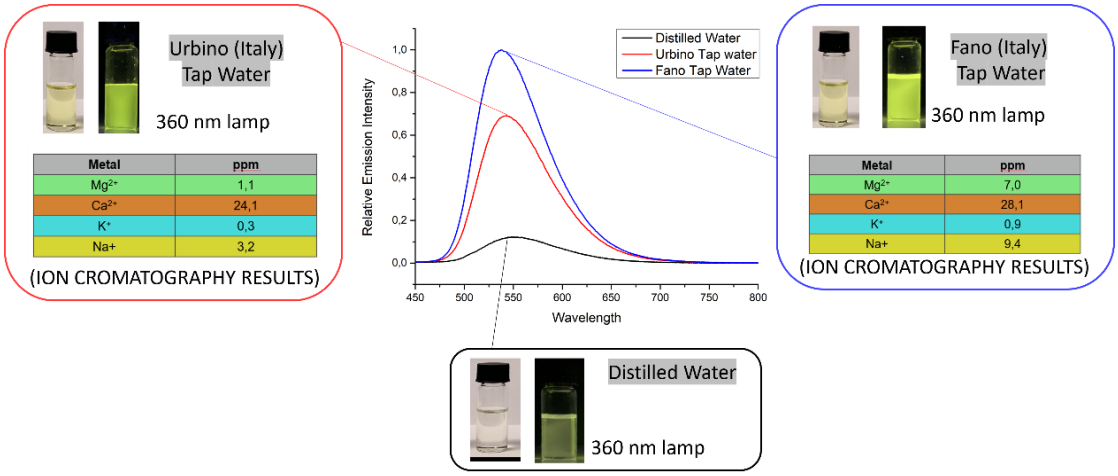

Figure 37. Emission spectra recorded by exciting (λex) at 450 nm. [**L2**] = $1.2 \cdot 10^{-5}$ mol dm^{-3} DMSO + 1.5 % H_2O; *I*= $1.2 \cdot 10^{-3}$ mol dm^{-3} NMe_4Cl. $(I-I_0) / I_0 = 0$ corresponds to the emission of the free Ligand. The spectra were recorded after the addition of 37.5 µL of tap water to a DMSO solution of **L2**. The metal ions content was determined by ion chromatography. Pictures show the colour change and the enhancement of fluorescence visible to the naked eye under a 360 nm lamp.

2.2.4 Conclusion

A series of fluorescent ligands based on HNBO fluorophore moiety, **La**, **Lb** and **L2,** were tested towards alkali and alkaline earth metals. The series was synthesized trying to increase the molecular complexity. **La** contains a single HNBO fluorophore moiety, bearing at benzylic position a dimethylamine fragment as binding unit. In **Lb**, a N,N,N'-Trimethylethylenediamine binding unit is bound to a single HNBO fluorophore moiety. **L2**, the most complex ligand of the series, is composed by two HNBO moieties both linked to a N,N'-Dimethylethylenediamine fragment.

All three ligands were screened towards alkali and alkaline earth metal ions and are all able to signal the presence in solution of Mg(II), with **L2** being the performing sensor in DMSO (limit of linearity: 20 ppm ($1.2\cdot10^{-5}$ mol dm^{-3}, R=0.99); limit of detection: 1.0 ppm ($1.5\cdot10^{-6}$ mol dm^{-3}); limit of quantitation: 3.2 ppm ($4.9\cdot10^{-6}$ mol dm^{-3})).

The presence other alkali and alkaline earth as well as transition metals does not prevent the emission caused by Mg(II). **L2** is able to work also with real samples such as tap and commercial water. In these cases it is possible to detect the Mg(II) presence but not to quantify its content, due to the loss of linearity of the system in the presence of many others cations and anions.

The presence of Mg(II) in all cases can be detected through both a great enhancement of fluorescence emission, that is also visible to the naked eye under a UV lamp, and a clear colour change of the solution from colourless to yellow.

This is a good result in terms of selectivity, because in the literature most of the sensors for Mg(II) respond also to Ca(II) and Zn(II) metal ions.

2.3 Results and Discussion of L3

The content of this chapter has been published in: G.Ambrosi, M.Fanelli, P.Paoli, M.Formica, D.Paderni, P.Rossi, M.Micheloni, L.Giorgi, V.Fusi. *Dalton. Trans.*, 2020, 49, 7496.

Conjugated systems in which aromatic fragments are directly appended at positions 2 and 5 of a 1,3,4-oxadiazole (ODA) ring have been attracting great interest of the scientists working in different fields (Scheme 8). This is due to the excellent properties of conjugated compounds containing ODA rings. Some of them show biological activity such as antitumoral[126-128] and antiproliferative[129-131] activities, others have been involved in pesticide chemistry studies.[132] ODA-derived compounds are also used in the field of material chemistry due to their high thermal stability and excellent optoelectronic properties leading to their use as polymeric light-emitting diodes (OLED), laser dyes, photovoltaic cells and photosensitive materials.[133-138] These systems also have an interesting behaviour in terms of chemosensing in solution, opening the possibility to develop fluorescent probes with applications in environmental monitoring and biological analysis.[139-141] They have good luminescent properties such as high emission quantum yield in the blue-green wavelength range. This makes the ODA-ring an interesting building block in the design of different fluorophores for the development of chemosensors.

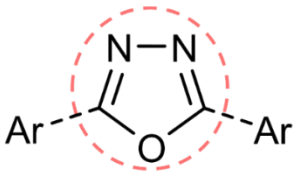

Scheme 8. ODA ring-conjugated systems in which aromatic fragments are directly appended at positions 2 and 5.

Recently, the Supramolecular chemistry group of the University of Urbino synthesized a series of ligands containing the ODA-ring able to bind metal ions such as Zn(II), Cd(II), Pb(II), Pt(II) and Ag(I). Scheme 9 reports the ligands containing a 2,5-diphenyl-1,3,4-oxadiazole

(PPD) group as the fluorophore moiety linked to different polyamine receptor units, either macrocyclic or open chain.[142,143]

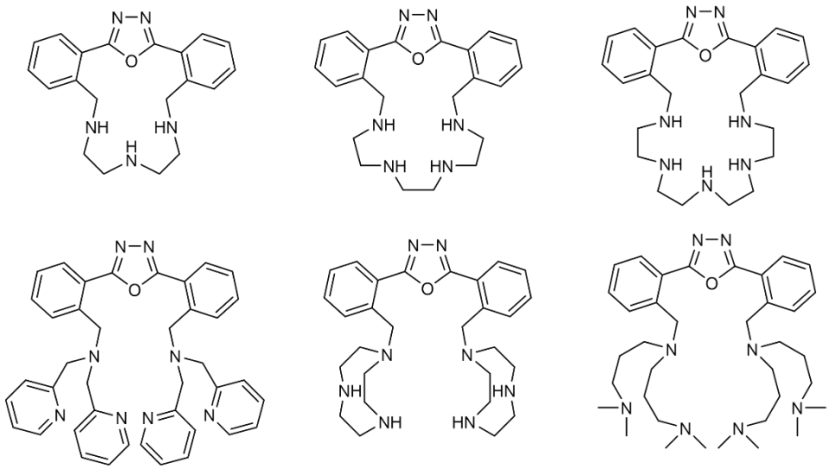

Scheme 9. Ligands containing 2,5-diphenyl-1,3,4-oxadiazole group as the fluorophore moiety synthesized by the Supramolecular Chemistry group of the University of Urbino.

In order to deepen the knowledge on the fluorescent properties of these systems,[144,145] a macrocyclic ligand (**L3**) containing a new ODA-ring based fluorophore fragment, namely 2,6-bis(5-(2-methylphenyl)-1,3,4-oxadiazol-2-yl)pyridine (POXAPy), has been designed and synthesized. The POXAPy fragment is composed by a central pyridine featuring at positions 2 and 6 two ODA-rings, both linked to a further phenyl ring (Scheme 10).[146] After the cyclization between the new fluorophore and the 1,4,7-trimethyl-1,4,7-triazaheptane polyamine, the ligand (13,16,19-trimethyl-36,37-dioxa-3,4,13,16,19,28,29,35-octaazahexacyclo [29.3.1.1(2,5).1(27,30).0(6,11).0(21,26)]eptatriaconta2,4,6,8,10,21,23,25, 27,29,31,33,1(35)-tridecene) (**L3**) was obtained. To the best of our knowledge, **L3** is the first example of a macrocycle containing ODA-rings in a sequence of five aromatic rings.

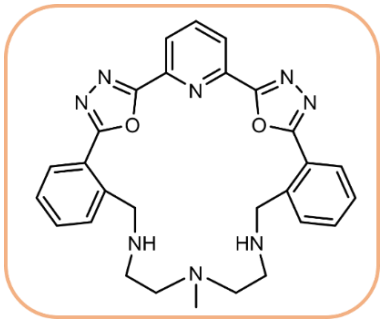

Scheme 10. Structure of **L3**.

2.3.1 Solid-state studies

The crystal structure of **L3** was determined by means of single crystal X-ray diffraction, with the crystal system resulting to be triclinic. Two independent molecules of the ligand (A and B in the following) are present in the asymmetric unit of **L3**. The X-ray structure of molecule A is reported in Figure 38.

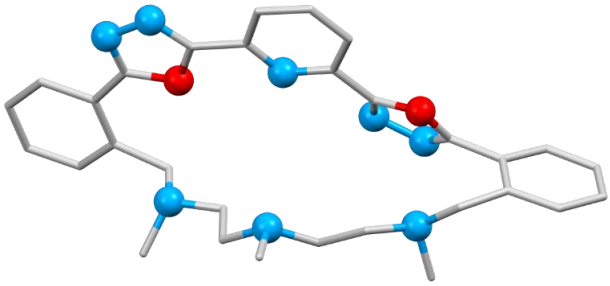

Figure 38. Structure of molecule A of L3. Non-H,C atoms are depicted in Ball and stick style, C atoms are depicted in capped stick style. C = gray; O = red; N = blue. Hydrogen atoms have been omitted for the sake of clarity (ellipsoid probability = 30%).

Molecule B shows some disorder in parts of the aliphatic chain and one phenyl ring (Figure 39). This was refined by using two models for B, Ba and Bb in the following, which have occupancy factors of 0.56 and 0.44, respectively.

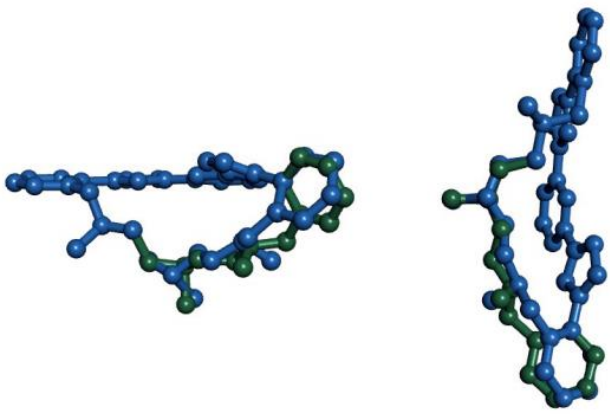

Figure 39. Superimposition of the a (green) and b (pale blue) model of the B independent molecules of **L3**.

As evidenced in Figure 40, molecule A overlaps fairly well with molecule Ba.

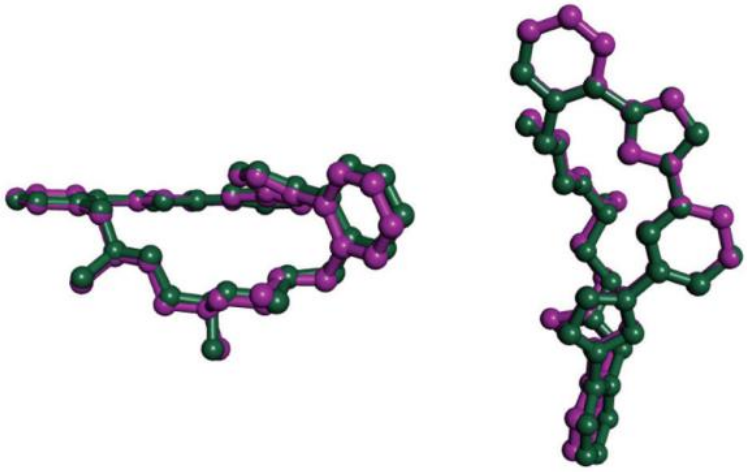

Figure 40. Superimposition of the independent molecules of **L3**: A (magenta) and Ba (green).

The conformation of the POXAPy moiety in both independent molecules is comparable with that observed in the 2,2'-(1,3-phenylene)bis(5-phenyl-1,3,4-oxadiazole) molecule retrieved in the Cambridge Structural Database[147] (CSD refcode = SEQRIR[148]). In particular, the five aromatic rings are not all coplanar, and the different orientation of the oxadiazole rings with respect to the central pyridine makes the overall conformation of the POXAPy moiety in **L3** and in SEQRIR quite asymmetrical (Figure 41).

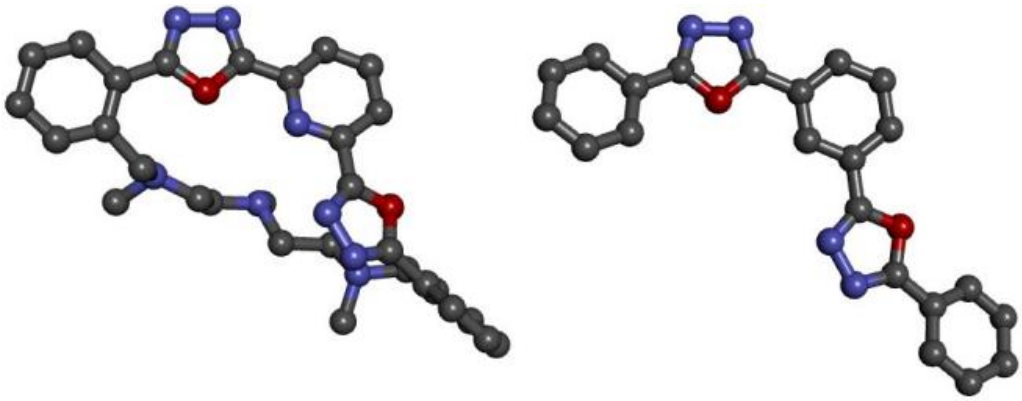

Figure 41. Ball and stick representations of the A molecule in **L3** (left) and SEQRIR.

Indeed, the oxygen atom of one oxadiazole ring in **L3** points towards the cavity of the macrocycle, while that of the other ring points outside. In addition, the first oxadiazole ring is quite coplanar with the central pyridine ring (the angle between the mean planes defined by the non-hydrogen atoms of the two rings is 4.4(1) and 7.9(2)° for A and B, respectively), while the second forms an angle of about 20° with the central ring (Table 5).

Table 5. Angle values (°) between the mean planes 1, 2, 3, 4 and 5. For the B molecules, due to disorder, two values (for Ba and Bb, respectively) are reported for the angles involving the plane number 5.

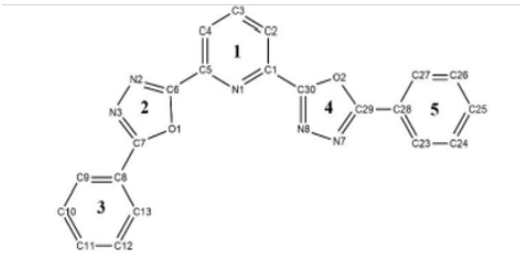

		2	3	4	5
A	1	4.4(1)	12.3(1)	22.6(2)	68.6(2)
	2		8.7(2)	25.4(2)	72.7(2)
	3			26.6(2)	76.2(2)
	4				50.0(2)
B	1	7.9(2)	12.7(2)	17.0(2)	64.3(4)/61.7(4)
	2		5.5(2)	20.5(2)	71.3(4)/54.9(4)
	3			21.3(2)	73.7(4)/52.9(3)
	4				53.2(4)/74.1(3)

Finally, three of the five rings (i.e. the central pyridine 1, the oxadiazole ring with the oxygen atom pointing inside the cavity 2 and the phenyl ring to which it is bonded 3) are quite coplanar, while the remaining two rings (i.e. the oxadiazole ring with the oxygen atom pointing outside the cavity 4 and the phenyl ring to which it is bonded 5) significantly deviate from the mean plane. The angle between the mean planes defined by the non-hydrogen atoms of these two ring groups is indeed 46.0(2), 26.60(9) and 22.4(1)° for A, Ba and Bb, respectively. In terms of the overall form of the two independent molecules of **L3**, both A and B have a V-shape (Figure 42), where the cavity has approximatively 6 × 10 Å dimensions. No significant intermolecular interactions are present in the crystal packing.

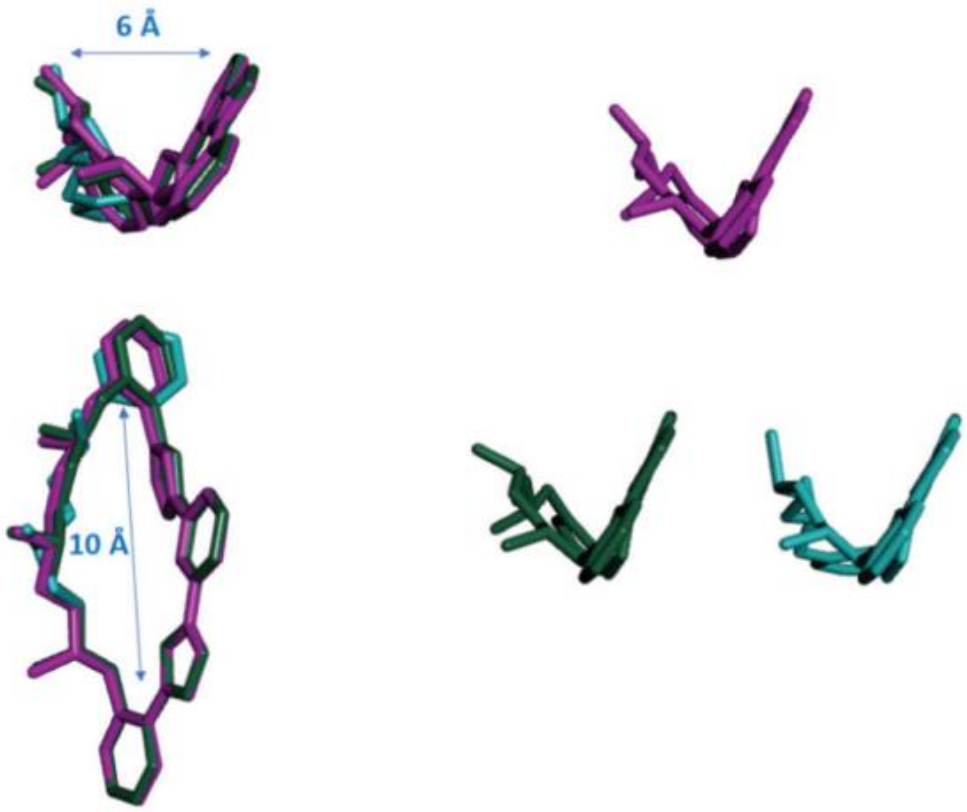

Figure 42. Left: Side (top) and front (bottom) views of the V-shape cavity in superimposed A and B molecules of **L3**. Hydrogen atoms have been omitted for the sake of clarity; the approximate dimensions of the cavity are indicated. Right: side views of the independent molecules: A (magenta, top), B (Ba = green, Bb = pale-blue, bottom).

2.3.2 Acid-base behaviour

Due to the poor solubility of **L3** in water, the UV-Vis and fluorescence studies were performed in a water/acetonitrile (70/30) mixed solvent. To understand the acid-base behaviour of the new system spectra were recorded at different pH values (Figure 43).

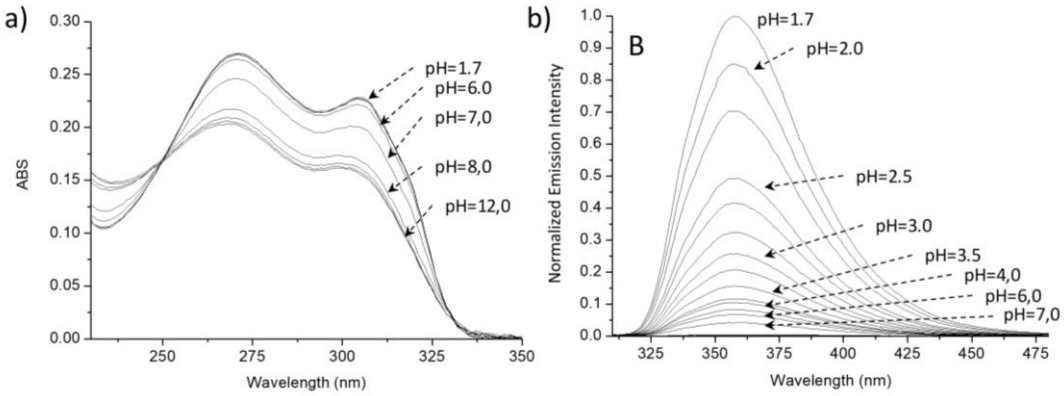

Figure 43. UV-Vis absorption (A) and emission (B) spectra of **L3** registered in a water/acetonitrile 70/30 v/v solvent mixture in the 1.7–12.0 pH range. [**L3**] = 1×10^{-5} mol dm^{-3} , 0.15 mol dm^{-3} $NaClO_4$, pH adjusted by adding $HClO_4$ and NaOH aqueous solutions. Emission spectra were acquired by excitation at λex = 306 nm and were corrected by taking into account the fall in absorbance at the excitation wavelength.

In acidic medium (pH = 1.7) **L3** shows two absorption bands at λmax = 306 nm (ε = 19 100 cm^{-1} mol^{-1} dm^3) and 272 nm (ε = 27 200 cm^{-1} mol^{-1} dm^3). By increasing the pH the absorbance of both bands drops with a very small displacement of the maxima: at pH = 12, the λ_{max} shifted, respectively, from 272 nm to 267 nm (ε = 19 400 cm^{-1} mol^{-1} dm^3) and from 306 nm to 300 nm (ε = 15 600 cm^{-1} mol^{-1} dm^3) (Figure 43a).

The same experiments carried out in fluorescence by exciting at λex = 306 nm show that **L3** is highly fluorescent in acidic medium, with an emission band centred at 358 nm (fluorescence quantum yield Φf = 0.15, Stokes-shift = 4750 cm^{-1}) (Figure 43b). By increasing the pH, the signal intensity decreases and is totally quenched at pH = 8. This phenomenon can be rationalized in terms of the excited state quenching effect (CHEQ) due to the PET from

the HOMO of the donor benzyl nitrogen atoms to the HOMO of the excited fluorophore moiety,[24] that can be observed only in the deprotonated form of **L3**, with the availability of a free lone pair on the nitrogen atoms.

Figure 44 reports the trend of the fluorescence emission at 358 nm as a function of pH. From pH = 2 to 4 an intensity drop (around 87%) is observed, followed by a plateau up to pH = 6, where the systems start to be completely quenched.

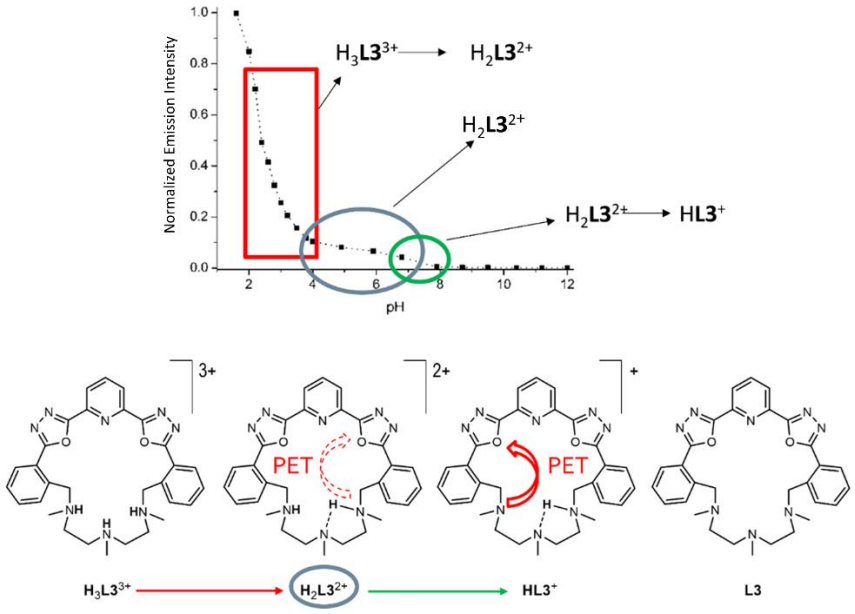

Figure 44. Proposed mechanism for the observed trend of the emission intensity at 358 nm as a function of pH. Experimental conditions: [**L3**] = 1 × 10^{-5} mol dm^{-3}, 0.15 mol dm^{-3} $NaClO_4$, pH adjusted by adding $HClO_4$ and NaOH aqueous solutions, λex = 306 nm. The emission intensity was corrected by taking into account the fall in the absorbance at the excitation wavelength.

This behaviour can be exploited in terms of PET effect, due to the different protonated species that are present in solution. The H_3**L3**$^{3+}$ species, where the three amine groups of the aliphatic chain are protonated, prevails at pH = 2. Indeed, in this species no free lone pairs are available for the establishment of the PET effect, causing the highest intensity of the signal. The drop in the emission from pH = 2 to 4 suggests the occurrence of the first deprotonation step involving an aliphatic amine and producing the H_2**L3**$^{2+}$ species (pKa1 =

2.2), generating a species able to give PET effect. Most of the fluorescence is indeed lost, although a residual emission can be observed probably due to the formation of an H-bond network between the free lone pair of the unprotonated amine and the protonated ones, partially preventing the PET effect. The plateau in the 4 - 6 pH range can be thus attributed to the H_2**L3**$^{2+}$ species that prevails in this range (pKa2 = 4.8). The fluorescence emission further drops in the 6 - 8 pH range, suggesting the occurrence of the second deprotonation step to form the H**L3**$^{+}$ species (pKa3 = 6.9). This deprotonation probably involves the benzylic position, that being close to the fluorophore moiety allows for the complete restoration of the PET effect, causing the total quenching of the emission. The final deprotonation step to give the **L3** species does not affect the emission behaviour.

The acid-base behaviour of **L3** was also studied through a ^{1}H NMR titration at various pH values in acetonitrile-*d3*/D_2O 50/50 v/v. The pH was adjusted to pH = 12 directly in the NMR tube by adding KOD and successively the pH was lowered by using DCl (Figure 45 a and b).

At pH 10 the ^{1}H NMR spectrum of **L3** shows five aliphatic and six aromatic signals: two singlets at δ = 1.84 ppm, integrating three protons (3H) and attributed to the resonance of H1 (H1, s, 3H), and 1.87 ppm (H4, s, 6H); two triplets at 2.09 ppm (H2, t, *J* = 7.6 Hz, 4H) and 2.38 ppm (H3, t, *J* = 7.6 Hz, 4H); a singlet at 3.81 ppm (H5, s, 4H); a multiplet ranging from 7.46 and 7.52 ppm (H6 and H8, m, 4H); a triplet at 7.60 ppm (H7, dt, *J* = 7.4, 1.2 Hz, 2H); a doublet at 7.85 ppm (H9, d, *J* = 7.6, 2H); a triplet at 8.28 ppm (H11, t, *J* = 8.0 Hz, 1H); a doublet at 8.45 ppm (H10, d, J = 7.6 Hz, 2H) (Figure 45a). The ^{13}C spectrum exhibits a total of 16 signals (see data in the Experimental Section, chapter 3.2.3), 11 for the aromatic and five for the aliphatic resonances. The ^{13}C spectrum, together with the ^{1}H spectrum, indicates a C2v symmetry of **L3** mediated on the NMR timescale. By lowering the pH to 8, all the aliphatic resonances undergo a downfield shift, with the signals of protons 1 and 2 showing the highest shift (Figure 45a). This suggests the occurrence of a protonation step to form the H**L3**$^{+}$ species, in which a H-bond is involved. The spectrum recorded at pH = 5 shows a downfield shift mainly

for the signals of protons 4, 5 and 3, suggesting a second protonation step leading to the formation of the H_2**L3**$^{2+}$ species. This result confirms the same behaviour deduced by the fluorescence experiments, namely the involvement of the aliphatic amines in benzylic positions. After lowering the pH to 2 another displacement of the H1 resonance is observed, suggesting a protonation step to form the H_3**L3**$^{3+}$ species involving the central aliphatic amine group (Figure 45b).

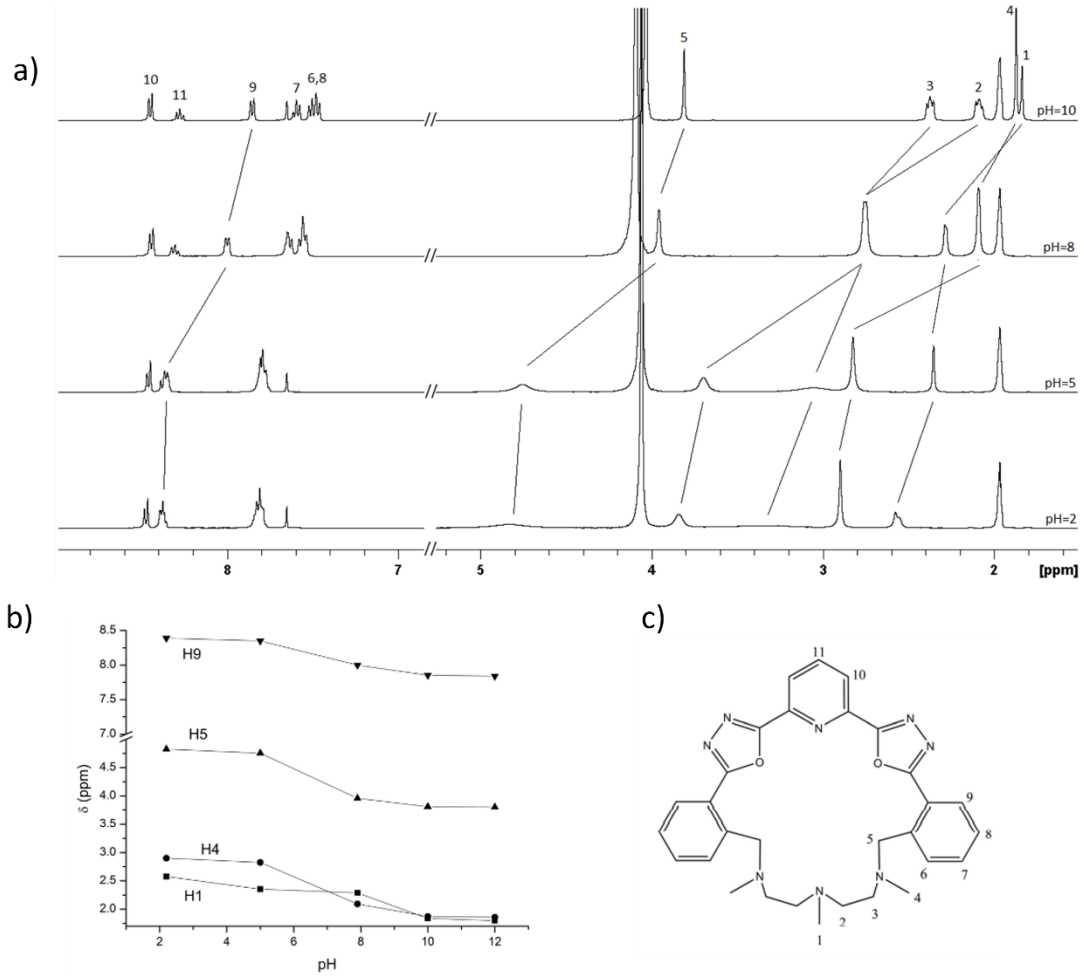

Figure 45. a) ^{1}H NMR spectra of **L3** recorded in acetonitrile-*d3*/D_2O 50:50 solution at pH = 10, 8, 5 and 2. b) Trend of selected ^{1}H NMR signals of **L3** protons in acetonitrile-*d3*/D_2O 50:50 solution as a function of pH (■ = H1, ● = H4, ▲= H5, ▼= H9). c) molecular structure of L3 together with atom labelling.

The ^{1}H aromatic signals of **L3** are not significantly perturbed by the variation of pH, suggesting that the POXAPy unit is not involved in any protonation step. Indeed, looking at the chemical

shifts of H10 and H11 attributed to the protonable pyridine moiety, they remained substantially unvaried by changing the pH. This result is in agreement with the spectrofluorimetric experiments, highlighting that no protonation step occurs on the POXAPy fluorophore. There is only a slight downfield shift attributed to H9, probably caused by the increased positive charge density on the polyamine fragment, that mainly affects the closest phenyl rings.[149]

The protonation of **L3** causes a broadening of the aliphatic resonances probably due to the stiffening of the structure that affects the conformational mobility on the NMR timescale. This result also confirms that only the aliphatic amines are involved during the protonation steps. Table 6 shows the protons distribution in the protonated species of **L3** deduced by the spectrophotometric, spectrofluorimetric and NMR experiments.

Table 6. Proposed position of the protons in the **L3** species based on fluorescence and ^{1}H NMR studies.

Highly fluorescent	**Slightly fluorescent**	**Non fluorescent**	
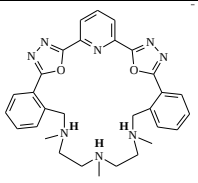	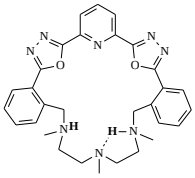	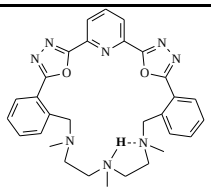	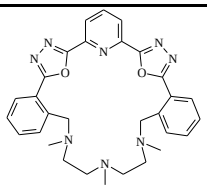
H_3**L3**$^{3+}$	H_2**L3**$^{2+}$	H**L3**$^{+}$	**L3**

2.3.3 Coordination behaviour

Spectrophotometric and spectrofluorimetric analysis were performed to investigate the coordination behaviour of **L3** towards metal ions. It is known, from the acid-base studies, that the emission properties of **L3** are PET-regulated through electron transfer from the lone pairs of the deprotonated aliphatic amine group to the excited fluorophore. For this reason, the coordination of a suitable metal ion into the cavity of free **L3** should change the emission intensity, preventing the PET effect.

L3, dissolved in water/acetonitrile 70/30 v/v solution at pH = 7.0 (HEPES buffer 10^{-3} mol dm^{-3}) shows two absorption bands at 270 nm (ε = 24 400 cm^{-1} mol^{-1} dm^3) and 305 nm (ε = 13 600 cm^{-1} mol^{-1} dm^3). Titrations were carried out by adding aqueous solutions of transition metal ions as a perchlorate salts. As shown in Figure 46, the addition of transition metal ions such as Ni(II), Cu(II), Zn(II) and Cd(II) does not change the shape of the absorption spectrum.

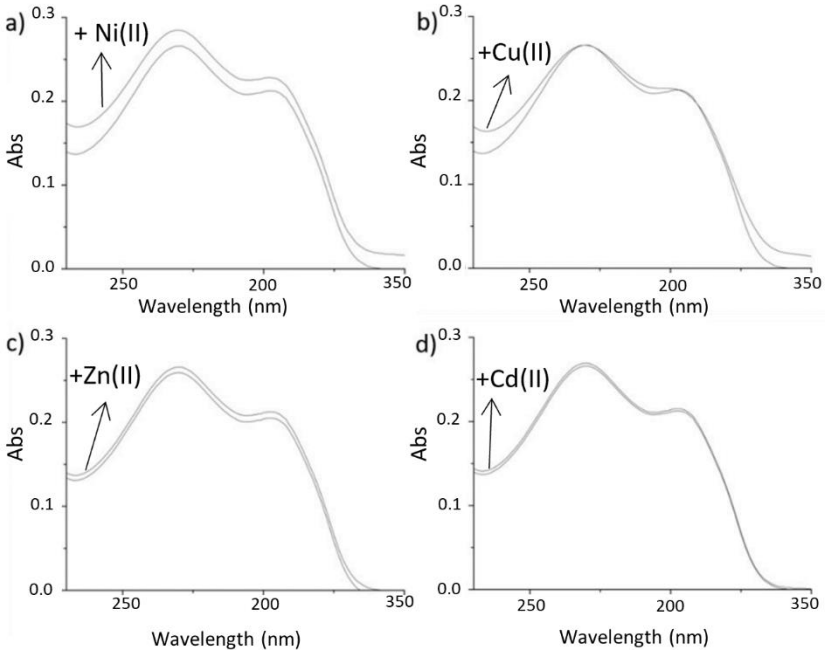

Figure 46. Absorption spectra of **L3** recorded in water/acetonitrile 70/30 v/v in the presence of a HEPES buffer (10^{-3} mol dm^{-3}) at pH = 7.0 and after addition of 2 equivalents of a) $Ni(ClO_4)_2$, b) $Cu(ClO_4)_2$, c) $Zn(ClO_4)_2$ and d) $Cd(ClO_4)_2$. ([**L3**] = $2 \cdot 10^{-5}$ mol dm^{-3}).

This can be justified by the involvement in the coordination of the sole aliphatic polyamine chain, meaning that the fluorophore does not participate in stabilizing the metal ion. Fluorescence emission of free **L3** at pH = 7.0 has a quantum yield Φf of 0.01 (λex = 300 nm), with the maximum at 360 nm. The addition of Cu(II) and Ni(II) ions displays a large CHQF effect, while the addition of d^{10} metal ions Zn(II) and Cd(II) induces a CHEF effect. Either way, the change in intensity occurs without a significant shift of the maximum emission wavelength (Figure 47). This is the typical behaviour of all PET-regulated sensors, where the metal ion is coordinated by the amine functions of the aliphatic chain linked to the fluorophore through a spacer.

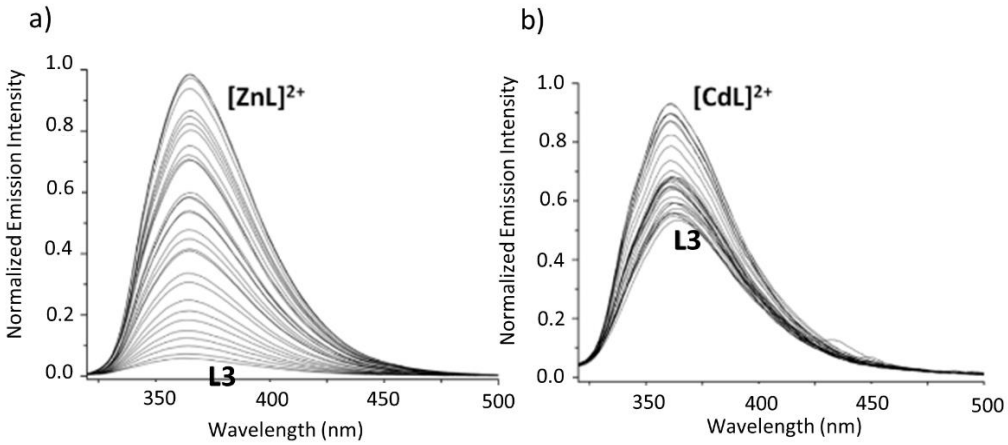

Figure 47. Fluorescence spectra of **L3** (λ_{ex} = 300 nm) registered in water/acetonitrile 70/30 v/v in the presence of a HEPES buffer (10^{-3} mol dm^{-3}) at pH = 7.0 by adding $Zn(ClO_4)_2$ (**A**) and $Cd(ClO_4)_2$ (**B**). ([**L3**] = $2 \cdot 10^{-5}$ mol dm^{-3}).

Cu(II) and Ni(II) ions, being paramagnetic metal ions, totally quench the emission, while diamagnetic close shell ions are able to restore the intrinsic fluorescence of the fluorophore preventing the PET effect.

In the case of Zn(II), the fluorescence emission intensity increases linearly up to one equivalent and then remains constant, suggesting the formation of the mononuclear species

(Figure 47a and 48). It was not possible to determine the value of the formation constant for the [Zn**L3**]$^{2+}$ species because it is too high to be reliably determined spectrophotometrically.

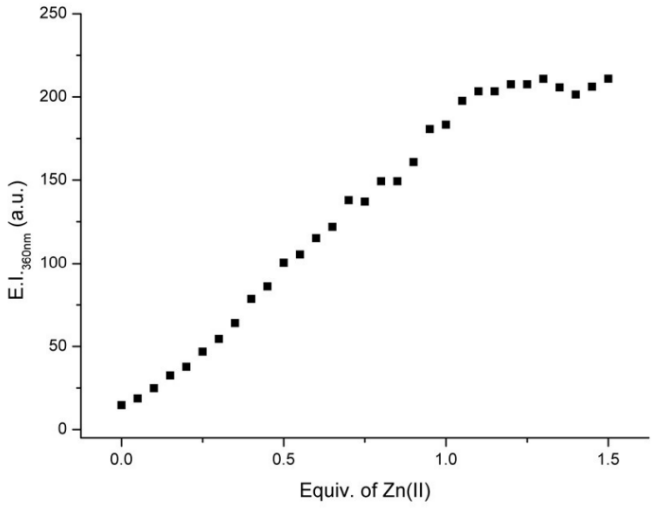

Figure 48. Variation of the emission intensity at 360 nm as a function of the added equivalents of Zn(II) registered in water/acetonitrile 70/30 v/v in the presence of a HEPES buffer (10^{-3} mol dm^{-3}) at pH = 7.0 (λex = 300 nm, [**L3**] = $2 \cdot 10^{-5}$ mol dm^{-3}).

Cd(II) ion gives the same effect as Zn(II), but while Zn(II) increases the intensity by about 17 times with respect to the free **L3**, Cd(II) only doubles it (Figure 47b).

In any case, the addition of further equivalents of metal ions does not change the fluorescence emission intensity, suggesting the formation of sole mononuclear species [M**L3**]$^{2+}$.

Other metal ions, such as Na(I), K(I), Mg(II) and Ca(II) were tested under the same conditions, resulting in a non-perturbation of the absorption and emission spectra of **L3**, revealing no interaction between **L3** and such ions. Competition experiments were carried out by adding two equivalents of all studied metal ions (Ni(II), Cu(II), Cd(II)) to a pH 7.0 buffer solution containing the preformed [Zn**L3**]$^{2+}$ complex (Figure 49). The results suggest that the presence of other metals does not perturb the emission caused by Zn(II), except for Cu(II), for which the system shows a partial quenching of the emission.

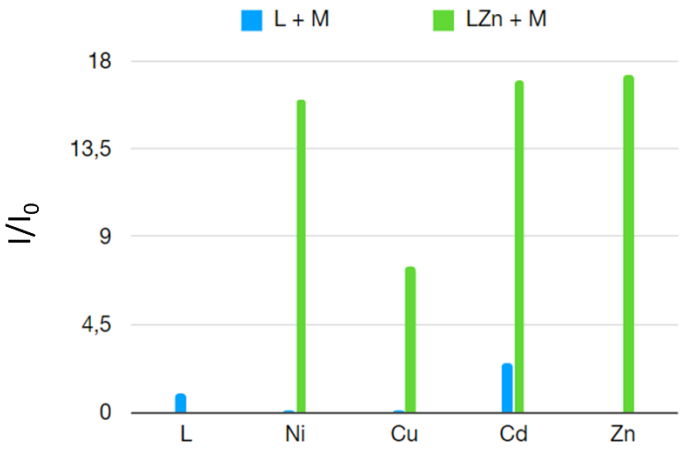

Figure 49. Relative emission intensity (I/I_0) upon the addition of selected metal ions (one equiv.) to **L3** in water/acetonitrile 70/30 v/v in the presence of a HEPES buffer (10^{-3} mol dm^{-3}) at pH = 7.0. I and I_0 are the emission intensities of the ligand in the presence and absence of the metal ion, respectively.

An NMR titration with Zn(II) was performed to better investigate the binding properties of **L3**. In the mixed water/acetonitrile 70/30 (v/v) solvent the complex is poorly soluble, thus the ^{1}H NMR titration was performed by adding the guest to a 1×10^{-2} mol dm^{-3} solution of **L3** in acetonitrile-d3. The ^{1}H NMR spectrum of **L3** shows six aromatic and five aliphatic signals: δ = 8.47 ppm (H10, d, J = 7.6 Hz, 2H); 8.24 ppm (H11, t, J = 7.6 Hz, 1H); 7.87 ppm (H9, dd, J = 7.6, 1.2 Hz, 2H); 7.59 ppm (H7, dt, J = 7.6, 1.6 Hz, 2H); 7.51 ppm (H8, dt, J = 7.2, 1.2 Hz, 2H); 7.47 ppm (H6, d, J = 7.2 Hz, 2H); 3.83 ppm (H5, s, 4H); 2.37 ppm (H3, m, 4H); 2.03 ppm (H2, m, 4H); 1.87 ppm (H4, s, 6H); 1.85 ppm (H1, s, 3H). The ^{1}H spectrum, together with the ^{13}C spectrum, which shows 16 signals (see Experimental chapter), five for the aliphatic and 11 for the aromatic resonances, suggests a C2v symmetry of the free ligand. The spectra obtained upon the addition of a 5×10^{-2} mol dm^{-3} solution of Zn(II) to **L3** are reported in Figure 50. By adding Zn(II) ions, it is possible to observe a downfield shift of all signals due the coordination of Zn(II) that determines a decrease of the electronic density. The aliphatic signals are more perturbed by the presence of Zn(II) ions than the aromatic ones, probably because in acetonitrile the metal ion is mainly coordinated by the tertiary aliphatic amine

groups. The signals attributed to the protons of the central pyridine moiety remained unvaried, meaning that this fragment is not involved in the coordination.

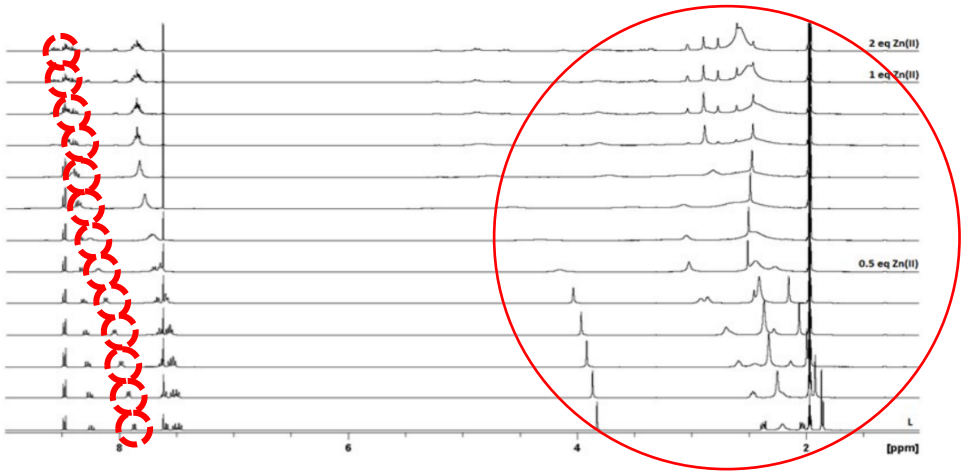

Figure 50. ^{1}H NMR spectra of **L3** recorded in acetonitrile-*d3* upon stepwise addition of Zn(II) ion as perchlorate salt. ([**L3**] = $1 \cdot 10^{-2}$ mol dm^{-3}, [Zn(II)] = $5 \cdot 10^{-2}$ mol dm^{-3}, 298 K).

The observed anomalous downfield shift of the H9 resonance is probably due to the stiffening of the structure upon the ion coordination that allows for the formation of an H-bond network between H9 and the nitrogen atoms of the ODA ring (Figure 51).

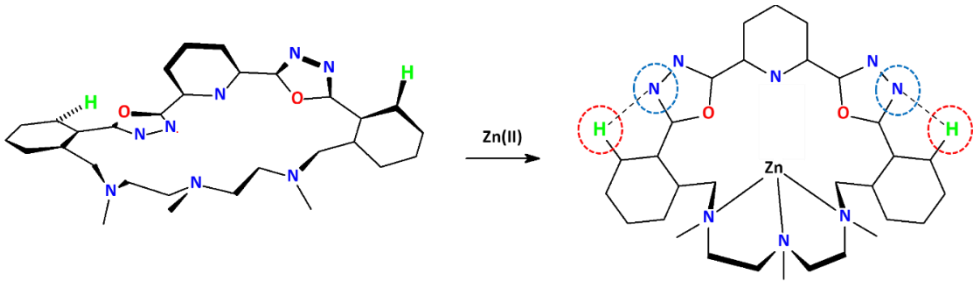

Figure 51. Probable H-bond network formation.

The broadening of the NMR spectrum and the non-equivalence of the signals of the methylene and methyl groups suggest the loss of symmetry of the ligand upon complex formation and a possible coexistence of more complex species in equilibrium with each other on the NMR timescale. Finally, the NMR and spectrophotometric studies are in agreement, both suggesting the formation of the sole mononuclear [Zn**L3**]$^{2+}$ species.

2.3.4 Conclusion

Macrocycle **L3** was obtained through the cyclization between the new POXAPYy (2,6-bis(5-(2-methylphenyl)-1,3,4-oxadiazol-2-yl)pyridine) fluorophore fragment and the 1,4,7-trimethyl-1,4,7-triazaheptane polyamine. The yield of the process to obtain both the POXAPy fragment and **L3** is very high. The free ligand was also characterized in the solid state. **L3** is composed by two distinct units: a penta-connected aromatic rings, with a central pyridine featuring at positions 2 and 6 two ODA rings both linked to a further phenyl ring, as the fluorescent sensing unit, and an aliphatic polyamine suitable for metal ion coordination.

L3 is fluorescent only at acidic pH when the amines of the aliphatic chain are protonated, meaning that it is a PET-mediated chemosensor. It has a lambda em at 360 nm, and is visible to the naked eye uder a UV lamp. **L3** is able to detect the presence of Cd(II) and Zn(II) metal ions through an enhancement of the fluorescence emission in aqueous medium (H_2O/ACN 70/30) at pH = 7. Solution studies suggested the formation of the mononuclear species between **L3** and the metal ion. The metals switch ON the emission with a CHEF effect (17-times for Zn(II)). While the absorption wavelength of the new synthesized POXAPy fluorophore (306 nm) is significantly longer compared to that of PPD (280 nm), their emission wavelengths fall in the same spectral range (360 nm for **L3** vs 350 nm for PPD-based systems).[17,18] This means that the extension of the π-system in POXAPy did not give a red-shift of the emission band with respect to that of PPD. This is probably due to the fact that in the excited state the five rings of POXAPy are not all coplanar, similarly to what observed in the solid state, and only the coplanar portion of the fluorophore is emissive. Probably, only three consecutive rings of the POXAPy fragment of **L3** can be stably coplanar, as suggested by the emission wavelength (λem = 360 nm) and confirmed by the X-ray crystal structure.

To the best of our knowledge, **L3** is the first sensor to be based on the POXAPy fluorophore unit. It is able to selectively detect Zn(II) metal ion in an aqueous media also in the presence of other transition, alkali and alkaline earth metal ions.

It is certainly interesting to continue the study on this new fluorophore system by designing further macrocycle- and open-chain ligands by varying the aliphatic polyamine receptor moiety.

2.4 Results and Discussion of L4

The following ligands have been designed to work as ratiometric sensors for transition metal ions. Most of the sensors for such guests are constituted by a polyamine chain, as the receptor moiety, linked to a fluorophore through a spacer, with a final linear or macrocyclic topology, and usually act via a PET mechanism. When the metal ion is coordinated to the ligand, the lone pairs of the amine nitrogen are not available and the PET effect is prevented; as a consequence, the fluorescence emission increases.[150] The biggest issue of PET-based sensors is to be easily perturbed by the pH, and the protonation of the polyamine chain can be misunderstood. To avoid this problem, sensors working through other mechanisms have been developed.[6,111]

For example, ESIPT mechanism was demonstrated to be active in ligands featuring an intramolecular hydrogen bond between a proton donor functional group, such as the hydroxyl group, and a proton acceptor moiety, such as an imine, hydrazide or hydrazine group. Upon excitation these molecules undergo a photo-induced tautomerization with formation of the conjugate keto form that emits at longer wavelength than the enol form, giving rise to a high Stokes shift.

Several receptors based on ESIPT paradigm have been synthesized by linking a suitable ESIPT fluorophore to a receptor unit.[115,151,152]

This chapter describes the preliminary studies on the coordination and photochemical properties of a new 2,6-bis(2-oxazolyl)phenol-based macrocycle (**L4**), which is part of a new series of ligands that was synthesized by incorporating different fluorophore moieties, namely 2,6-bis(2-ossazolyl)phenol (BPhB), 2,6-bis(2-ossazolyl)pyridine (BPyB) and 1,3-bis(2-ossazolyl)phenyl (BBzB), in a polyamine-macrocycle, respectively **Lc**, **Ld** and **L4** (Scheme 11). The macrocyclic structures of the ligands, constituted by a 1,3-bis(2-ossazolyl)aryl derivatives fluorophore and a triethylentetraamine chain, were synthesized by using the Richmann-

Atkins anellation between 1,3-bis(4-bromomethylbenzoxazol-2-yl)aryl derivates and 1,4,7,10-tetrakis(4-toluensulphonyl)-1,4,7,9-tetraazadecane, followed by the removal of the four sulphonyl groups on the amines by treatment with HBr in acetic acid in the presence of phenol as scavenger. The ligands were purified as tetrahydrobromide salt (**L**·4HBr) by re-crystallization from hot ethanol.

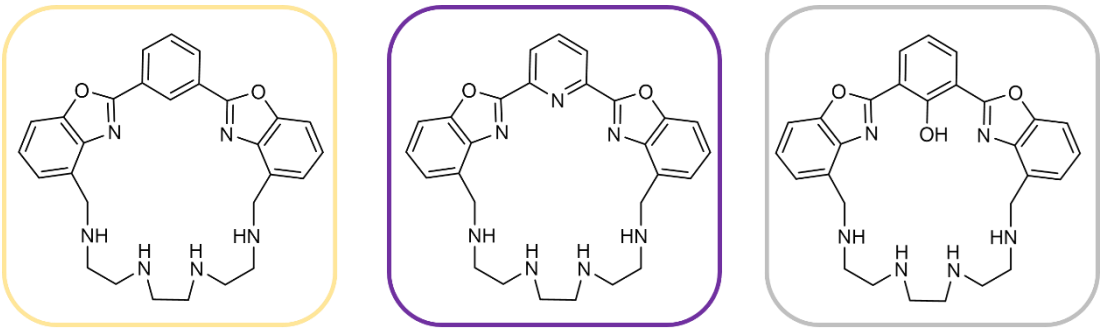

Scheme 11. Structures of the synthesized macrocycles.

The three ligands, differing for the fluorophore, can be activated by different photochemical mechanisms.

L4 can act as an ESIPT system, since it features suitable properties. Indeed, the most common ESIPT fluorophores are based on systems containing a phenol as H-bond donor and an N-heterocycle as H-bond acceptor, such as 2-(2-hydroxyphenyl)benzimidazole (HBI), 2-(2-hydroxyphenyl)benzoxazole (HBO) and 2-(2-hydroxyphenyl)benzothiazole (HBT) (Figure 52) (see chapter 1.3.3 for ESIPT mechanism paradigm).

In the ground state, the fluorophore is stable as enol form (E), but upon photoexcitation (E*) a redistribution of the electronic density takes place resulting in a greater acidity for the hydrogen bond donor group and an increased basicity for the hydrogen bond acceptor within the enol form. This determines the transfer of the acidic H^+ ion from the H-bond donor to the acceptor giving rise to the keto-tautomer, that is the most stable form in the excited state

(K*). In the case in which the excited keto-form radiatively decays, a fluorescence emission is detected. The emission wavelength is strongly red shifted with respect to the excitation one, due to the fact that in the ground state the enol form is more stable than the keto form, while in the excited state the stability is inverted, resulting in a higher absorption energy gap between E and E* than between K* and K. After the emission, in the ground state K converts into E through a reverse proton transfer (RPT) process.

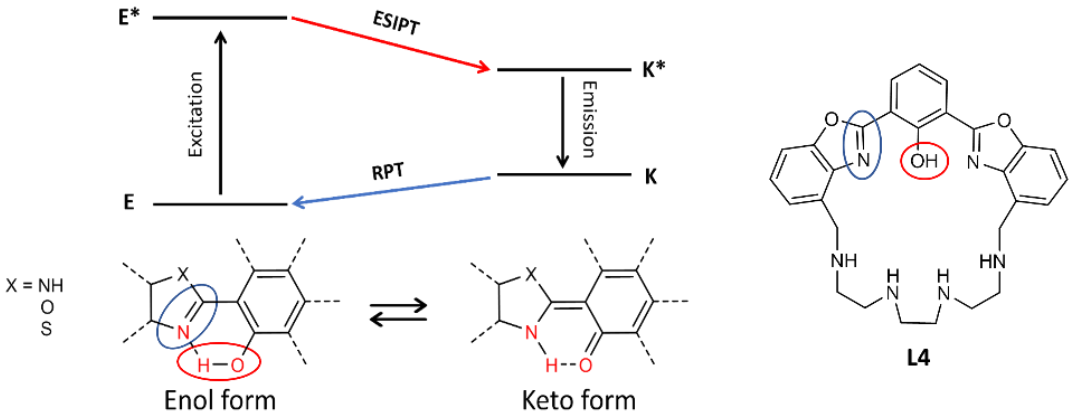

Figure 52. Schematic representation of the structural characteristics of **L4** that make it an ESIPT sensor. Circled in red: the phenol group acting as H-bond donor. Circled in blue: the N-heterocycle acting as H-bond acceptors

Spectrophotometric and spectrofluorimetric studies were performed to evaluate the acid-base behaviour and coordination properties of **L4** towards some selected transition metal ions such as Zn(II), Cd(II) and Pb(II), and in particular to understand the role of the hydroxyl group of the central phenol ring in the interaction.

2.4.1 Spectrochemical properties as a function of pH

The spectrochemical behaviour of **L4** has been studied acquiring by UV-Vis absorption and emission spectra in aqueous solution at various pH conditions (Figure 53). An aqueous solution of **L4** ($1 \cdot 10^{-5}$ mol dm^{-3}) was adjusted at pH 2.0 with 0.1 mol dm^{-3} aqueous HCl and a 0.1 mol dm^{-3} aqueous solution of NaOH was added dropwise until pH = 12.0. At pH 2.0 the absorption spectrum exhibits two main bands, at 293 nm (ε = 23700 cm^{-1} mol^{-1} dm^3), attributed to the π−π* transition, and 342 nm (ε = 16600 cm^{-1} mol^{-1} dm^3), attributed to the n−π* transition. By increasing the pH, a gradual drop in absorptivity of these bands together with the growth of a new band at 405 nm take place (Figure 53). This new band has been attributed to the n−π* transition of the deprotonated form of the BPhB moiety. At pH=12 the absorption at 342 nm totally disappears and the band at 405 nm reaches its maximum intensity (ε = 8700 cm^{-1} mol^{-1} dm^3), thus the trend of these two bands can be considered as an indicator of the protonation state of the fluorophore. A well defined isosbestic point at 367 nm is observed.

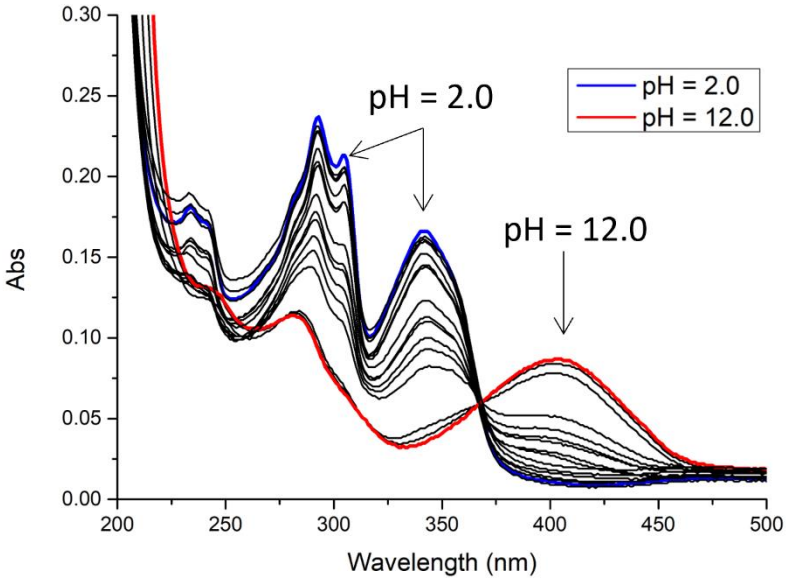

Figure 53. UV-Vis absorption spectra of **L4** registered in aqueous solution in the 2.0 − 12.0 pH range at 298 K. Experimental conditions: [**L4**] = $1 \cdot 10^{-5}$ mol dm^{-3}, pH adjusted by adding HCl and NaOH aqueous solutions.

The emission behaviour as a function of pH is quite complex. By exciting at 342 nm, in acidic solution (pH=2) two emission bands at 380 and 507 nm were observed (Stokes shifts = 2924 and 9516 cm^{-1}, respectively) (Figure 54 and 56a). By increasing the pH, and keeping constant the excitation wavelength, both bands undergo a decrease of emission intensity due to the drop of absorptivity at the excitation wavelength (Figure 54 and 56a). At pH=6 the complete disappearance of the band at 380 nm takes place and from this pH only the emission at 507 nm is visible. At pH=12, when the deprotonated form of **L4** is prevalent in solution, a single intermediate emission band at 476 nm was detected (Figure 54 and 56a). Thus, considering the overall fluorescence behaviour of the ligand, we can attribute the emission band at higher energy (380 nm) to the enol form of **L4**, that at lower energy (507 nm) to the keto form and that at 476 nm to the deprotonated form.

In order to confirm this attribution a second set of emission spectra were acquired by exciting at 405 nm in correspondence of the absorption band of the deprotonated form, observing a single emission band at 476 nm (Stokes shift = 3992 cm^{-1}) that decreases in intensity going from basic to acid pH in agreement with the decrease in absorbance of the deprotonation excitation band (Figure 56b).

A final set of pH-dependent emission spectra was acquired by exciting at the isosbestic point (λ_{ex} = 367 nm, Figure 56c) with the aim to appreciate the transition between the keto emission band at 507 nm, observable at acidic pH values, and the deprotonation emission band at 476 nm, observable at pH values up to 10. As previously affirmed, when the fluorophore is in the protonated form, ESIPT is allowed and the main emission takes place at 507 nm, while when the fluorophore is in the deprotonated form the emission band at 476 nm is observed. By gradually increasing the pH from 2 to 12 the superimposition of the two bands was observed, resulting in a sort of continuous transition of the emission band wavelength from 507 nm to 476 nm, as depicted in Figure 56c.

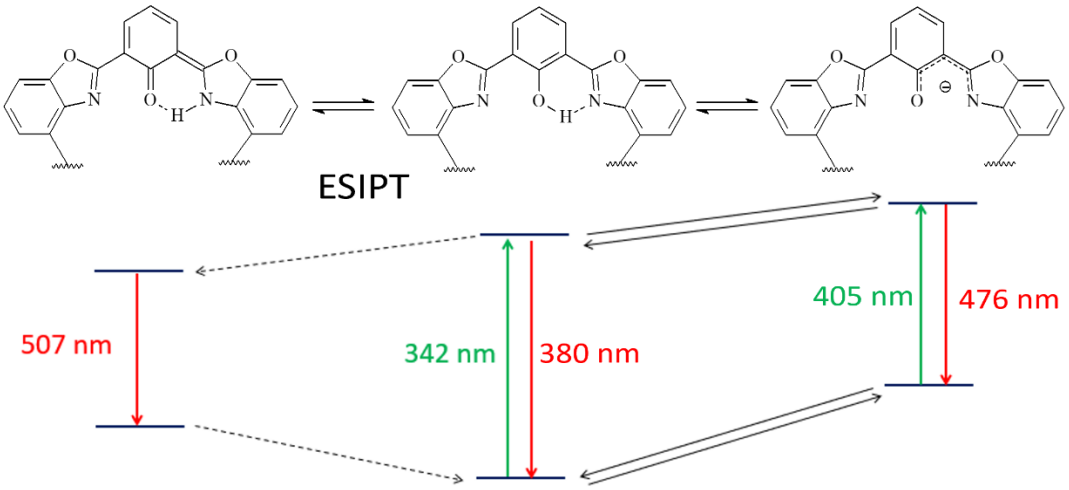

Figure 54. Schematic representation of ESIPT mechanism.

By examining the trend of the displacement of the emission wavelength as a function of pH emerges that the deprotonation of the BPhB fluorophore takes place around pH 9.5 (Figure 55).

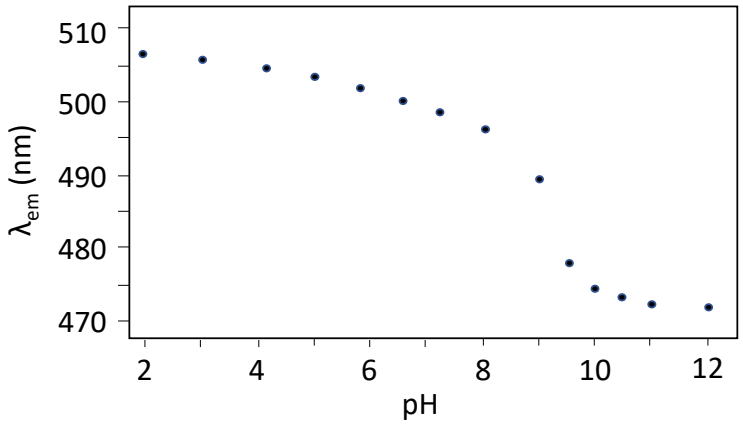

Figure 55. Trend of the observed emission maximum wavelength of **L4** as a function of pH.

Noteworthy, due to the ESIPT process, while the absorption band of the protonated form is located at higher energy than that of the deprotonated one, the emission bands behave contrarily. Another peculiarity is that in this ligand the polyamine chain does not influence the emission behaviour at any pH value.

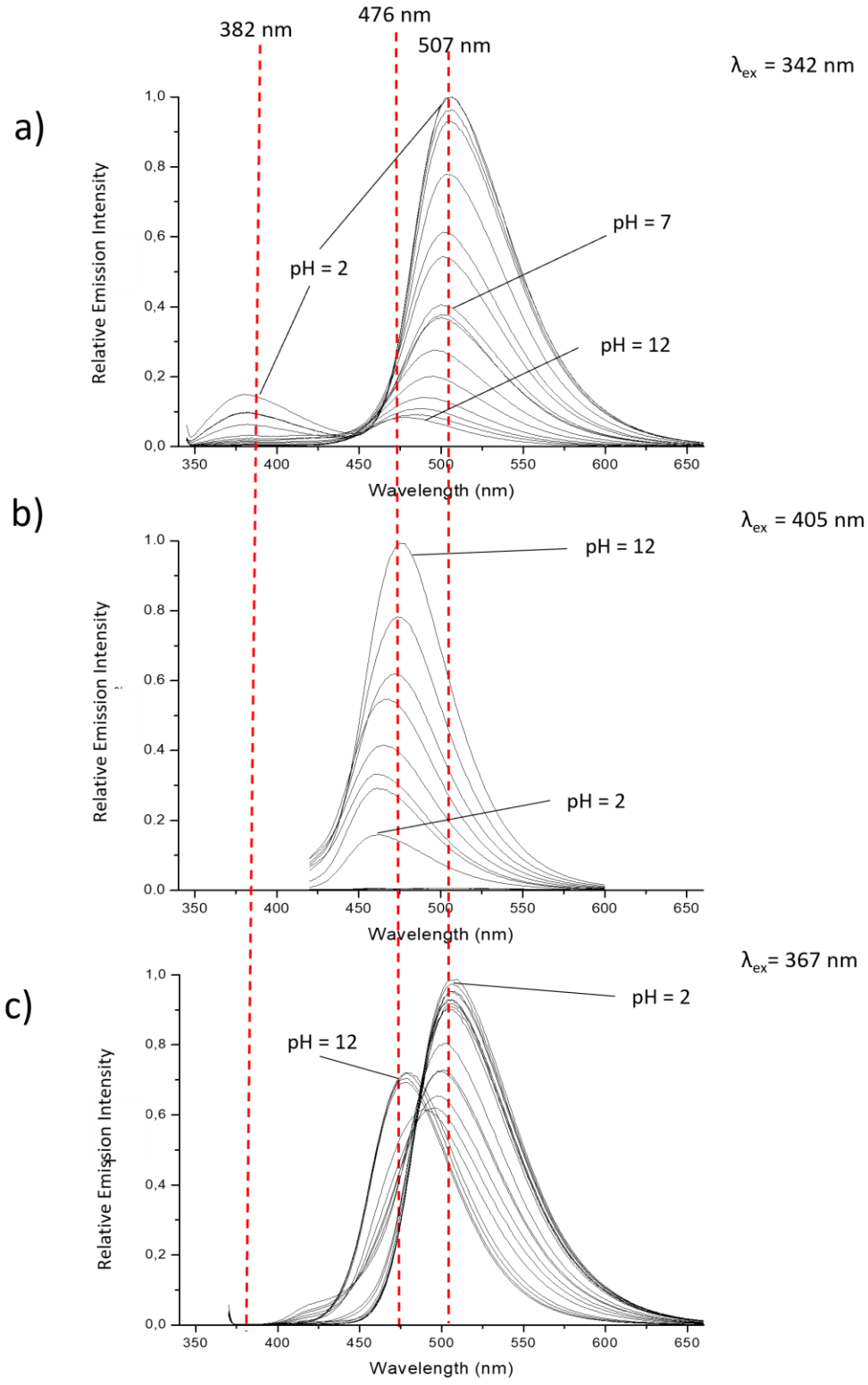

Figure 56. Fluorescence spectra of **L4** registered in aqueous solution in the pH range of 2.0 − 12.0 at 298 K. Experimental condition: [**L4**] = $1 \cdot 10^{-5}$ mol dm^{-3}, pH adjusted by adding HCl and NaOH aqueous solutions. a) λex = 342 nm; b) λex = 405 nm, c) λex = 367 nm.

2.4.2 Coordination behaviour

Spectrophotometric and spectrofluorimetric titrations were carried out by adding Zn(II), Cd(II) and Pb(II) metal ions as perchlorate salts to an aqueous solution of **L4** buffered at pH = 7.0 (TRIS). As shown in Figure 57, the addition of the metal ions caused a decrease in the absorption band at 342 nm, attributed to the enol form, and the growth of a new band at 405 nm, attributed to the deprotonated form of **L4**. The presence of this new band suggests the involvement of the phenol -OH group in the coordination, in fact the interaction of a metal ion increases the acidity of the phenolic function. The addition of Zn(II) ions caused a linear increase of the absorbance of the band at 405 nm up to two equivalents, then a plateau is reached, suggesting the formation of the species with a 1:2 **L4** to Zn(II) ratio (Figure 57a). On the contrary, the addition of Cd(II) and Pb(II) ions caused an increase of the absorbance of the same band only until one equivalent, suggesting the formation of the mononuclear species (Figure 57b and 57c).

These trends are confirmed by the fluorescence titrations performed by adding the metal ions to a buffered solution of **L4** at pH = 7 (TRIS 10^{-3} mol dm^{-3}, [**L4**] = $1 \cdot 10^{-5}$ mol dm^{-3}) and exciting at the isosbestic point (λex = 367 nm). In these conditions **L4** shows an intense emission band at 507 nm (Figure 58). The addition of a metal ion caused the decrease of the keto band for all three metal ions tested. In particular, the addition of Zn(II) caused a decrease of the keto band and the growth of a new emission band at 476 nm, relative to the deprotonated form, whose emission increases up to two equivalent of Zn(II) and then remains constant (Figure 58a). The addition of Cd(II) caused a decrease of the keto band and the appearance of the band at 476 nm (Figure 58b), while the addition of Pb(II) caused a total quench of the band relative to the keto form after the addition of one equivalent of the metal ion (Figure 58c), without the appearance of the emission at 476 nm.

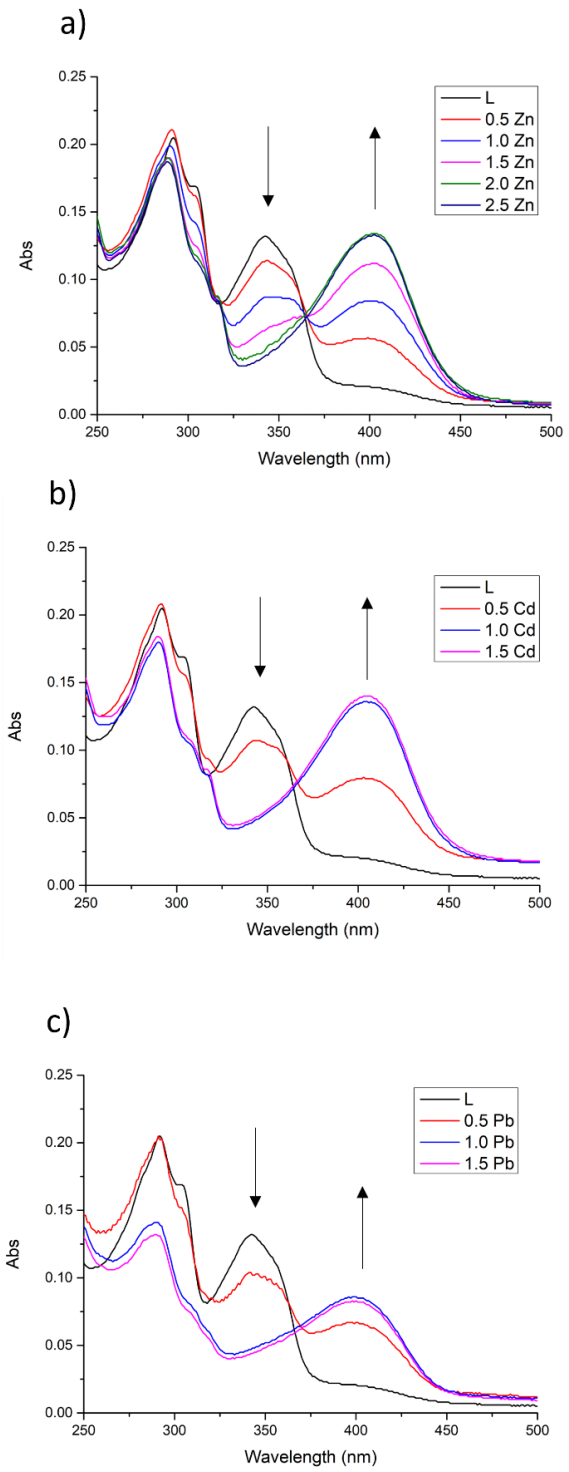

Figure 57. UV-Vis absorption titrations of **L4** with a) Zn(II); b) Cd(II); c) Pb(II), added as perchlorate salt, registered in aqueous solution at pH = 7 (TRIS 0.001 mol dm^{-3}) at 298 K. [**L4**] = $1 \cdot 10^{-5}$ mol dm^{-3}.

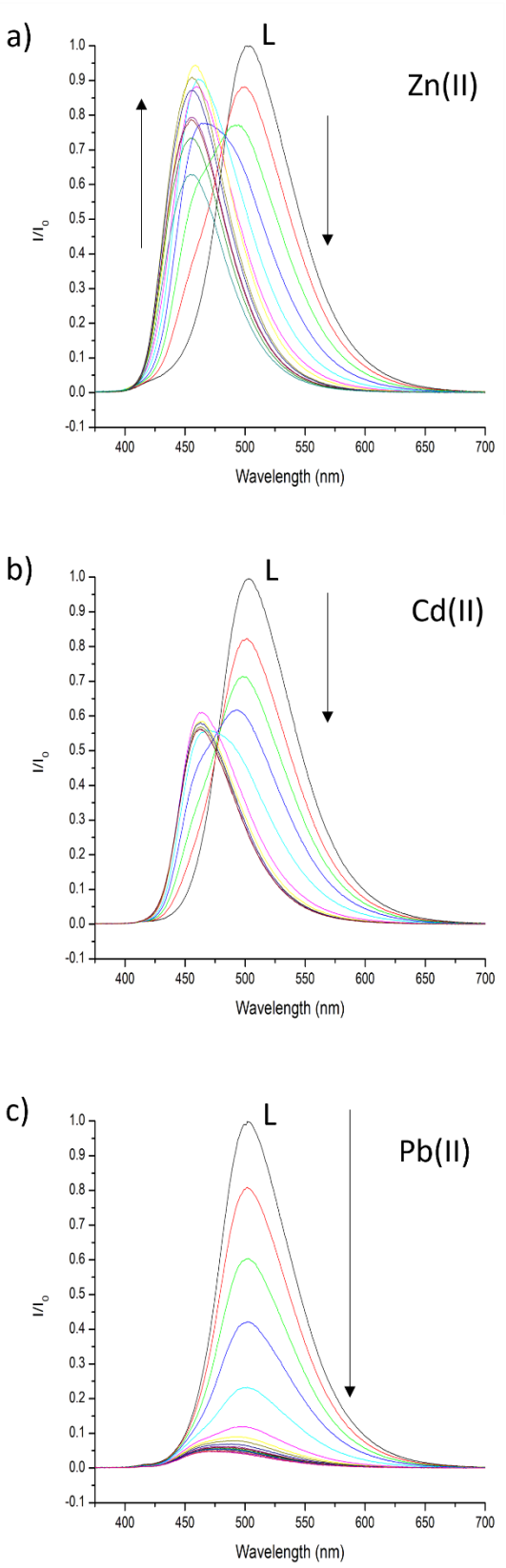

Figure 58. Fluorescence titrations of **L4** with a) Zn(II); b) Cd(II); c) Pb(II), added as perchlorate salt, registered in aqueous solution at pH = 7 (TRIS 0.001 mol dm^{-3}) at 298 K. [**L4**] = $1 \cdot 10^{-5}$ mol dm^{-3}.

These results confirmed the stoichiometry already suggested by the UV-Vis studies, namely **L4** forms a complex with a 1:2 ligand to Zn(II) ratio, while the mononuclear species forms with Cd(II) and Pb(II). The Pb(II) complex is not fluorescent, probably due to the reducing nature of Pb(II) that can quench the emission of the fluorophore by metal-to-ligand PET mechanism. This aspect must to be studied more in depth by evaluating the lifetime of the excited states.

The possibility for **L4** to host two Zn(II) ions to form the 1:2 complex was studied by DFT calculations, as showed in Figure 59, in which are reported the possible conformations of **L4** upon the Zn(II) ion coordination. The four structures represented in Figure 59 have been optimized using DFT method and demonstrate that the cavity of **L4** can host one or two Zn(II) metal ions (grey balls in the figure). In each structure the phenolic OH group is involved in the coordination of the metal ion in its deprotonated form. In the dinuclear species this group bridges the two Zn(II) ions that are forced to stay close to each other and could cooperate in the coordination of an external host, for example a chloride anion (the green ball in the figure). A similar arrangement was found in the dinuclear nickel (II) complex of the polyamino phenolic macrocycle reported in Figure 60.[153]

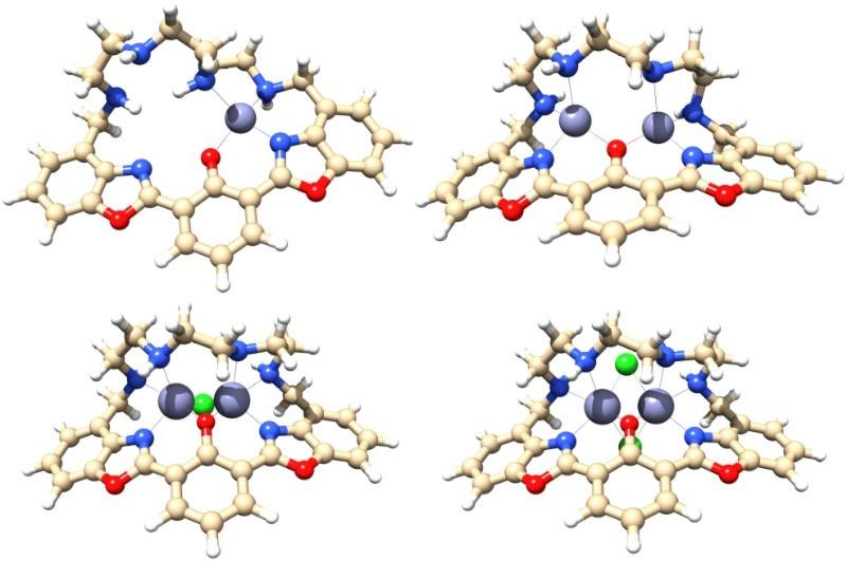

Figure 59. DFT calculations on the possible conformations of **L4** with Zn(II).

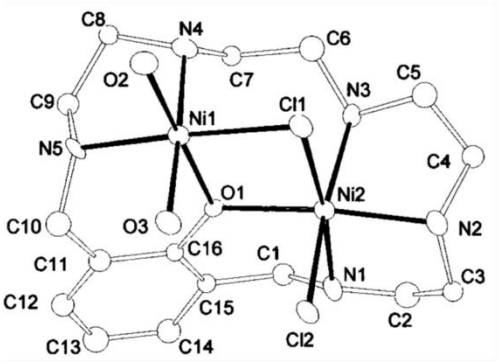

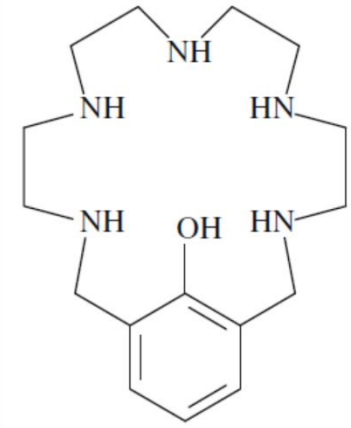

Figure 60. Dinuclear nickel (II) complex of the the polyamino phenolic macrocycle reported in this figure.

Finally, the interaction of **L4** with the metal ions can be evaluated with the naked eye by lighting up an aqueous solution of **L4** at pH = 7 with an UV lamp at 365 nm. In this conditions, the free **L4** appears green. Due to the ratiometric nature of the signal the presence of Zn(II) and Cd(II) ions determines a clear change of colour from green to blue (Figure 61). Further studies are in progress to characterize the emission using the chromatic coordinate in order to obtain information about the concentration of the sample.

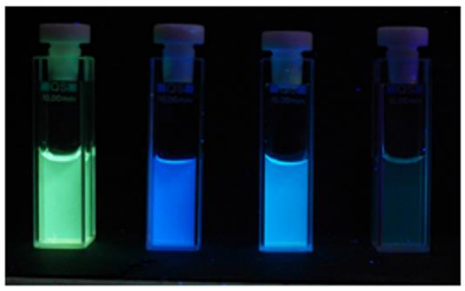

Figure 61. The colour change from green to blue after the addition of Zn(II) and Cd(II) and the quenching of the fluorescence after the addition of Pb(II), visible under a 365 nm UV lamp.

2.4.3 Conclusion

In this chapter, preliminary studies on the coordinative and photochemical properties of **L4** in aqueous solution at pH = 7 are reported. **L4** features a 2,6-bis(2-ossazolyl)phenol fragment that acts as the signalling moiety working through an ESIPT mechanism of signal transduction with a double peculiar emission band relative to the keto and enol form. **L4** is able to bind Zn(II), giving rise to the complex with a 1:2 ligand to metal ratio, also confirmed by DFT calculations. On the contrary, only the mononuclear species form with Cd(II) and Pb(II). The ligand binds the metal ions involving the oxygen atom of the phenol -OH group. Among the metal tested only Zn(II) causes an increase of the emission band relative to the deprotonated form of the **L4**. Due to the ratiometric nature of the ligand the presence of Zn(II) and Cd(II) can also be detected through a clear change of colour from green to blue. The ratio between the emission intensity of the keto and the deprotonated form could provide a direct measure of the Zn(II) level in the sample at pH = 7. Indeed, a future perspective is to further investigate this quantification method. In the future, the coordinative and photochemical properties of **Lc** and **Ld** macrocycles are going to be studied, probably showing different signal transduction mechanisms.

Chapter 3 - Experimental Section

3.1 General Overview of the Scientific Methods & Instruments

Synthesis and Characterization of the Ligands

All reactions involving moisture-sensitive reagents were carried out under a nitrogen atmosphere using standard vacuum line techniques and glassware that was flame-dried before use. All other solvents and reagents were used as supplied (analytical or HPLC grade) without prior purification. All chemicals were purchased from Aldrich, Fluka and Lancaster in the highest quality commercially available. All the solvents were dried prior to use.

NMR Spectroscopy

^{1}H- and ^{13}C-NMR spectra were recorded on a Bruker Avance 400 instrument, operating at 400.13 and 100.61 MHz, respectively, and equipped with a variable temperature controller. The temperature of the NMR probe was calibrated using 1,2-ethandiol as calibration sample. For the spectra recorded in $CDCl_3$, and DMSO-d_6 the ^{1}H and ^{13}C peak positions are reported with respect to the residual solvent. Chemical shifts (δ scale) are reported in parts per million (ppm values) and coupling constants (*J* values) are given in hertz (Hz). ^{1}H-^{1}H and ^{1}H-^{13}C correlation experiments were performed to assign the signals.

Elemental Analysis

Elemental analyses were performed with a Thermo Finnigan Flash 1112 EA CHN analyser.

UV-Vis and Fluorescence Spectroscopy

UV-Vis absorption spectra were recorded at 298.1 K on a Varian Cary-100 spectrophotometer equipped with a temperature control unit. Fluorescence emission spectra were recorded at 298.1 K on a Varian CaryEclipse spectrofluorimeter and the spectra are uncorrected. Emission quantum yields were calculated using 2,2'-biphenol in acetonitrile as standard ($\varphi^{\cdot}em$ = 0.29).[154] The HypSpec computer program (HYPERQUAD package) was used to process the

spectrophotometric data.[154] The pH-metric UV-Vis and fluorescence titration were carried out adjusting the pH by adding of NaOH or HClO4 and values were corrected considering the autoprotolysis product of the solvent mixture (pKw = 14.62).[155] At least three sets of spectrophotometric titration curves for each metal/L system were performed. All sets of curves were treated either as single sets or as separate entities, for each system; no significant variations were found in the values of the determined constants. LOD, LOQ and LOL were calculated by linear regression of normalized emission intensity as a function of concentration of the metal.[123]

3.2 Synthesis of the Ligands

3.2.1 Synthesis and Characterization of [Pd(H$_{-2}$L1)]

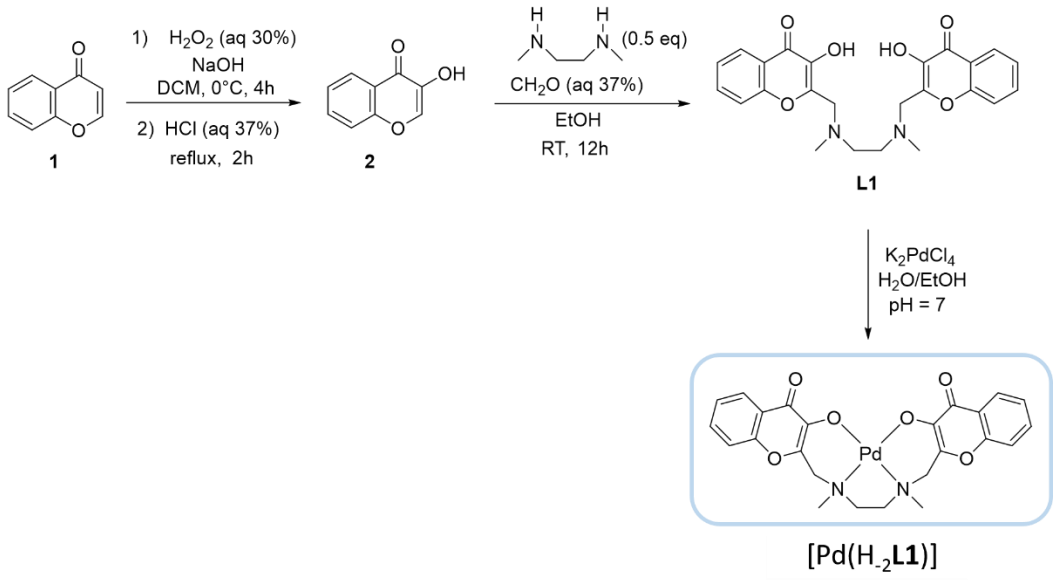

Scheme 12. Synthesis of [Pd(H$_{-2}$**L1**)]

3-hydroxychromone (2)

Based on a literature procedure[156], NaOH (71.0 mg, 1.77 mmol) was dissolve in a hydrogen peroxide 30% solution (0.2 ml, 0.89 mmol) at 0°C. Then this solution was slowly added to a solution of chromone (**1**) (200 mg, 0.89 mmol) in dichloromethane (DCM) (3 ml). The mixture was stirred 3 h at 0°C, and added more solution of NaOH and Hydrogen peroxide until the starting was finished. The reaction was quenched with water and extracted with DCM (4 x 15 ml). The combined organic layers were dried over Na_2SO_4 and evaporated under reduce pressure to yield the epoxide as an amorphous solid (100 mg, 0.61 mol), y = 50%, which was used in the next step without purification. To the epoxide previously obtained, conc. HCl (2 ml) was added and the resulting mixture was heated to reflux at 70 °C for 2 h. After cooling, water (3ml) was added which lead to the formation of a white precipitate. The mixture was extracted with DCM (4 x 5 ml). The combined organic layers were washed with saturated

aqueous $NaHCO_3$, dried over Na_2SO_4, filtered and concentrated under reduce pressure to yield an orange crystal solid (70 mg, 0.47 mmol), which was use in the next step without purification. Y = 70%. ^{1}H NMR (400 MHZ, $CDCl_3$, 25°C) δ 7.43 (ddd, J_1 = 8.1, J_2 = 7.1, J_3 = 1.0 Hz, 3H); 7.52 (dd, J_1 = 8.6, J_2 = 1.1 Hz, 3H); 7.70 (ddd, J_1 = 8.6, J_2 = 7.1, J_3 = 1.7 Hz, 3H); 8.03 (s, 3H); 8.28 (dd, J_1 = 8.1, J_2 = 1.7, 3H) ppm.

N,N'-bis(3-hydroxy-4-chromone-2-ylmethyl)- N,N'-dimethylethylendiamine (L1)[157]

0.25 cm^3 of 37% aqueous formaldehyde (100 mg, 3.4 mmol) was added to 141 mg of N,N'-dimethylethylenediamine (1.5 mmol) dissolved in 2 cm^3 of ethanol. The mixture was stirred 1 h at RT and added dropwise to 500 mg of 3-hydroxy-4-chromone (**2**) (3.1 mmol) dissolved in 10 cm^3 of ethanol under nitrogen atmosphere. The reaction was stirred at RT until a white precipitate gradually appear. After 12 h the mixture was cooled at 0°C and filtered. The white solid obtained was crystallized from hot ethanol, filtered, washed with cold ethanol and dried obtaining **L1** as white crystals (490 mg, 74% yield). ^{1}H-NMR (400 MHz, DMSO-d_6, 25°C) δ = 2.29 (s, 6H) ppm; 2.67 (s, 4H); 3.75 (s, 4H); 7.41 (dd, J_1 = 8.0 Hz, J_2 = 7.1 Hz, 2H); 7.55 (d, J = 8.2 Hz, 2H); 7.70 (dd, J_1 = 8.2 Hz, J_2 = 7.1, 2H); 8.07 (dd, J_1 = 8.0 Hz, J_2 = 1.5 Hz, 2H) ppm. ^{13}C-NMR (100 MHz, DMSO-d_6, 25°C) δ = 42.7; 54.1; 54.6; 118.7; 122.5; 124.8; 125.4; 133.8; 140.4; 149.4; 155.1; 172.6) ppm. Anal. for C24H24N2O6 (436.5): calcd C 66.05, H 5.54, N 6.42; found C 65.9, H 5.6, N 6.5.

Palladium N,N'-bis(4-chromone-3-olate-2-ylmethyl)-N,N'-dimethylethylendiamino hexahydrate [Pd(H$_{-2}$L1)](H$_2$O)$_6$.[157]

A freshly prepared aqueous solution of K_2PdCl_4 (15 mg, 0.046 mmol, 0.5 cm^3) and 0.1 M aqueous TRIS/HCl buffer solution (pH=7, 0.5 cm^3) were added to an ethanolic solution of **L1** (20 mg, 0.046 mmol, 5 cm^3). The mixture was kept at RT and after 24 h the complex [Pd(H$_{-2}$**L1**)](H$_2$O)$_6$ precipitated as yellow needles suitable for X-ray

analysis. Anal. for $C_{24}H_{34}N_2O_{12}Pd$ (649.0): Calcd C 44.42, H 5.28, N 4.32; Found C 44.2, H 5.5, N 4.1.

Crystallographic data.

Intensity data for [Pd(H_{-2}**L1**)](H2O)$_6$ were collected, at 100 K, on an Oxford Diffraction Excalibur diffractometer using Cu(Kα) radiation (λ(Cu) = 1.54184 Å). Data collection and data reduction were performed with the program CrysAlisPro;[158] absorption correction was performed with the program ABSPACK implemented in CrysAlisPro. The structure was solved by using the SIR-2004 package[159] and refined by full-matrix least squares against F2 using all data (SHELXL-2018/3).[160] All the non-hydrogen atoms were anisotropically refined; concerning the hydrogen atoms, those of the (H_{-2}**L1**)$^{-2}$ ligand where set in calculated position, while those of the water molecules were found in the Fourier density map and their coordinated were freely refined. Geometrical calculations were performed by PARST97[161] and molecular plots were produced by the programs Mercury (v4.3.1)[162] and Discovery Studio Visualizer 2019.[163] In Table 3 (see chapter 2.1.1) crystallographic data and refinement parameters of [Pd(H_{-2}**L1**)](H2O)$_6$ are reported, while in Table 2 (see chapter 2.1.1) a list of selected distances and angles is shown. In Figure 15 a ball and stick representation of [Pd(H_{-2}**L1**)] is reported.[157]

3.2.2 Synthesis and Characterization of La, Lb, L2

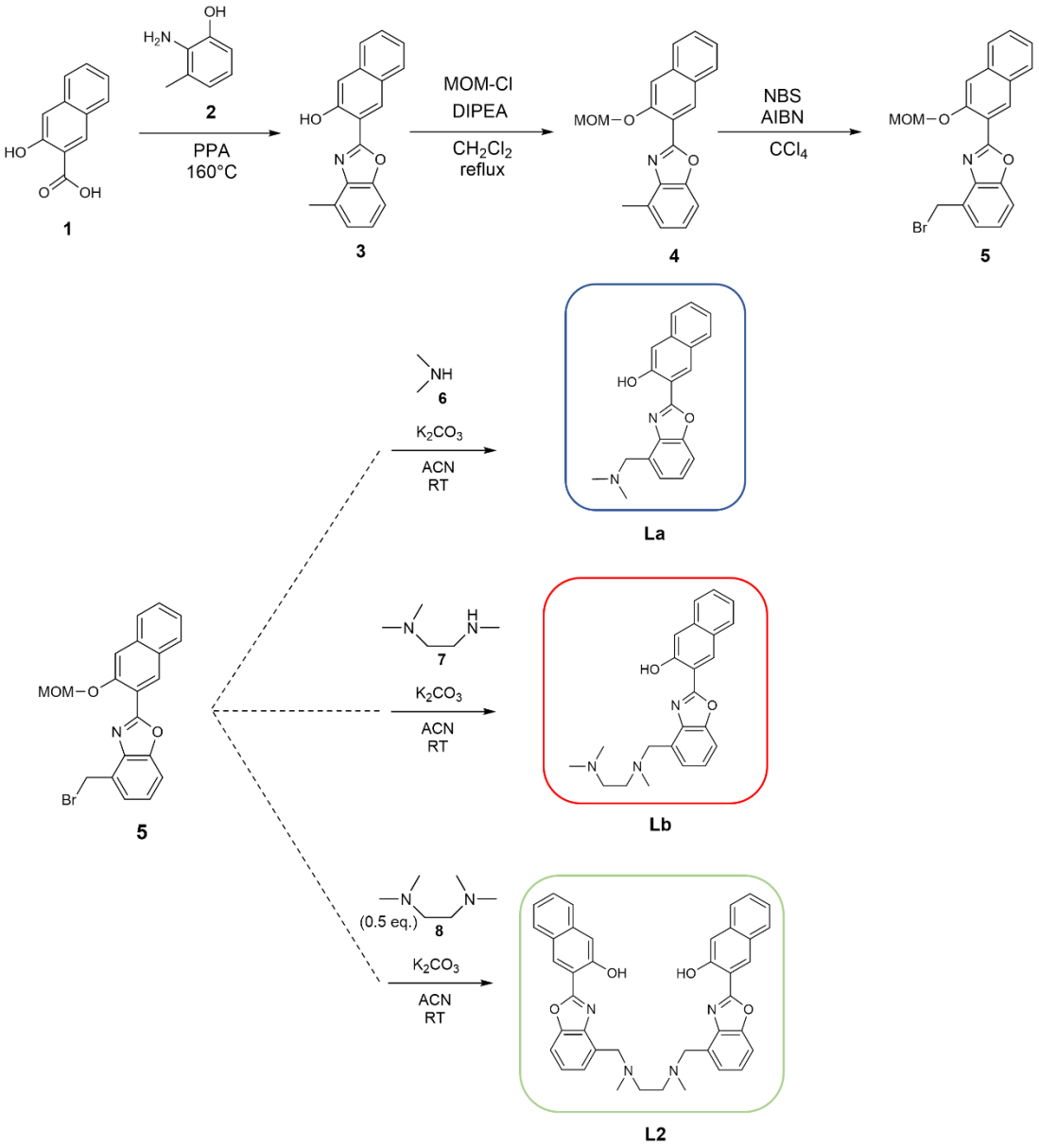

Scheme 13. Synthesis of La, Lb, **L2**

2-(2'-Hydroxy-3'-naphtyl)-4-methylbenzoxazole (HNBO, 3).

Based on a literature procedure[125], 2-amino-m-cresol (**2**) (3.3 g, 123.1 mmol) and 3-hydroxy-2-naphthoic acid (**1**) (5.0 g, 26.6 mmol) were suspended in polyphosphoric acid (25.0 g) and heated overnight at 160°C. the reaction mixture was cooled to room temperature and poured into 1 L of water at 0°C. After neutralization with Na_2CO_3, the mixture was filtered and washed with water and extracted with Soxhlet (hexane) obtaining 4.5 g of orange solid (y = 62%). ^{1}H NMR (400 MHz, CDCl3, 25°C) δ = 2.68 (s, 3H), 7.21-7.23 (dt, J_1 = 7.5 Hz, J_2 = 1.0 Hz, 1H), 7.31-7.38 (m, 2H), 7.47-7.53 (m, 3H), 7.74-7.76 (d, J = 8.3 Hz, 2H), 7.88-7.90 (d, J = 8 Hz, 2H), 8.64 (s, 1H) ppm.

2-(2'-Methoxymethyloxy-3'-naphtyl)-4-methylbenzoxazole (4).

Based on a literature procedure,[125] HNBO (**3**) and diisopropylethylamine (2.00 g, 7.27 mmol), were dissolved in CH_2Cl_2 (100 ml) under nitrogen, followed by the addition of Chloromethyl methyl ether (2.73 ml, 22.68 mmol) portion wise at 0°C. Then the reaction mixture was refluxed overnight until the starting material was consumed. The reaction mixture was cooled to room temperature and water was added to the solution and extracted with CH_2Cl_2 (40 ml, three times). The combined organic phases were washed sequentially with HCl (0.5 M), distilled water, NaOH (1 M) and brine, dried over Na_2SO_4 and evaporated to dryness to give pure **4** as an orange solid (2.31 g, y = 97%). ^{1}H NMR (400 MHz, $CDCl_3$, 25°C) δ = 2.74 (s, 3H), 3.62 (s, 3H), 5.46 (s, 2H), 7.19 (dt, J = 7.5, 0.9 Hz, 1H), 7.30 (d, J = 7.6 Hz, 1H), 7.48 – 7.40 (m, 1H), 7.46 (s, 1H), 7.59 – 7.44 (m, 2H), 7.80 (dd, J = 8.2, 1.1 Hz, 1H), 7.92 (dd, J = 8.4, 0.9 Hz, 1H), 8.66 (s, 1H) ppm.

4-Bromomethyl-2-(2'-methoxymethyloxy-3'-naphthyl)-benzoxazole (5).

Based on a literature procedure,[125] a solution of **4** (2.00 g, 6.26 mmol), N-bromosuccinimide (1.23 g, 6.89 mmol) and 2,2'-azobis(2-methylpropionitrile) (0.20 g, 1.20 mmol) in CCl_4 was refluxed for 24 h, under nitrogen, until the starting material was consumed and then cooled

at room temperature. The white precipitate was filtered off and filtrate was concentrated under vacuum. The crude residue was purified by flash column chromatography on silica gel using CH_2Cl_2 as eluent to provide pure **5** as a white solid. (2.50 g, y = 50%). ^{1}H NMR (400 MHz, $CDCl_3$, 25°C) δ = 3.64 (s, 3H), 5.01 (s, 2H), 5.46 (s, 2H), 7.35-7.39 (t, *J* = 7.8 Hz, 1H), 7.43-7.47 (m, 2H), 7.53-7.60 (m, 3H), 7.80-7.82 (d, *J* = 8.0 Hz, 1H), 7.92-7.94 (d, *J* = 8.0 Hz, 1H), 8.68 (1s, 1H) ppm.

N-(2-(2'-hydroxy-3'-naphthyl)benzoxazol-4-ylmethyl)-N,N-dimethylamine (La).

Under nitrogen, **5** (0.40 g, 1.0 mmol) dissolved in 20 ml of acetonitrile was added dropwise to an acetonitrile solution (20 ml) containing 40 % aqueous dimethylamine (0.12 ml, 1.0 mmol) and K_2CO_3 (0.41 g, 3.0 mmol), The reaction mixture was stirred at room temperature overnight. The resulting white precipitate was removed by filtration. The filtrate was concentrated under vacuum obtaining a yellow sticky oil that is dissolved in MeOH (4 ml) under nitrogen in which it was added portionwise a solution (1 ml) of p-toluenesulfonic acid monohydrate (0.95 g, 5.0 mmol). The solution was stirred at room temperature for 24 h until the starting material was consumed. The reaction mixture was concentrated under vacuum obtaining a white solid that was put into an aqueous K_2CO_3 solution (1 M, 5 ml) and extracted with CH_2Cl_2 (10 ml, three times). The combined organic phases were dried over Na_2SO_4 and evaporated to dryness to give 0.18 g of **La** as a yellow solid (y = 58%). ^{1}H NMR (400 MHz, d_6-DMSO, 25°C) δ = 2.25 (s, 6H), 3.84 (s, 2H), 6.99 (s, 1H), 7.04 (t, *J* = 7.3 Hz, 1H), 7.28 (t, *J*= 7.6 Hz, 1H), 7.38 (m, 2H), 7.47 (d, *J* = 8.1 Hz, 1H), 7.65 (m, 1H), 7.77 (d, *J* = 8.1 Hz, 1H), 8.40 (s, 1H) ppm. ^{13}C NMR (100 MHz, d_6-DMSO, 25°C) δ = 45.7, 58.2, 109.5, 111.7, 120.9, 125.0, 125.2, 127.7, 129.1, 130.6 ppm. Anal. for $C_{20}H_{18}N_2O_2$ (318.4): Calcd C 75.45, H 5.70, N 8.80; Found C 75.3, H 5.8, N 8.9.

N-(2-(2'-hydroxy-3'-naphthyl)benzoxazol-4-ylmethyl)-N,N',N'-trimethylethylendiamine dihydrochloride (Lb·2HCl).

Under nitrogen atmosphere, **5** (0.40 g, 1.0 mmol) dissolved in 20 ml of acetonitrile was added dropwise to an acetonitrile solution (20 ml) containing N,N,N'-trimethylethylenediamine (0.13ml, 1.0 mmol) and K_2CO_3 (0.41 g, 3.0 mmol), The reaction mixture was stirred at room temperature overnight. The resulting white precipitate was removed by filtration. The filtrate was concentrated under vacuum obtaining a yellow sticky oil that is dissolved in MeOH (4 ml) under nitrogen in which it was added portionwise a solution (1 ml) of p-toluenesulfonic acid monohydrate (0.95 g, 5.0 mmol). The solution was stirred at room temperature for 24 h until the starting material was consumed. The reaction mixture was concentrated under vacuum obtaining a yellow oil that was put into an aqueous K_2CO_3 solution (1 M, 5 ml) and extracted with CH_2Cl_2 (10 ml, three times). The combined organic phases were dried over Na_2SO_4 and evaporated to dryness to give **Lb** as a yellow oil. The pure **Lb** was obtained as hydrochloride salt by the addition of a 10% ethanolic solution of HCl to an ethanolic solution (1 ml) of the crude obtaining 0.21 g of yellow solid (y = 49%). ^{1}H NMR (400 MHz, d_6-DMSO, 25°C) δ = 2.14 (s, 6H), 2.24 (s, 3H,), 3.92 (s, 2H), 6.39 (s, 1H), 6.65 (td, J_1 = 7.4, J_2 = 1.1 Hz, 1H), 6.99 (td, J_1 = 7.5, J_2 = 1.3 Hz, 1H), 7.11 (d, J = 8.4 Hz, 1H), 7.26 (t, J = 7.6 Hz, 1H), 7.32 (dd, J_1 = 7.7, J_2 = 1.2 Hz, 1H), 7.43 (d, J = 8.2 Hz, 1H), 7.51 (dd, J_1=7.7, J_2 = 1.3 Hz, 1H), 8.06 (s, 1H) ppm. ^{13}C NMR (100 MHz, d_6-DMSO, 25°C) δ = 131.4, 128.8, 126.1, 124.0, 123.7, 123.4, 116.9, 112.1, 108.9, 57.7, 56.6, 55,4, 42.9, 46.0 ppm. Anal. for $C_{23}H_{27}Cl_2N_3O_2$ (448.4): Calcd C 61.61, H 6.07, N 9.37; Found C 61.4, H 6.2, N 9.5.

N,N'-bis(2-(2'-hydroxy-3'-naphthyl)benzoxazol-4-ylmethyl)-N,N'-dimethylethylendiamine dihydrochloride (L2).

Under nitrogen, **5** (0.40 g, 1.0 mmol) dissolved in 20 ml of acetonitrile was added dropwise to an acetonitrile solution (20 ml) containing N,N'-dimethyl ethylenediamine (0.053 ml, 0.5

mmol) and K_2CO_3 (0.41 g, 3.0 mmol), The reaction mixture was stirred at room temperature overnight. The resulting white precipitate was removed by filtration. The filtrate was concentrated under vacuum obtaining a yellow sticky oil that is dissolved in MeOH (4 ml) under nitrogen in which it was added portionwise a solution (1 ml) of p-toluenesulfonic acid monohydrate (0.95 g, 5.0 mmol). The solution was stirred at room temperature for 24 h until the starting material was consumed. The reaction mixture was concentrated under vacuum obtaining a white solid that was put into an aqueous K_2CO_3 solution (1 M, 5 ml) and extracted with CH_2Cl_2 (10 ml, three times). The combined organic phases were dried over Na_2SO_4 and evaporated to dryness to afford 0.17 g of **L2** as a yellow solid (y = 50%). ^{1}H NMR (400 MHz, d_6-DMSO, 25°C) δ = 2.25 (s, 6H), 2.69 (s, 4H), 3.96 (s, 4H), 6.35 (s, 2H), 6.61 (td, J_1 = 7.3, J_2 = 1.1 Hz, 2H), 6.97 (td J_1 = 7.6, J_2 = 1.3 Hz, 2H), 7.10 (d, J=8.1 Hz, 2H), 7.25 (t, J = 7.8 Hz, 2H), 7.34 (dd, J = 7.3 Hz, 2H), 7.41 (d, J = 7.8 Hz, 2H), 7.50 (d, J = 7.8 Hz, 2H), 8.06 (s, 2H) ppm. ^{13}C NMR (100 MHz, d_6-DMSO, 25°C) δ = 43.0, 55.7, 56.8, 108.8, 112.1, 116.6, 123.5, 123.7, 124.0, 126.0, 128.9, 131.4 ppm. Anal. for $C_{40}H_{34}N_4O_4$ (634.7): Calcd C 75.69, H 5.40, N 8.83; Found C 75.5, H 5.5, N 8.9.

3.2.3 Synthesis and Characterization of L3

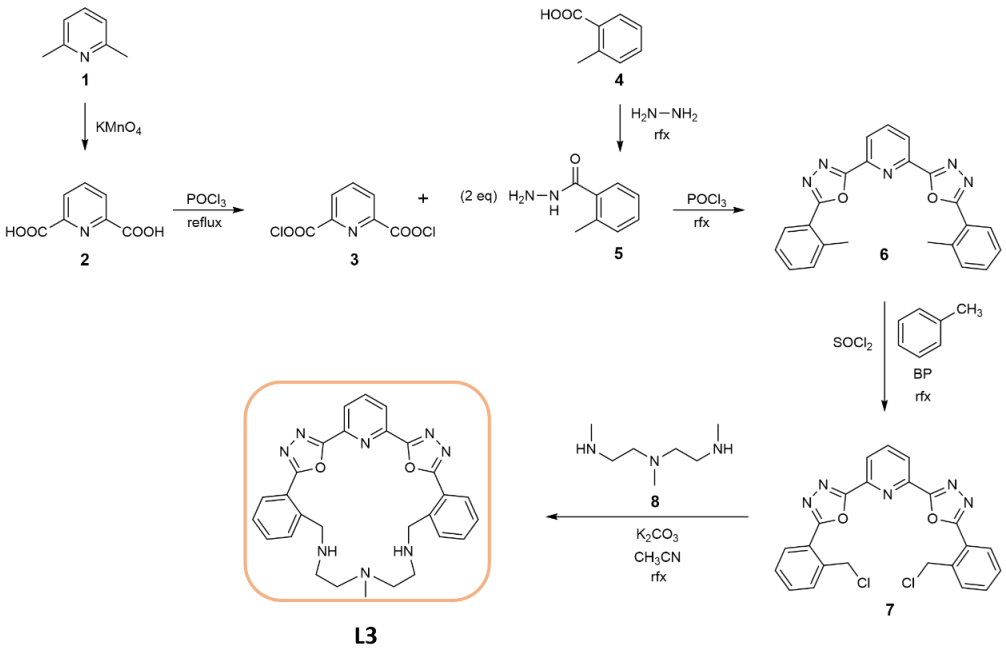

Scheme 14. Synthesis of **L3**

The oxidation of 2,6-dimethyl pyridine (**1**) lead to the formation of pyridine dicarboxylic acid (**2**).[146] 1,4,7-trimethyl-1,4,7-trizaheptane (**8**) was obtained as reported in literature.[164] Intermediate **5** was prepared by mixing hydrazine and compound (**4**) refluxing overnight.

2,6-Bis(5-(2-methylphenyl)-1,3,4-oxadiazol-2-yl)pyridine (6).

Under nitrogen atmosphere, **2** (10.0 g, 60 mmol) was suspended in 200 cm^3 of phosphorus oxychloride ($POCl_3$) and then refluxed until complete dissolution. After 3 h the resulting pink solution containing the intermediate **3** was used without purification. **5** (18.0 g, 120 mmol) was slowly added in the solution containing **3** at 0°C. After the addition, the resulting yellow solution was warmed to RT stirring for 2 h and then refluxed overnight. When the reaction was completed, the solution was cooled to RT and putted in a 3 dm^3 of ice/water mixture and neutralized adding Na_2CO_3 until the crude product **6** precipitates. The solid was filtered,

washed with cold water and dried. Flash-chromatography on silica gel using $CHCl_3$ as eluent lead to obtaine **6** as pure product (15 g, yield 63%). 1 H-NMR (400 MHz, CDCl3, 25°C) δ = 2.84 (s, 6H), 7.42–7.39 (m, 4H), 7.49 (t, J = 7.6 Hz, 2H), 8.14 (t, J = 7.8 Hz, 1H), 8.19 (d, J = 7.6 Hz, 2H), 8.49 (d, J = 7.8 Hz, 2H) ppm.

2,6-Bis(5-(2-(chloromethyl)phenyl)-1,3,4-oxadiazol-2-yl)pyridine (7).

A mixture of dibenzoyl peroxide 70% in water (50 mg, 0.15 mmol), sulfuryl dichloride (SO_2Cl_2, 1.5 cm^3 , 2.5 g, 19 mmol) and **6** (3 g, 7.6 mmol) was suspended in 50 cm^3 of chlorobenzene and refluxed under nitrogen atmosphere. After 12 h the resulting solution was warmed to RT. Residual sulfuryl dichloride and the solvent were evaporated under reduce pressure obtaining the crude solid product that was purified by flash-chromatography (silica gel, CH2Cl2) to obtain pure **7** (2.5 g, yield 70%). 1 H-NMR (400 MHz, CDCl3, 25°C) δ = 5.31 ppm (s, 4H), 7.57 (t, J = 7.2 Hz, 2H), 7.63 (t, J = 7.2 Hz, 2H), 7.73 (dd, J1 = 7.6, J2 = 1.6, 2H), 8.17 (t, J = 7.9 Hz, 1H), 8.27 (dd, J1 = 7.6, J2 = 1.6 Hz, 2H), 8.53 (d, J = 7.9 Hz, 2H) ppm.

13,16,19-Trimethyl-36,37-dioxa3,4,13,16,19,28,29,35octaazahexacyclo[29.3.1.1(2,5) .1 (27 ,30).0(6,11).0(21,26)] eptatriaconta2,4,6,8,10,21,23,25,27,29,31,33,1(35)-tridecene (L3).

Under nitrogen atmosphere, **8** (1.4 g, 2.9 mmol) was dissolved in a suspension of K2CO3 (4 g, 29 mmol) in 200 cm^3 of anhydrous acetonitrile (ACN) at 60 °C. In this suspension was added, over a period of 8 h, a solution of **7** (420 mg, 2.9 mmol) in 100 cm^3 of anhydrous ACN. After the addition, the mixture was stirred for further 12 h at 60°C. The reaction was cooled to RT, the solid residues were filtered off, then the liquid phase was concentrated to obtain a white solid that was purified by flash-chromatography (aluminum oxide, chloroform) obtaining pure **L3** as white solid (670 mg, yield 65%). ^{1}H-NMR (400 MHz, CDCl3) δ = 1.95 (s, 6H), 1.98 (s, 3H), 2.17 (br, 4H), 2.46 (br, 4H), 7.39–7.44 (m, 4H), 7.50 (t, J = 7.6 Hz, 2H), 7.87 (dd, J1 = 7.6 Hz, J2 = 1.2 Hz, 2H), 8.13 (t, J = 7.9 Hz, 1H), 8.51 (d, J = 7.9 Hz, 2H) ppm. ^{13}C NMR

(100 MHz, CDCl3, 25°C) δ = 29.7, 42.1, 55.1, 61.3, 123.7, 124.8, 127.7, 130.8, 130.9, 131.5, 138.5, 139.9, 144.5, 166.2, 167.0 ppm. Elemental analysis calcd (%) for C30H32N8O2: C 67.15, H 6.01, N 20.88; found: C 67.0, H 6.2, N 20.6.

Crystals of free L3.

L3 (15 mg, 0.028 mmol) was dissolved in a 50/50 H_2O/ethanol mixture solvent and stirred at 50°C for 30 minutes. After 24 h, the slow evaporation of ethanol caused the precipitation of free **L3** as crystals suitable for X-ray analysis.

Crystallographic data.

Crystal structure of **L3** was determined by means of single crystal X-ray diffraction. Measurement was carried out with an Oxford Diffraction Excalibur diffractometer using the Cu-Kα radiation (λ = 1.54184 Å). Data collection was performed with the program CrysAlis CCD,[165] while data reduction was carried out with the program CrysAlis RED.[165] Finally, absorption correction was performed with the program ABSPACK in CrysAlis RED. Structure was solved by using the SIR-2004 package[166] and subsequently refined on the F2 values by the full-matrix leastsquares program SHELXL-2018.[167] Geometrical calculations were performed by PARST97,[168] and molecular plots were produced by the programs ORTEP-3[169] and Discovery Studio Visualizer.[170] The structure was solved as a twin by using the twinning law suggested by Platon.[171] One of two independent molecules of **L3** present in the asymmetric unit contains a disordered fragment. Such disorder was modelled by refining two positions for all the atoms of the fragment (occupancy factors 0.56 and 0.44). For all the non-hydrogen atoms anisotropic thermal parameters were used, while all the hydrogen atoms were introduced in calculated position and refined in agreement with the atom to which they are bound.

3.2.4 Synthesis and Characterisation of Lc, Ld, L4

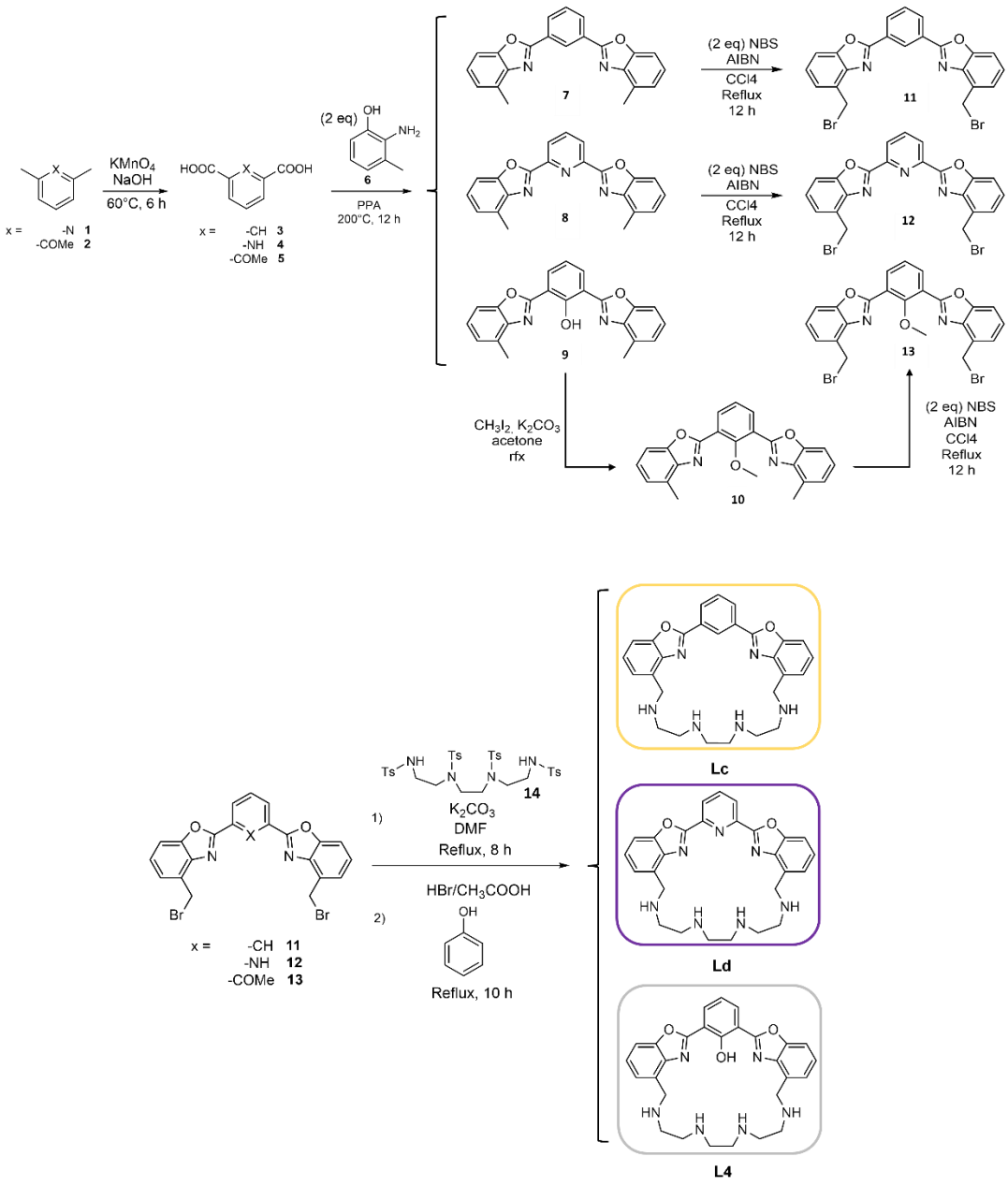

Scheme 15. Synthesis of Ligands **Lc**, **Ld**, **L4**

The synthesis of **Lc** starts form the commercially available isophthalic acid **3**. The synthesis of **Ld** starts from the oxidation of 2,6-dimethyl pyridine (**1**) lead to the formation of pyridine dicarboxylic acid (**4**)[146]. The synthesis of **L4** starts form the commercially available 2,6-dimethylanisole (**2**). The protected polyamine (**14**) was obtained as reported in literature.[153]

2-Methoxyisophtalic acid (5)

A mixture of 2,6-dimethylanisole (**2**) (15.5 g, 114mmol), $KMnO_4$ (50 g, 316 mmol), and NaOH (6.20 g, 155 mmol) in water (1 L) was heated at 60 °C for 5 h. Additional $KMnO_4$ (50 g, 316 mmol) was added in several portions, and refluxed for 1 h. The mixture was cooled to room temperature and then filtered on a thin layer of celite. The filtrate was acidified with concentrated HCl and the resulting white precipitate was collected by filtration. The product was dried under reduced pressure to afford 15.3 g of white solid (y = 68%). ^{1}H NMR (400 MHz, CDCl3, 25°C) δ = 3.64 (s, 3H), 6.96-6.99 (t, *J* = 8 Hz, 1H), 7.18-7.19 (d, *J* = 7.6 Hz, 2 H) ppm.

General Procedure:

1,3-bis(4-methyl-2-ossazolyl)phenyl (7); 2,6-bis(4-methyl-2-ossazolyl)pyridine (8); 2,6-bis(4-methyl-2-ossazolyl)phenol (9).

2-Amino-m-cresol (**2**) (18.4 g, 150 mmol) and aromatic dicarboxylic acid (**3**: 12.4 g **, 4**: 12.5 g**, 5**: 14.7 g) (75 mmol) were suspended in polyphosphoric acid (120.0 g) and heated overnight at 160°C. The reaction mixture was cooled to room temperature and poured into 3 L of water at 0°C. After neutralization with Na_2CO_3, the mixture was filtered, and the residue was washed with methanol and dried under reduced pressure obtaining the product as grey solid (y = (**7**) 18.6 g, 73%; (**8**) 18.9 74%; (**9**) 19.1 72%). ^{1}H NMR (400 MHz, CDCl3, 25°C) δ = (**7**) 2.73 (s, 6H), 7.18-7.19 (dt, J_1 = 7.5 Hz, J_2 = 1.0 Hz, 2H), 7.28-7.31 (t, *J* = 8 Hz, 2H), 7.46-7.49 (dt, J_1 = 8.1 Hz, J_2 = 0.9 Hz, 2H), 7.68-7.72 (t, *J* = 8.0 Hz, 1H), 8.45-8.47 (dd, J_1 = 7.8 Hz, J_2 = 1.7 Hz, 2H),

9.14-1.15 (t, J = 1.6 Hz, 1H) ppm; (**8**) 2.75 (s, 6 H), 7.22-7.24 (dt, J_1 = 7.4 Hz, J_2 = 1.0 Hz, 1H), 7.33-7.37 (m, J = 7.8 Hz, 1H), 7.55-7.57 (d, J_1 = 8.0 Hz, 1H), 8.10-8.14 (t, J_1 = 7.9 Hz, 1H), 8.55-8.57 (d, J = 7.8 Hz, 1H) ppm; (**9**) 2.70 (s, 1H), 7.17-7.22 (m, 3H), 7.27-7.33 (t, J = 7.8 Hz, 2H), 7.48-7.50 (dt, J_1 = 8.1 Hz, J_2 = 0.9 Hz, 2H), 8.29-8.31 (d, 7.8 Hz, 2H), 13.02 (s,1H) ppm.

2,6-bis(4-methyl-2-ossazolyl)anisole (10)

Under nitrogen atmosphere, **9** (8.0 g, 0.02 mmol) was dissolved in 300 ml of acetone, then 2 equivalent of K_2CO_3 was suspended. The mixture was heated at 50°C and then CH_3I (8.8 g, 0.06 mmol) was added portion wise. The reaction was refluxed overnight, then was cooled to room temperature and concentrated under reduce pressure. The residue was dissolved in CH_2Cl_2 and washed with saturated aqueous $NaHCO_3$ and brine, dried over Na_2SO_4, filtered and concentrated under reduce pressure to obtain **10** with a 91% of yield (7.5 g, 0.019 mmol). ^{1}H NMR (400 MHz, CDCl3, 25°C) δ = δ 2.72 (d, J = 0.7 Hz, 6H), 4.03 (s, 3H), 7.20 (dq, J = 7.5, 0.9 Hz, 2H), 7.30 (t, J = 7.8 Hz, 2H), 7.43 (t, J = 7.8 Hz, 1H), 7.47 (dt, J = 8.1, 0.9 Hz, 2H), 8.35 (d, J = 7.8 Hz, 2H) ppm.

General Procedure:

1,3-bis(4-bromomethyl-2-ossazolyl)phenyl (11); 2,6-bis(4-bromomethyl-2 ossazolyl) pyridine (12); 2,6-bis(4-bromomethyl-2-ossazolyl)anisole (13).

A solution of the fluorophore moiety (**7** (2.0 g), **8** (2.0 g), **10** (2.4 g)) (6.0 mmol), N-bromosuccynimide (7.0 mmol) and 2,2'-azobis(2-methylpropionitrile) (1.20 mmol) in 50 ml of CCl_4 was refluxed for 24 h, under nitrogen atmosphere, until the starting material was consumed and then cooled at room temperature. The white precipitate was filtered off and filtrate was concentrated under vacuum. The crude residue was crystalized with MeOH giving pure **11** (1.5 g), **12** (1.5 g) and **13** (1.7 g) as pink solids. (y = 50%). ^{1}H NMR (400 MHz, $CDCl_3$, 25°C) δ = (**11**) 5.00 (s, 3H), 7.63 – 7.41 (m, 7H), 8.50 (dd, J = 7.8, 1.8 Hz, 1H), 9.16 (t, J = 1.8

Hz, 1H) ppm; (**12**) 5.01 (s, 4H), 7.58 – 7.36 (m, 3H), 7.70 (dd, *J* = 8.0, 1.2 Hz, 2H), 8.15 (t, *J* = 7.9 Hz, 1H), 8.63 (d, *J* = 7.9 Hz, 2H) ppm; (**13**) 4.13 (s, 3H), 4.99 (s, 4H), 7.54 – 7.35 (m, 5H), 7.60 (dd, *J* = 8.0, 1.1 Hz, 2H), 8.42 (d, *J* = 7.8 Hz, 2H) ppm.

General Procedure:

hexacyclo[28.3.1.1^{2,5}.1^{26,29}.0^{9,4}.0^{22,27}]-35,36-dioxa-3,11,14,17,20,28-hexaaza-2,4,6,8,22,24,26,28,30,32,1^{34}-tetratricontaendecaene tetraperchlorate (Lc·4HClO$_4$);

hexacyclo[28.3.1.1^{2,5}.1^{26,29}.0^{9,4}.0^{22,27}]-35,36-dioxa-3,11,14,17,20,28,34-eptaaza-2,4,6,8,22,24,26,28,30,32,1^{34}-tetratricontaendecaene tetraperchlorate (Ld·4HClO$_4$);

hexacyclo[28.3.1.1^{2,5}.1^{26,29}.0^{9,4}.0^{22,27}]-35,36-dioxa-3,11,14,17,20,28-hexaaza-2,4,6,8,22,24,26,28,30,32,1^{34}-tetratricontaendecaen-34-ol (L4·4HClO$_4$).

Under nitrogen atmosphere, the brominated fluorophore (**11** (1.5 g), **12** (1.5 g) and **13** (1.7 g)) (3 mmol) was dissolved in a suspension of K2CO3 (4 g, 30 mmol) in 200 cm^3 of anhydrous dimethylformamide (DMF) and refluxed. In this suspension was added, over a period of 8 h, a solution of **14** (3.0 mmol) in 100 cm^3 of anhydrous DMF. After the addition, the mixture was stirred for further 12 h at reflux. Then, the reaction was cooled to RT, the solid residues were filtered off, the liquid phase was concentrated and put into cold water obtaining a yellow precipitated that filtered and dried and used in the next step without further purification. The solid obtained was refluxed overnight, under nitrogen atmosphere, in 15ml of HBr/HCOOH with phenol (2.5 g, 27.0 mmol). A brown precipitate gradually appears. After 24 h, the reaction was stopped and cooled to RT and filtered. The brown solid was dissolved in a 2 ml mixture ethanol/water (99/1), obtaining pure product (**Lc**·4HClO$_4$, 1.48 g (Y% = 56), **Ld**·4HClO$_4$, 1.3 g (Y% = 49), (**L4**·4HClO$_4$, 1.24 (Y% = 46)) as perchlorate salt by adding to this solution two drops of a 10% HClO$_4$ ethanolic solution.

hexacyclo[28.3.1.1^{2,5}.1^{26,29}.0^{9,4}.0^{22,27}]-35,36-dioxa-3,11,14,17,20,28-hexaaza-2,4,6,8,22,24,26,28,30,32,1^{34}-tetratricontaendecaene tetraperchlorate (Lc·4HClO$_4$).

^{1}H NMR (400 MHz, D_2O, 25°C) δ 9.14 (t, *J* = 1.8 Hz, 1H), 8.46 – 8.38 (m, 2H), 7.88 – 7.77 (m, 3H), 7.56 – 7.45 (m, 3H), 4.75 (s, 9H), 4.65 (s, 10H), 3.48 (t, *J* = 6.4 Hz, 3H), 3.35 – 3.23 (m, 5H), 3.12 (d, *J* = 1.6 Hz, 3H) ppm. ^{13}C NMR (100 MHz, D_2O, 25°C) δ = 46.2, 49.6, 50.7, 51.4, 108.7, 112.4, 118.3, 122.1, 123.5, 125.5, 129.2, 138.3, 143.1, 148.6, 151.4 ppm. Anal. for $C_{28}H_{34}Cl_4N_6O_{18}$ (884.4): Calcd C 38.03, H 3.87, N 9.50; Found C 37.9, H 4.0, N 9.4.

hexacyclo[28.3.1.1^{2,5}.1^{26,29}.0^{9,4}.0^{22,27}]-35,36-dioxa-3,11,14,17,20,28,34-eptaaza-2,4,6,8,22,24,26,28,30,32,1^{34}-tetratricontaendecaene tetraperchlorate (**Ld**·4HClO$_4$).

^{1}H NMR (400 MHz, D_2O, 25°C) δ = 3.20 (s, 4H), 3.31 (t, *J* = 6.7 Hz, 4H), 3.37 (t, *J* = 6.7 Hz, 4H), 4.57 (s, 4H), 7.46 – 7.41 (m, 4H), 7.68 (t, *J* = 4.6 Hz, 2H), 8.18 (dd, *J* = 8.5, 7.2 Hz, 1H), 8.31 (d, *J* = 7.8 Hz, 2H). ^{13}C NMR (100 MHz, D_2O, 25°C) δ = 50.2, 50.9, 51.1, 52.3, 109.1, 112.6, 121.1, 125.6, 129.2, 142.3, 143.2, 149.8, 152.6, 157.6 ppm. Anal. for $C_{27}H_{33}Cl_4N_7O_{18}$ (885.4): Calcd C 36.63, H 3.76, N 11.07; Found C 36.5, H 3.9, N 11.2.

hexacyclo[28.3.1.1^{2,5}.1^{26,29}.0^{9,4}.0^{22,27}]-35,36-dioxa-3,11,14,17,20,28-hexaaza-2,4,6,8,22,24,26,28,30,32,1^{34}-tetratricontaendecaen-34-ol (**L4**·4HClO$_4$).

^{1}H NMR (400 MHz, D_2O, 25°C) δ = 3.21 (s, 4H), 3.39 (s, 8H), 4.62 (s, 4H), 7.21 (t, *J* = 7.9 Hz, 1H), 7.38 (d, *J* = 7.2 Hz, 4H), 7.65 (d, *J* = 7.2 Hz, 2H), 8.21 (d, *J* = 7.9 Hz, 2H) ppm. ^{13}C NMR (100 MHz, D_2O, 25°C) δ = 46.3, 49.7, 50.2, 51.5, 108.9, 112.6, 122.3, 123.6, 125.6, 129.2, 138.1, 143.2, 149.8, 153.2, 162.7 ppm. Anal. for $C_{28}H_{34}Cl_4N_6O_{19}$ (900.4): Calcd C 37.35, H 3.81, N 9.33; Found C 37.2, H 3.8, N 9.4

References

[1] F. Pina, M. A. Bernardo, E. Garcia-Espana. Eur. J. Inorg. Chem. 2000, 10, 2143-2157.

[2] L. Prodi, F. Bolletta, M. Montaldi, N. Zaccheroni. Coordination Chemistry Review, 2000, 205, 59-83.

[3] C. Loidero, J. L. Capelo, J. C. Mejuto, E. Oliveira, H. M. Santos, B. Pedras, C. Nunez. Chem. Soc. Rev., 2010, 39, 2948-2976.

[4] A. Pal, S. R. Bhatta, A. Thakur. Coordination Chemistry Reviews, 2021, 431, 213685.

[5] Chemosensors: Principles, Strategies, and Applications. Binghe Wang, Eric V. Anslyn, 2011 John Wiley & Sons.

[6] D. Paderni, L. Giorgi, V. Fusi, M. Formica, G. Ambrosi and M. Micheloni. Coord. Chem. Rev., 2021, 429, 213639.

[7] Jonathan W. Steed, J. L. Atwood. Supramolecular Chemistry, Second Edition. 2009 John Wiley & Sons.

[8] J. P. Behr. The Lock and key Principle. 1994 John Wiley & Sons, New York.

[9] F. Vogtle. Supramolecular Chemistry, 1991 John Wiley & Sons, Ltd: Chichester.

[10] George A. Jeffrey. An introduction to hydrogen bonding. 1997 Oxford university

[11] E. V. Ansyln. Modern Physical Organic Chemistry. 2006 University Science Books, Sausalito, CA, USA.

[12] K. A. Connors. Binding constant, 1987 John Wiley & Sons, Ltd: Chichester.

[13] J. Polster, H. Lanchmann. Spectrometric Titration, 1989 John Wiley & Sons, VHC:Weinheim 1989.

[14] D. J. Cram. Angew. Chem. Int. ed. Engl., 1988,27, 1021-1027.

[15] A. Harriman, O. Trompette ,R. Ziessel. J. Am. Chem. Soc. 1999, 121, 2516–2525

[16] Y. Shen, B. P. Sullivan. Inorg. Chem. 1995, 34, 6235.

[17] J. Gagnon, C. Loeber, D. Matt. Inorg. Chim. Acta, 242, 137-142.

[18] P. D. Beer, O. Kocian, R. J. Mortimer, C. Ridgway. J. Chem. Soc. Dalton Trans., 1993, 2629-2638.

[19] F. Barigelletti, L. Flamigni, G. Calogero, L. Hammarström, J. P. Sauvage, J. P. CollinChem. Commun., 1998, 2333-2334.

[20] J. M. Lehn. Angew. Chem. Int. ed. Engl., 1988, 27, 1021-1027.

[21] B. C. Tzeng, W. C. Lo, C. M. Che, S. M. Peng Chem. Commun., 1996, 181-182.

[22] A. M.Josceanu, P. M. Simon, C. Rawle, P. Sheldon, S. M. Smith. Inorg. Chim. Acta, 1995, 240, 159-168.

[23] I. E. Tolpygin, V. A. Bren', A. D. Dubonosov, V. I. Minkin, V. P. Ryabalkin. Russian Journal of Organic Chemistry, 2003, 39, 1364-1366.

[24] D. W. Domaille, E. L. Que, C. J. Chan. Nat. Chem. Biol., 2008, 4, 168-175.

[25] R. B. Thompson. Curr. Opin. Chem. Bio., 2005 9, 526-532.

[26] K. Rurack, U. R. Genger. Chem. Soc. Rev., 2002, 31, 116-127.

[27] B. Valeur. Molecular Fluorescence. Weinheim, Wiley-VCH; 2006.

[28] E. M. Nolan, S. J. Lippard. Acc. Chem. Res. 2009, 42, 193.

[29] E. Kimura, S. Aoki. BioMetals, 2001, 14, 191-204.

[30] K. Kikuchi, K. Komatsu, T. Nagano. Curr. Opin. Chem. Bio., 2004, 8, 182-191

[31] P. J. Jiang, Z. J. Guo. Coordination Chemistry Reviews, 2004, 248, 205-229.

[32] N. C. Lim, H. C. Freake, C. Bruckner. Chem. Eur. J., 2005, 11, 38-49.

[33] G. Lisak. Environmental Pollution, Pollution 2021, 289 , 117882.

[34] E. L. Que, D. W. Domaille, C. J. Chang. Chem. Rev. 2008, 108, 1517-1549.

[35] E. Zdrachek, E. Bakker. Anal. Chem. 2019, 91, 2-26.

[36] C. J. Mei, S. A. Alang, A. Ahmad. Arabian Journal of Chemistry, 2021, 14, 103303.

[37] Q. Zhao, F. Li, C. Huang. Chem. Soc. Rev., 2010, 39, 3007-3030.

[38] Y. You, S. Cho, W. Nam. Inorg. Chem. 2014, 53, 1804-1815.

[39] G. Alberti, C. Zanoni, L. R. Magnaghi, R. Biesuz. Journal of Analytical Science and Technology, 11, 30, 2020.

[40] X. Wang, C. Shen, C. Zhou, Y. Bu, X. Yan. Chemical Engineering Journal, 417, 2021, 129125.

[41] A. E. Martell, R. D. Hancock, R. J. Motekaitis. Coord. Chem. Rev. 1994, 133, 39-65.

[42] P. Kar, M. Suresh, D. K. Kumar, D. A. Jose, B. Ganguli, A. Das. Polyhedron 26 (2007) 1317-1322.

[43] P. Strazzullo, C. Leclercq. Sodium. Adv. Nutr. 2014, 5, 188–190.

[44] F. Galletti, E. Agabiti-Rosei, G. Bernini, R. Boero, G. Desideri, F. Fallo, F. Mallamaci, A. Morganti, M. Castellano, P. Nazzaro. J. Hypertens. 2014, 32, 48–56.

[45] A. M. Villani, P. M. Clifton, J. B. Keogh. J. Hum. Nutr. Diet. 2012, 25, 129–139.

[46] P. Traiwatcharanon, W. Siriwatcharapiboon, C. Wongchoosuk. Chemosensors 2020, 8, 3, 58.

[47] D. Wu, A. C. Sedgwick, T. Gunnlaugsson, E. U. Akkaya, J. Yoon, T. D. James. Chem Soc. Rev., 2017, 46, 7105.

[48] G. Wang, J. Qin, L. Fan, C. R. Li, Z. Yang. Journal of Photochemistry and Photobiology A: Chemistry, 2016, 314, 29-34.

[49] B. Sontia, R.M. Touyz. Arch. Biochem. Biophys. 2007, 458, 33–39.

[50] W. Jahnen-Dechent, M. Ketteler. Clin. Kidney J., 2012, 5, i3–i14.

[51] R.Y. Walder, B. Yang, J.B. Stokes, P.A. Kirby, X. Cao, P. Shi, C.C. Searby, R.F. Husted, V.C. Sheffield. Hum. Mol. Genet., 2009, 18, 4367–4375.

[52] M. Piskacek, L. Zotova, G. Zsurka, R.J. Schweyen. J. Cell. Mol. Med., 2009, 13, 693–700.

[53] M. Barbagallo, L.J. Dominguez. Arch. Biochem. Biophys. 2007, 458, 40–47.

[54] R.M. Toyuz. Front. Biosci., 2004, 1, 1278–1293.

[55] Y. Rayssiguier, E. Gueux, W. Nowacki, E. Rock, A. Mazur. Magnesium Res., 2006, 19, 237–243.

[56] T. S. Lazarou and D. Buccella. Curr. Opin. Chem. Biol., 2020, 57, 27–33.

[57] Y. Li and M. Y. Chi. J. Am. Chem. Soc., 2005, 127, 3527–3530.

[58] L. Li, S. Yun, Z. Yuan-Hui, M. Lan, Z. Xi, C. Redshaw and W. Gang. Sensors Actuators, B Chem., 2016, 226, 279–288.

[59] E. Arunkumar, P. Chithra and A. Ajayaghosh. J. Am. Chem. Soc., 2004, 126, 6590–6598.

[60] Y. Li, J. Wu, X. Jin, J. Wang, S. Han, W. Wu, J. Xu, W. Liu, X. Yao and Y. Tang. Dalt. Trans., 2014, 43, 1881–1887.

[61] S. H. Mashraqui, S. Sundaram, A. C. Bhasikuttan, S. Kapoor and A. V. Sapre. Sensors Actuators B Chem., 2007, 122, 347–350.

[62] S. Amatori, G. Ambrosi, M. Fanelli, M. Formica, V. Fusi, L. Giorgi, E. Macedi, M. Micheloni, P. Paoli and P. Rossi. Chem. - A Eur. J., 2014, 20, 11048–11057.

[63] L. Lvova, C. G. Gonçalves, C. Di Natale, A. Legin, D. Kirsanov and R. Paolesse. Talanta, 2018, 179, 430–441.

[64] D. J. Bonda, H. Lee. Metallomics, 2011, 3, 267-270.

[65] E. L. Que, D. W. Domaille, . J. Chem. Rev., 2008, 108, 1517-1549.

[66] A. Kuźniar, P. Kurys, B. Floriańczyk, S. Szymonik-Lesiuk, K. Pasternak, S.Zimmer. BioMetals, 2001, 14, 127-130.

[67] W. G. Telford,P. J. Fraker. J. Cell. Physiol, 1995; 164: 259-270.

[68] H. Kozlowski, A. J. Klos, J. Brasun, E. Gaggelli, D. Valensin, G. Valensin. Coord. Chem. Rev. 2009, 253, 2665-2685

[69] L. Tapia, M. Suazo, C. Hodar, V. Cambiazo, M. Gonzalez. Biometals, 2003; 16(1), 169-174.

[70] G. Multhaup, A. Schlicksupp, L. Hesse, D. Beher , T. Ruppert, C. L. Masters, K. Beyreuther. Science, 1996, 271, 1406-1409

[71] A. Renzoni, F. Zino ,E. Franchi. E. Environ. Res. Sect. A, 1998; 77:68-72.

[72] Y. Mikata, M. Wakamatsu, S. Yano. Dalton Trans, 2005, 3, 545-550.

[73] Z. X. Han, X. B. Zhang, Z. Li, Y. J. Gong, X. Y. Wu, Z. Jin et al. Anal. Chem., 2010, 82, 3108-3113.

[74] N. C. Lim, J. V. Schuster, M. C. Porto, M. A. Tanudra, L. Yao, H. C. Freake et al. Inorg. Chem. 2005, 44, 2018-2030.

[75] Z. C. Xu, H. H. Baek, H. N. Kim, J. N. Cui, X. H. Qian, D. R. Spring et al. J. Am. Chem. Soc., 2010, 132, 601-610.

[76] Y. K. Wu, X. J. Peng, B. C. Guo, J. L. Fan, Z. C. Zhang, J. Y. Wang et al. Org. Biomol. Chem., 2005, 3, 1387-1392.

[77] Z. P. Dong, Y. P. Guo, X. Tian, J. T. Ma. J Lumin 2013, 134, 635-639.

[78] L. W. Zhang, D. Z. Duan, X. M. Cui, J. Y. Sun, J. G. Fang. Tetrahedron, 2013, 69, 15-21.

[79] S. A. Ingale, F. J. Seela. Org. Chem. 2012, 77, 9352-1956.

[80] Y. Y. Tang, Y. B. Ding, X. Li, H. Agren, T. Li, W. B. Zhang et al. Sens Actuators B, 2015, 206, 291-302.

[81] Y. B. Ding, Y. S. Xie, X. Li, J. P. Hill, W. B. Zhang, W. H. Zhu. Chem. Commun., 2011, 47, 5431-5433.

[82] X. A. Zhang, K. S. Lovejoy, A. Jasanoff, S. J. Lippard. Proc. Natl. Acad. Sci, 2007, 104, 10780-10785.

[83] W. Lin, D. Buccella, S. J. J. Lippard. Am. Chem. Soc., 2013, 135, 13512-13520.

[84] H. Kim, J. Kang, K. B. Kim, E. J. Song, C. Kim. Spectrochim. Acta A, 2014, 118, 883-887.

[85] L. Xue, C. Liu, H. Jiang. Chem. Commun. 2009, 9, 1061-1063.

[86] Z. P. Dong, X. D. Le, P. P. Zhou, C. X. Dong, J. T. Ma. RSC Adv. 2014, 4, 18270-18277.

[87] L. W. Zhang, D. Z. Duan, X. M. Cui, J. Y. Sun, J. G. Fang. Tetrahedron, 2013, 69, 15-21.

[88] G. F. Nordberg, R. F. M. Heber, L. Alessio. Cadium in the human Environment: toxicity and carcinogenicity. International Agency for Research on Cancer, 1992, IARC Scientific Publication N. 118.

[89] H. H. Harris, I. J. Pickering, G. N. George. Science, 2003, 301, 1203.

[90] D. Schüler, M. Buchert, R. Liu, S. Degreif, C. Merz, Study on Rare Earths and Their Recycling, OKO-insititut e.V, Germany, Darmstadt, 2011.

[91] Engineering Technical Support Center Land Remediation and Pollution Control Division National Risk Management Research Laboratory Office of Research and Development Cincinnati, Rare Earth Elements: A Review of Production, Processing, Recycling, and Associated Environmental Issue, National Service Center for Environmental Publications (NSCEP), EPA, 2012.

[92] J. C. G. Bűnzli. Acc. Chem. Res., 2006, 39 53−6.

[93] V. Balaram. Geoscience Frontiers, 2019, 10, 1285-1303.

[94] F. Faridkot, M. Sedaghat, M. Hosseini, M.R. Ganjali, M. Khoobi, A. Shafiee, P. Norouzi. Acta Part A Mol. Biomol. Spectrosc., 2015, 137, 1231–1234.

[95] Z. Liang, Z. Liu, Y. Gao. Tetrahedron Lett., 2007, 48, 3587–3590.

[96] I.E. Tolpygin, K.S. Tikhomirova, Y.V. Revinskii, Z.V. Bren, A.D. Dubonosov, V.A. Bren. Russ. J. Org. Chem., 2017, 53, 1651–1654.

[97] M. Liu, Z. Xu, Y. Song, H. Li, C. Xian. J. Lumin., 2018, 198, 337–341.

[98] T. Yu, J. Meng, Y. Zhao, H. Zhang, X. Han, D. Fan. Acta Part A Mol. Biomol. Spectrosc. 2011, 78, 396–400.

[99] R.S. Kumar, S.K.A. Kumar, K. Vijayakrishna, A. Sivaramakrishna, C.V.S.B. Rao, N. Sivaraman, S.K. Sahoo. Acta Part A Mol. Biomol. Spectrosc. 2019, 214, 32–39.

[100] W.S. Xia, R.H. Schmehl, C.J. Li. Tetrahedron 200, 56, 7045–7049.

[101] P. Dapporto, M. Formica, V. Fusi, L. Giorgi, M. Micheloni, P. Paoli, R. Pontellini, P. Rossi. Inorg. Chem. 2001, 40, 6186-6192.

[102] G. Ambrosi, M. Micheloni, D. Paderni, M. Formica, L. Giorgi, V. Fusi. Supramolecular Chemistry, 2020, 32, 1-11.

[103] G. A. Melson. coordination of macrocyclic compound, 1979 plenum, New York.

[104] R. Izatt. Synthetic Multidentate Macrocyclic Ligands, Academic Press, New York, 1978.

[105] G. W. Gokel. Macrocyclic Polyether Synthesis, 1982 Springer, Heidelberg,.

[106] R. M. Izatt, J. J. Christensen. Synthesis of Macrocycles, the Design of Selective Complexing Agents. 1987 Wiley, New York.

[107] J. M. Lehn. Angew. Chem. Int. ed. Eng., 1988, 27, 89-112.

[108] F. Diederich. Angew. Chem. Inte. Ed. eng., 1988, 27, 362-386.

[109] H. J. Schneider, and A. K. Yatsimirsky. Chem. Soc. Rev. 2008, 37, 263-277.

[110] N. F. Curtis. J. Chem. Soc., 1960, 4409-4413.

[111] M. Formica, V. Fusi, L. Giorgi, M. Micheloni. Coord. Chem. Rev. 2012, 256, 170-192.

[112] J. Seo, S. Kim, Soo Young Park. J. Am. Chem. Soc., 2004, 126, 11154-11155.

[113] P. Pasman, G. F. Mes, N. W. Koper, J. W. Verhoeven. J. Am. Chem. Soc., 1985, 107, 21.

[114] Z. Zece, L. Weiyu, C. Yang. Sensors and Actuators B: Chemical, 2016, 224, 31-36.

[115] M. Formica, G. Favi, V. Fusi, L. Giorgi, F. Mantellini, M. Micheloni. Journal of Luminescence, 2018, 195, 193-200.

[116] C. Benelli, E. Borgogelli, M. Formica, V. Fusi, L. Giorgi, E. Macedi, M. Micheloni, P. Paoli, P. Rossi. Dalton Trans., 2013, 42, 5848.

[117] S. Amatori, G. Ambrosi, M. Formica, V. Fusi, L. Giorgi, E. Macedi, M. Micheloni, P. Paoli, P. Rossi. Chem. Eur. J. 2014, 20, 11048-11057.

[118] R. A. Sheldon. ACS Sustainable Chem. Eng. 2018, 6, 1, 32-48.

[119] C. R. Groom, I. J. Bruno, M. P. Lightfoot, S. C. Ward. Acta Cryst., 2016, B72, 171.

[120] P. Rossi, S. Ciattini, M. Formica, V. Fusi, L. Giorgi, E. Macedi, M. Micheloni, P. Paoli. Inorg. Chim. Acta, 2018, 470, 254.

[121] K. Chevalier, A. Gruen, A. Stamm, Y Schmitt, M. Gerhards, R. Diller. J. Phys. Chem. A, 2013, 117, 11233.

[122] G. E. Dobretsov, T. I. Syrejschikovaa, N. V. Smolin. Biophysics, 2014, 59, 183.

[123] A. Shrivastava, V. B. Gupta. Chronicles of Young Scientists, 2011, 2, 21.

[124] A. Garau, L. Lvova, Eleonora Macedi, G. Ambrosi, M. C. Aragoni, M.Arca, C. Caltagirone, S. J. Coles, M. Formica, V. Fusi, L. Giorgi, F. Isaia, V. Lippolis, J. B. Orton, R. Paolesse. New J. Chem., 2020, 44, 20834.

[125] J. E. Kwon, S. Lee, Y. You, K. H. Baek, K. Ohkubo, J. Cho, S. Fukuzumi, I. Shin, Soo Y. Park, W. Nam. Inorg. Chem. 2012, 51, 8760-8774.

[126] C. S. de Oliveira, B. F. Lira, J. M. Barbosa-Filho. Molecules, 2012, 17, 10192-10231.

[127] N. A. Khalil, A. M. Kamal, S. H. Emam. Biol. Pharm. Bull., 2015, 38, 763-773.

[128] M. M. G. El-Din, M. I. El-Gamal, M. S. Abdel-Maksoud, K. H. Yoo, C. H. Oh. Eur. J. Med. Chem., 2015, 90, 45-52.

[129] R. Gudipati, R. N. R. Anreddy, S. Manda. Pharm. J., 2011, 19, 153-158.

[130] N. B. Patel, A. C. Purohit, D. P. Rajani, R. Moo-Puc, G. Rivera. Eur. J. Med. Chem., 2013, 62, 677-687.

[131] S. Rapolu, M. Alla, V. R. Bommena, R. Murthy, N. Jain, V. R. Bommareddy, M. R. Bommineni. Eur. J. Med. Chem., 2013, 66, 91-100.

[132] H. Rajak, P. Singour, M. D. Kharya, P. Mishra. Chem. Biol. Drug Des., 2011, 77, 152-158.

[133] M. Homocianu, A. Airinei. J. Fluoresc., 2016, 26, 1617-1635.

[134] S. Wen, J. Pei, Y. Zhou, L. Xue, B. Xu, Y. Li, B. Xu, W. Tian. J. Polym. Sci., Part A: Polym. Chem., 2009, 47, 1003-1012.

[135] Y. K. Fang, C. L. Liu, G. Y. Yang, P. C. Chen, W. C. Chen. Macromolecules, 2011, 44, 2604-2612.

[136] E. Schab-Balcerzak, A. Iwan, M. Grucela-Zajac, M. Krompiec, M. Podgorna, M. Domanski, M. Siwy, H. Janeczek. Synth. Met., 2011, 161, 1660-1670.

[137] E. Schab-Balcerzak, M. Grucela-Zajac, M. Krompiec, H. Janeczek, M. Siwy, D. Sek. Synth. Met., 2011, 161, 2268-2279.

[138] A. P. Kulkarni, C. J. Tonzola, A. Babel, S. A. Jenekhe. Chem. Mater., 2004, 16, 4556-4573

[139] L. Zhu, C. Gu, Y. He, G. Wang. J. Lumin., 2014, 153, 439-445.

[140] J. Han, F. L. Wang, Y. X. Liu, F. Y. Zhang, J. B. Meng, Z. J. He. ChemPlusChem, 2014, 77, 196-200.

[141] C. Y. Yu, T. Y. Shih. Synth. Met., 2014, 191, 12-18.

[142] A. Terenzi, M. Fanelli, G. Ambrosi, S. Amatori, V. Fusi, L. Giorgi, V. T. Liveria, G. Barone, Dalton Trans., 2012, 41, 4389.

[143] G. Ambrosi, M. Formica, V. Fusi, L. Giorgi, E. Macedi, M. Micheloni, G. Piersanti, R. Pontellini. Org. Biomol. Chem., 2010, 8, 1471-1478

[144] G. Ambrosi, M. Formica, V. Fusi, L. Giorgi, E. Macedi, M. Micheloni, P. Paoli, P. Rossi, Inorg. Chem., 2009, 48, 10424-10434.

[145] G. Piersanti, F. Remi, V. Fusi, M. Formica, L. Giorgi, G. Zappia. Org. Lett., 2009, 11, 417-420.

[146] G. Ambrosi, M. Fanelli, P. Paoli, M. Formica, D. Paderni, P. Rossi, M. Micheloni, L. Giorgi, V. Fusi. Dalton Trans., 2020, 49, 7496.

[147] C.R. Groom, I.J. Bruno, M.P. Lightfoot, S.C. Ward. Acta Cryst., Sect. B: Struct. Sci., Cryst. Eng. Mater., 2016, 72, 171-179.

[148] Y. Chih-Chiang, C.-J. Hsu, P.-T. Chou, H. C. Cheng, Y. O. Su, M.-K. Leung. J. Phys. Chem. B, 2010, 114, 756-768.

[149] A. W. Czarnik, Fluorescent Chemosensor for Ion and Molecule Recognition, American Chemical Society, Washington, DC, 1993.

[150] V. Fusi, L. Giorgi, M. Formica, M. Micheloni, E. Macedi, G. Ambrosi, P. Paoli, P. Rossi, R. Pontellini. Inorg. Chem., 2010, 49, 9940-9948.

[151] T. Iijima, A. Momotake, Y. Shinohara, T. Sato, Y. Nishimura, T. Arai. Phys. J. Chem. A, 114, 2010, 114, 1603-1609.

[152] J.E. Kwon, S. Lee, Y. You, K.-H. Baek, K. Ohkubo, J. Cho, S. Fukuzumi, I. Shin, S.Y. Park, W. Nam. Inorg. Chem., 2012, 51, 8760–8774.

[153] P. Dapporto, M. Formica, V. Fusi, M. Micheloni, P. Paoli, R. Pontellini, P. Romani, P. Rossi. Inorg. Chem., 2000, 39, 2156-2163.

[154] P. Gans, A. Sabatini, A. Vacca. Talanta, 1996, 43, 1739.

[155] J.-L. Brisset. Rev. Roum. Chim., 1983, 28, 941-949.

[156] L. Giordano, V. V. Shvadchak, J. A. Fauerbach, E. A. Jares-Erijman, T. M. Jovin. J. Phys. Chem. Lett. 2012, 3, 1011-1016.

[157] D. Paderni, L. Giorgi, E. Macedi, M. Formica, P. Paoli, P. Rossi, V. Fusi. Dalton, Trans., 2021. DOI: 10.1039/d1dt01753e.

[158] CrysAlisPro, Version 1.171.39.46, Rigaku OD, 2018.

[159] M. C. Burla, R. Caliandro, M. Camalli, B. Carrozzini, G. L. Cascarano, L. Da Caro, C. Giacovazzo, G. Polidori, R. Spagna. J. Appl. Crystallogr., 2005, 38, 381.

[160] G. M. Sheldrick. Acta Crystallogr., Sect. C: Struct. Chem., 2015, 71, 3.

[161] M. Nardelli. J. Appl. Crystallogr., 1995, 28, 659.

[162] C. F. Macrae, I. J. Bruno, J. A. Chisholm, P. R. Edgington, P. McCabe, E. Pidcock, E. Rodriguez-Monge, R. Taylor, J. van de Streek, P. A. Wood. J. Appl. Crystallogr., 2008, 41, 466.

[163] Dassault Systèmes BIOVIA, Discovery Visualizer, v19.1.0.18287, Dassault Systèmes, San Diego, 2019.

[164] A. Bencini, A. Bianchi, E. Garcia-Espana, V. Fusi, M. Micheloni, P. Paoletti, J. A. Ramirez, A. Rodriguez, B. Valtancoli. J. Chem. Soc., Perkin Trans., 1992, 2, 1059-1065.

[165] CrysAlisPro, Agilent Technologies, 2011.

[166] M. C. Burla, R. Caliandro, M. Camalli, B. Carrozzini, G. L. Cascarano, L. Da Caro, C. Giacovazzo, G. Polidori, R. Spagna. J. Appl. Crystallogr., 2005, 38, 381-388.

[167] G. M. Sheldrick. Acta Crystallogr., Sect. C: Struct. Chem., 2015, 71, 3-8.

[168] M. Nardelli. J. Appl. Crystallogr., 1995, 28, 659.

[169] L. J. Farrugia. J. Appl. Crystallogr., 2012, 45, 849-854.

[170] Dassault Systèmes BIOVIA, Discovery Studio Visualizer, v 19.1.0.18287, Dassault Systèmes, San Diego, 2019.

[171] A. L. Speck. Acta Crystallogr., Sect. D: Biol. Crystallogr., 2009, 65, 148-155.

Aknowledgements

Thanks to:

my Tutor, Professor Luca Giorgi for his fundamental role in my professional growth,

Dr. Eleonora Macedi for her enormous support, you are a Friend,

Professor Mauro Formica for his kind help,

Professor Mauro Micheloni for his good soul,

Professor Vieri Fusi for his precious advice,

and to:

Professor Paola Paoli,

Professor Patrizia Rossi,

Professor Enrique Garcia-Espana,

for their great contributions in this research project.